COMPOSITE REGENERATION AND PARTICULATE FILTRATION BY APPLICATION OF MICROWAVE ENERGY FOR EXHAUST EMISSION CONTROL OF CI ENGINES

A thesis submitted to the
University of Petroleum and Energy Studies

For the award of
Doctor of Philosophy
in
Mechanical Engineering

BY
Caneon Kurien

March 2020

SUPERVISOR
Dr. Ajay Kumar Srivastava

UPES
UNIVERSITY WITH A PURPOSE

Department of Mechanical Engineering
School of Engineering
University of Petroleum &Energy Studies,
Dehradun – 248007: Uttarakhand

COMPOSITE REGENERATION AND PARTICULATE FILTRATION BY APPLICATION OF MICROWAVE ENERGY FOR EXHAUST EMISSION CONTROL OF CI ENGINES

A thesis submitted to the
University of Petroleum and Energy Studies

For the award of
Doctor of Philosophy
in
Mechanical Engineering

BY
Caneon Kurien
(SAP ID- 500056861)

March 2020

SUPERVISOR
Dr. Ajay Kumar Srivastava
Professor
Department of Mechanical Engineering
University of Petroleum and Energy Studies
Dehradun, Uttarakhand

UPES
UNIVERSITY WITH A PURPOSE

Department of Mechanical Engineering
School of Engineering
University of Petroleum &Energy Studies,
Dehradun – 248007: Uttarakhand

August 2020

DECLARATION

I declare that the thesis entitled "**Composite Regeneration and Particulate Filtration by Application of Microwave Energy for Exhaust Emission Control of CI Engines**" has been prepared by me under the guidance of **Dr. Ajay Kumar Srivastava**, Professor of Mechanical Engineering Department, University of Petroleum & Energy Studies. No part of this thesis has formed the basis for the award of any degree or fellowship previously.

Caneon Kurien

Department of Mechanical Engineering,
School of Engineering
University of Petroleum & Energy Studies
Dehradun-248007: Uttarakhand

Date: **28/08/20**

CERTIFICATE

CERTIFICATE

I certify that **Caneon Kurien** has prepared his thesis entitled "**Composite Regeneration and Particulate Filtration by Application of Microwave Energy for Exhaust Emission Control of CI Engines**," for the award of PhD degree of the University of Petroleum & Energy Studies, under my guidance. He has carried out the work at the Department of Mechanical Engineering, University of Petroleum & Energy Studies, Dehradun.

Supervisor

Dr. Ajay Kumar Srivastava
Professor
Department of Mechanical Engineering
University of Petroleum and Energy Studies

Date: **28.08.2020**

ABSTRACT

The toxic nature of these exhaust emissions has resulted in stringent emission norms limiting the permissible emission levels of components in the exhaust. Various emission control techniques have been developed over the years, which can be broadly classified into pre-treatment techniques (engine modifications) and post-treatment techniques like diesel oxidation catalysis (DOC), diesel particulate filtration (DPF), selective catalytic reduction (SCR) and lean NOx trap. The post-treatment technique includes the application of an emission control system in the exhaust manifold to treat the exhaust gas and reduce toxicity levels prior to releasing it to the atmosphere. Oxidation of hydrocarbon and carbon monoxide emissions take place in the diesel oxidation catalysis system, where carbon dioxide and water vapor are released as by-products.

Diesel Particulate Filtration system uses wall flow filtration technique, where the particles are trapped in the spatial layers of the wall by depth filtration and cake filtration. The wall flow filtration leads to clogging of filter channels and causes higher backpressure. The engine efficiency and other operational parameters will be affected once the backpressure rises above the allowable limit. Hence regeneration of DPF has to be carried out periodically by burning the accumulated soot particles. Various active regeneration techniques by application of electric heaters, plasma discharge, corona discharge, burner, and vector network analyzers have been developed in the previous research works, whereas the commercially available technique is fuel-based regeneration. Regeneration strategy for DPF requires optimization since the commercially available fuel-based regeneration is resulting in excessive fuel penalty and also the catastrophic failure of DPF substrate due to uncontrolled combustion. Development of an alternate regeneration technique that can selectively burn the accumulated soot particles without affecting the

filter substrate material is one of the major challenges faced by the automotive industry.

This work aims to develop an emission control system comprising of diesel oxidation catalysis (DOC) and diesel particulate filtration (DPF) system with microwave-assisted composite regeneration. Diesel oxidation catalysis filter consists of a ceramic filter substrate which has straight channels at a density of 300 or 400 cells per square inch, and the inner surface of the filter channels are coated with a layer of alumina washcoat. Noble metals like platinum and palladium are impeded in the alumina washcoat layer, which acts as catalyst for oxidation of carbon monoxide and reduction of nitrates and hydrocarbons. The exhaust gas is directed to the diesel particulate filtration system after the treatment in diesel oxidation catalysis filter. The diesel particulate filter has a ceramic substrate with alternately plugged straight channels of rectangular cross-section, i.e., a channel which is open at the inlet side will be closed at the outlet side thus the exhaust gas will be forced to flow through the porous wall. The soot particles will get accumulated in the porous wall of the diesel particulate filter, and hence the clean exhaust will be released via the outlet of the adjacent channel. The accumulated soot particles will lead to clogging of the filter channels and increase backpressure causing reverse flow, which will affect the engine performance. The soot particles collected on the filter walls have to be cleared for the effective functioning of the system. In commercially available systems, the soot particles are burned into ashes by injecting fuel into the filter substrate and then washed away by the exhaust gas flow. The injection of fuel to the filter substrate is causing uncontrolled combustion inside the system leading to filter damage.

Electromagnetic radiations in the microwave region, which are also used in household microwave ovens, are proposed to be used for clearing these clogged filter channels. An emission control system has been designed

using Computer Aided Designing (CAD) software, and simulations have been conducted in the virtual environment using Computational Fluid Dynamics (CFD) software for testing the suitability and effectiveness of the suggested design and developed system. The results of the simulation showed that the developed system could be an effective alternative in place of the existing emission control system with fuel-based regeneration, and it can also improve the service life of the filter substrates.

Performance and emission characteristics of multi-cylinder CI engine were evaluated after retrofitting the developed after-treatment emission control system comprising of Diesel Oxidation Catalysis (DOC) and microwave regeneration based Diesel Particulate Filtration (DPF) systems. The ceramic DOC substrate (400 cpsi) with a catalyst loading of platinum and palladium in the ratio 5:1 exhibited conversion efficiency of 54% for hydrocarbons, 27% for carbon monoxide and 55% for particle number emissions. Filtration efficiency of DPF substrate was observed to be 45% for hydrocarbons, 11% for carbon monoxide and 88% for particle number emissions. Soot accumulation rate and regeneration rate were experimentally investigated at different engine loads and magnetron input power levels. The experimental results showed that the developed after-treatment system (DOC + DPF) has an average filtration efficiency of 91% for particle number emissions and 59% for hydrocarbon emissions. The regeneration rate was observed to be a maximum of 0.21 g/min at 50% power levels owing to the non-linear behavior of magnetron.

The effect of soot accumulation and regeneration on the morphology, microstructure, chemical composition and particle size of DPF substrate were examined using characterization studies like Scanning Electron Microscopy – Energy Dispersive X-Ray Spectroscopy (SEM-EDS), Fourier Transform Infra-Red spectroscopy (FTIR), Particle Size Analysis (PSA) and microscopic

imaging. SEM-EDS results detailed the microstructure of the porous wall in unused DPF substrate and the morphological characteristics of the accumulated soot particles in the used DPF substrate, where the carbon content of 8.53% was found indicating the presence of soot particles. The FTIR results showed the presence of anatase in the DOC substrate indicating the oxidation of platinum catalyst and carcinogenic agents like tetra chloro ethylene was also detected in the case of DPF substrate. The intensity of particle size distribution in the DPF substrate was reduced to an average size of 328 nm (after soot loading) from 1172 nm (unused DPF substrate) and size was again increased to 938.5 nm in the case of DPF substrate after microwave energy based regeneration.

ACKNOWLEDGMENT

TABLE OF CONTENTS

LIST OF SYMBOLS

ϕ local porosity (dimensionless)

α darcy law viscous permeability of porous zone (m^2)

B magnetic induction (N s/ C m)

C_o velocity of light in vacuum (m/s)

c speed of light (m/s)

d_p penetration depth of microwave (m)

ρ density of fluid (kg/m^3)

D electric displacement (C/m^2)

E electric field intensity

ε complex permittivity

ε^* relative complex permittivity

ε' dielectric constant

ε'' dielectric loss factor

F_o power flux at the surface (w/m^2)

H magnetic field intensity (A/m)

$\vec{J_i}$ diffusive mass flux (kg/m^2 s)

$\vec{V}$ superficial velocity in the porous region (m/s)

S_ρ mass source arising in porous region due to soot consumption (kg/m^3 s)

P pressure (Pa)

P_v power per unit volume (W/m^3)

$\overset{=}{\tau}$ stress tensor (Pa)

μ viscosity (kg/m s)

μ_m magnetic permeability of material (H/m)

ω angular frequency (rad/s)

σ free space permittivity (8.54×10^{-12} F/m)

y_i mass fraction (dimensionless)

z spatial distance in z direction

LIST OF TABLES

LIST OF FIGURES

9

10

CHAPTER 1. INTRODUCTION

Reducing the toxicity levels of harmful emissions from automotive diesel engines is a major technical challenge. The exhaust emission from diesel engine includes carbon monoxide, carbon dioxide, hydrocarbons, nitrates, soot particles, and soluble organic fraction. These emissions have been included in the category "likely to be carcinogenic to humans" by organizations like the United States Environmental Protection Agency (US-EPA), World Health Organisation (WHO), etc. based on human epidemiology data. Exposure to diesel exhaust will affect the functioning of lungs, blood vessels and also results in cardiovascular diseases. Rising levels of pollution in cities are also a direct reflection of the adverse impact of automotive emissions on the environment. India is one of the 196 countries that have signed the Paris agreement for reducing the intensity of emissions so that the global temperature rise can be limited to 2 °C. Complete combustion of the fuel in the combustion chamber of engines will generate carbon dioxide and water vapor as by-products, whereas in real scenario incomplete combustion products including particulate matter, NOx, unburnt hydrocarbons and carbon monoxide are produced.

Global climate change has an adverse effect on human life, and studies have shown that sea levels are likely to rise about 0.5 to 1 m due to 4 °C global warming levels by 2060 [1][2][3]. Human activities like fossil fuel combustion have resulted in the atmospheric release of greenhouse gases enhancing the natural greenhouse effect [4][5][6]. As per the studies conducted by Intergovernmental Panel on Climate Change (IPCC), there must be a reduction in the greenhouse gas emissions (i.e. 50-85% of emission levels in year 2000) to restrict the global warming at 2 – 2.4 °C by the year 2050,

which can be achieved by reducing the emission of greenhouse gases from all the sectors [7][8].

Among the risk factor for deaths in the world as per the 25 years trend for the global burden of disease, particulate matter was ranked fifth since it was responsible for 4.2 million deaths globally in the year 2015 [9]. Laboratory experiments and epidemiological studies have exposed the carcinogenic nature of diesel engine exhaust, which consists of diesel particulate matter that is a complex mixture of polycyclic aromatic hydrocarbons [10][11][12]. Exposure to particulate matter was also observed to make a significant contribution to the risk of cardiovascular diseases (CVD), and American health association (AHA) has also included specific statements in their guidelines related to the link of PM exposure in the CVD risk factor [13][14]. Pollutants can affect the human system following three pathways, namely classical (inflammatory mediators), alternative (particle translocation and oxidative stress), and neurogenic pathway (autonomic nervous system) [15]. Some of the pathological consequences of the PM pollutant include atherosclerosis [16], vascular dysfunction [17], thrombosis, and coagulation [18]. Recent studies have also showed that exposure to particulate matter worsens diabetic's control by affecting glycaemic metabolism [19]. Mediating factors of cardiovascular diseases induced by particulate matter include insulin resistance [20], diabetes [21], metabolic syndrome [22], arterial hypertension [23], and autonomic imbalance [24].

Diesel engines have become an integral part of the automotive industry as well as other industries because of its higher thermal efficiency and longer life compared to gasoline engines [25][26]. But the exhaust emissions from these engines are found to be toxic in nature, contributing a significant part in environmental pollution [27][28]. Diesel engine ranks second among the anthropogenic sources releasing particulate matter ($PM_{2.5}$ and PM_{10}), which is

formed due to the combustion of fossil fuel and tribological parameters [29][30]. The exhaust emission from diesel engines includes unburnt hydrocarbons, particulate matter, and oxides of carbon & nitrogen [31][32]. Particulate matter consists of soluble organic fraction and soot particles. Insoluble organic components of particulate matter have agglomerates in size range of 0.5 to 5 μm while the inorganic non-combustible fraction (ash) will be in a size range of 45 to 160 nm. Soot particles released from diesel engines are found to be carcinogenic, creating a threat to human life [33]. The size and composition of soot particle determine its impact on human health, and lower size fine particles (< 2.5 μm) can reach the alveolar region of human lungs [34][35][36]. Particulate matter (> 2.5 μm) released by the engine exhaust can enter deep into the respiratory tract. Diesel engine utilizes the heat generated during compression of air to release chemical energy in the fuel, which gets converted to mechanical energy [37][38]. Complete combustion of the fuel in the combustion chamber will generate carbon dioxide and water vapor as by-products, whereas in real scenario incomplete combustion products including particulate matter, NOx, unburnt hydrocarbons and carbon monoxide are produced [39][40][41]. These emissions can be reduced by two techniques, namely pre-treatment and post-treatment [42].

Engine modifications like exhaust gas recirculation, combustion cylinder alteration, fuel injection strategies, and blending of fuels will come under pre-treatment techniques [43][44][45]. Pre-treatment techniques are employed to reduce the generation of toxic gases from the combustion inside the engine [46][47][48]. Post-treatment techniques are used to treat the exhaust gases released from the engine by the use of systems like Diesel Oxidation catalysis, Diesel Particulate Filtration, and Selective Catalytic Reduction. Oxidation of carbon monoxide, nitrides, and hydrocarbons takes place in the diesel oxidation catalyst (DOC) filter. The particulate matter is

trapped with the help of the Diesel particulate Filter (DPF). The particulate matter consists of soluble organic fraction and soot particles.

The soot particles will get accumulated in these channels leading to clogging of filters, and the backpressure will rise, reducing the efficiency of the engine [48]. Regeneration of the accumulated soot particles has to be carried out either by using active or passive regeneration techniques. The temperature of the exhaust gas plays an important role in passive regeneration which can also be carried out by using some catalysts to improve soot combustion [49]. But passive regeneration alone cannot remove the trapped soot particles to the required extent. The active regeneration technique has to be adopted to remove the accumulated soot. In commercial diesel particulate filters, active regeneration is carried out by injecting the fuel to the filter substrate and then burning it by producing a spark/or by self-ignition, which will result in uncontrolled combustion inside the filter substrate and will also damage the filter reducing the service life of the filter [49]..

1.1 MOTIVATION

- Effects of exhaust emission from diesel engines is a serious threat to environment and human health
- Solutions: Pretreatment and post treatment techniques
- Post treatment techniques: Diesel Oxidation Catalysis (DOC), Diesel Particulate Filtration (DPF) and Selective Catalytic Reduction (SCR).
- Compliance approaches for light-duty Euro 6 engines include (a) Smaller and medium-size engines (<2 liters) tend to use DOC+DPF and primarily LNT for NOx control; (b) Larger cars (>2L) use DOC+DPF+SCR; (c) Some manufacturers offer EGR-only NOx control (with no after-treatment control), and DOC+DPF on medium and larger cars.

- DPF is a mandatory retrofit in engines to bring down the emission levels to meet EURO VI norms and accumulated soot particles in DPF channels has to be regenerated at regular intervals for its effective functioning.
- Commercially available fuel-based regeneration is causing uncontrolled combustion and thus leading to catastrophic failure.
- Development of an alternate regeneration technique for selectively burning the accumulated soot particles is the major technical challenge faced by automotive industries.

1.2 NOVELTY STATEMENT

Microwave energy is a possible method for active regeneration since it can penetrate through the filter and even without heating the exhaust gases. The material of the filter has to be selected in such a way that it must have good dielectric properties, which will help in allowing microwave radiation to selectively burn the soot particles. Soot particles are a good absorber of microwave radiations [50]. The combined use of microwave energy and catalysts will help in the oxidation of soot at a higher reaction rate and lower temperature. The composite regeneration technique proposed in this work will be a possible solution for meeting emission norms effectively

1.3 OBJECTIVES

- Development of a post-treatment emission control system with a composite regeneration setup.

  – Modelling and fabrication

- Experimental analysis of the developed emission control system.

- Comparison of the conversion efficiency (metallic and ceramic DOC with different catalyst loading).

- Analysis of soot accumulation rate and filtration efficiency of DPF at different loads.

- Analyze the effectiveness of microwave-assisted composite regeneration system.

- Characterization of the filter substrate to determine the effects of filtration on substrate properties.

CHAPTER 2. LITERATURE SURVEY

The toxic nature of exhaust gases released by Compression Ignition (CI) engines has led to environmental concerns, affecting its sustainability [51]. The exhaust emission from diesel engines includes unburnt hydrocarbons, particulate matter, and oxides of carbon & nitrogen [52]. Soot particles contained in the particulate matter is also found to be carcinogenic in nature and also leads to various lung diseases [53]. The diesel oxidation catalysis system involves oxidation of hydrocarbons, nitrates, and soluble organic fraction [54]. Diesel particulate filtration blocks the soot particles with the help of alternately plugged diesel particulate filter with porous walls. The regeneration of accumulated soot is one of the significant challenges faced by automotive industries for the effective implementation of diesel particulate filtration system. A detailed review of the challenges faced in the application of emission control techniques has been carried out in this study, and it has been concluded from the results of the literature study that microwave-based regeneration system would be an effective technique.

2.1 EXHAUST EMISSIONS AND CONTROL TECHNIQUES

Diesel engines are one of the major sources of particulate matter emissions (PM2.5 and PM10), which is formed due to the combustion of fossil fuel and tribological parameters [55]. Particulate matter consists of soluble organic fraction and soot particles. Insoluble organic components of particulate matter have agglomerates in size range of 0.5 to 5 μm while the inorganic non-combustible fraction (ash) will be in a size range of 45 to 160 nm [56]. Soot particles released from diesel engines are found to be carcinogenic in nature, creating a threat to human life [57]. The size and composition of the soot particle determine its impact on human health. These emissions can be

reduced by two techniques, namely pre-treatment and post-treatment.

Engine Exhaust emissions pose a severe threat to the environment and human health. Combined application of pre-treatment and post-treatment techniques is the only solution to reduce these emissions. Pre-treatment techniques include engine modifications like combustion cylinder alteration, injection timing retard, exhaust gas recirculation, fuel injection strategies, and so on [58]. Optimization of fuel injection strategies will have a considerable effect on the reduction efficiency of hydrocarbons in exhaust emissions. The reduction efficiency of the particle oxidation catalyst was calculated for different values of the Start of Injection (SOI) and Fuel Injection Pressure (FIP) in [59]. Experimental results showed that higher reduction efficiency is achieved when FIP is in the range of 600 – 1000 bar and SOI in the range 0° to 15° crank angle before top dead center (CABTDC). Nitrogen oxide emissions from compression ignition engines can be controlled by exhaust gas recirculation technology, where a certain percentage of exhaust gas is recirculated to intake manifold [60].

Table 2.1. Literature study on particulate filtration and regeneration

Reference	Approach	Major Research Findings
Fang et al. 2019 [61]	Electric heater based DPF regeneration	The temperature distribution was not uniform, and the maximum temperature was observed at rear and center part of DPF
Fu et al. 2018 [62]	Burner based regeneration	The geometric parameters of the swirl burner have a significant influence on the distribution characteristics of the flow field.
Xiaoyu Pu et at. 2018 [63]	Regeneration of DPF using non-thermal plasma induced by dielectric barrier discharge	Comparative analysis of DPF regeneration at different oxygen flow rates was conducted using a Dielectric Barrier Discharge (DBD) - type Non-Thermal Plasma

		(NTP) reactor.
Penghao et al. 2018 [64]	DPF regeneration with NOx-PM coupled chemical reaction	The results showed that the presence of N_2O would reduce the light-off critical temperature of soot, thus enhancing the regeneration.
Dawei, Jun, and Yu 2017 [65]	Mathematical modelling of regeneration control.	Fuel based regeneration affects the durability of DPF and leads to lubricant oil dilution.
Feulner et al. 2017 [66]	MW energy generated by Vector Network Analyzer (VNA).	Temperature influence will also have to be considered since it will affect the transmission factor.
Bai et al. 2017 [67]	Experimental study on active control strategies for thermal exhaust management in the engine test bench.	The main factor for the increase in exhaust temperature is the fuel injection and higher fuel pressure, which influences the NOx emission.
V. Palma et al. 2016 [68]	DPF regeneration using electric heaters.	Energy consumption was higher and also the regeneration was limited to 5 cycles since efficiency reduced to 50%
Vincenzo Palma et al. 2016 [69]	Optimization of the preparation procedure of catalytic DPF and study on the feasibility of microwave-based regeneration.	MW considered the best alternative for regeneration since it will reduce energy consumption compared to fuel-based regeneration.
Yang, and Hunsicker 2016 [55]	Characterization of damaged DPF used in Industry by X-Ray Diffraction (XRD) and Scanning Electron Microscopy (SEM).	Uncontrolled combustion during fuel-based regeneration leads to the formation of cracks, pinholes, and melts.
Yamazaki et al. 2016 [70]	Application of Ceria based catalysts for diesel soot oxidation.	Cerium oxide – Ag-based catalyst reduces the oxidation temperature by 100 °C. Oxidation performance measured by Temperature Programmed Oxidation.
Jiaqiang et al. 2016 [71]	Mathematical model for NO_2 assisted passive regeneration of DPF.	Continuous regeneration technology - initial oxidation of soot by NO_2 released from DOC and further oxidation by active regeneration methods.

Bermúdez et al. 2015 [72]	Experimental study on Pre-DPF water injection to reduce the pressure drop.	Redistribution of accumulated soot particles by dragging it with the help of water will improve soot loading capacity and reduce regeneration frequency.
Vincenzo Palma et al. 2015 [73]	Study on performance of catalyzed DPF	Fuel borne catalysts (Ce/Fe/Cu based organic compounds) will oxidize a part of soot in the combustion chamber and improve soot light-off temperature in DPF.
Di Sarli and Di Benedetto 2015 [74]	Two dimensional mathematical model of soot regeneration using Computational Fluid Dynamics (CFD) for a single channel.	Combustion of soot by fuel-based regeneration results in overheating spots inside the filter.
Ramdas et al. 2015 [75]	Development of synthetic soot for analysis of oxidation activity of Ag-K	Catalyst lowered the combustion temperature by 200 ^{o}C but didn't have much effect on condensed poly-aromatic molecules.
Fornarelli et al. 2015 [76]	Three-dimensional flow and numerical simulations of the flow field in DOC	Validation of design by flow and pressure drop analysis. The sudden expansion of the diffuser resulted in the formation of a recirculation zone.
Zuo et al 2014 [77]	Regeneration model of DPF: field synergy theory	Microwave radiation enters in the form of a traveling waveguide and burns the deposited particles.
Graupner et al. 2013 [78]	Application of pulsed electric discharge for the regeneration of DPF	A high voltage pulse is applied to filter by discharging a capacitor for regeneration which resulted in the formation of pinholes and ringing.
Vincenzo Palma et al. 2013 [79]	Application of copper ferrite as a catalyst for soot oxidation.	Catalyst loading about 15-30% weight was found to reduce the temperature, time and energy required for DPF regeneration.
Corro et al. 2013 [80]	Application of Cu loaded ZnO as a catalyst in DPF	Oxidation temperature of particulate matter lowered to 150 ^{o}C and Cu ions act as active species for PM oxidation.
H.J Kim et al 2010 [81]	Electrostatic precipitation system for filtration of PM.	Corona discharge was found to be unstable when the speed and load were increased.

Blending of diesel with butanol and pentanol will also reduce the particulate matter emissions to a certain extent. Long-chain alcohols will have advantages like higher energy density, cetane number, better miscibility, and will be less hygroscopic [82]. Alternative fuels like BTL (Biomass to liquid) and GTL (Gas to liquid) will decrease the emission of pollutants in terms of nuclei & accumulation mode particles and also exhibits a similar behavior like diesel [83]. Post-treatment techniques involve the use of Diesel Oxidation Catalysis (DOC), Diesel Particulate Filtration (DPF) and Selective Catalytic Reduction (SCR) [84]. Diesel oxidation catalysis set up consists of a monolith substrate that has a wash coat, impeded with a thin layer of catalyst, and the whole set up is encased in a can. Since the Euro 5b emission norm in 2011, strict regulations have been made for particle number per km, which has forced the manufacturers to incorporate Diesel Particulate Filtration systems in the exhaust line of their vehicles [85]. Summary of the literature study on particulate filtration and regeneration is detailed in Table 2.1.

2.2 SOOT FORMATION AND IMPACT ON HUMAN HEALTH

Particulate matter in the engine exhaust is composed of soot and soluble organic fractions [72]. Soot particles are formed in the cylinder at fuel-rich regions where oxygen concentration is low, and soot absorbs soluble organic fraction on its surface [86][87]. Various stages involved in the formation of soot from fuel are as shown in Figure 2.1. Some of the major factors influencing the characteristics of soot particles formed in the engine cylinder are pressure, temperature, fuel injection strategy, and structure of fuel [88]. Precursors or the basic building block for soot is formed by fuel pyrolysis, where the molecular structure of organic compounds in fuel changes at high temperature in the presence of a lower concentration of oxygen [89]. The rate of fuel pyrolysis depends on temperature and oxygen concentration, which is related to the types of flames and the products of pyrolysis, including

polycyclic aromatic hydrocarbons and other hydrocarbon derivatives [90]. Particles are developed from gas-phase reactants by nucleation process at a temperature range of 1300 – 1600 K, where small size hydrocarbons combine to form large size aromatic molecules and particle nuclei has active sites for surface growth [91].
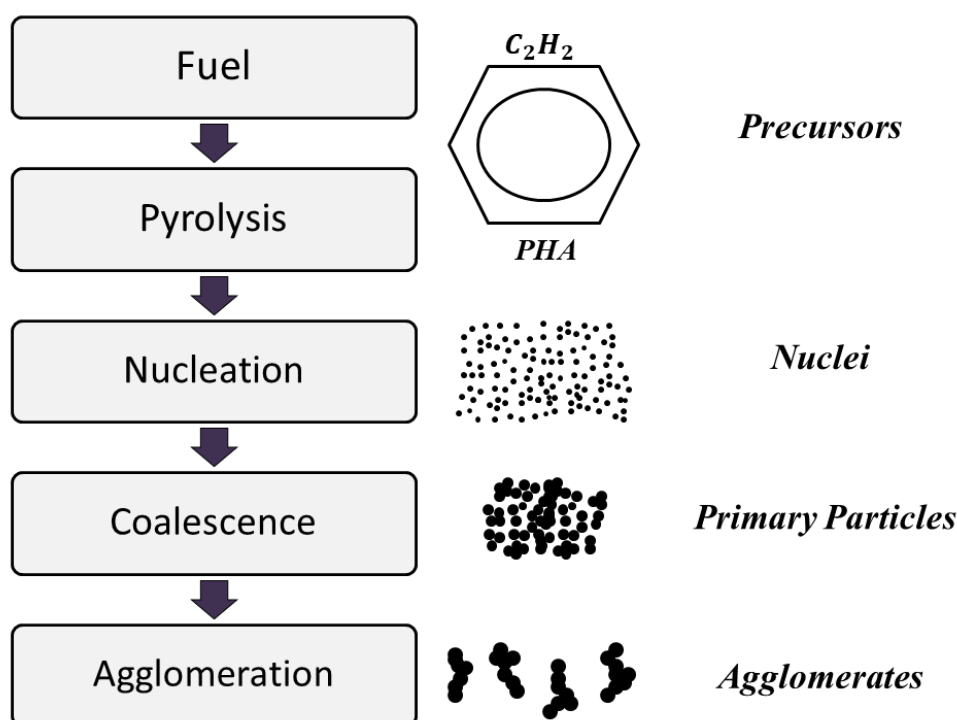
Figure 2.1. Stages involved the formation of soot

Nucleation takes place in three steps, out of which the first one is benzene ring formation, followed by dehydrogenation of rings and formation of polycyclic compounds [92]. Nucleation is followed by surface growth, where deposition of gas-phase hydrocarbons takes place in the spherules surface, and it contributes to the rise in soot mass, whereas the number of particles remains constant [93]. Inter collision of the developed particles will lead to agglomeration, resulting in the coagulation of the particles into a single large spheroid, as shown in Figure 2.2 [94]. Oxidation of soot into combustion

products might take place during any of the soot formation stages from pyrolysis to coagulation, which involves absorption of OH, O $^-$ and O radicals and desorption of these oxidation species as combustion products [95][96]. The composition and structure of the fuel have a direct influence on the formation of particulate matter, and the presence of sulfur, lead, and other additives in the fuel increase the mass of soot emissions [97].

Soot formation rate also depends on the carbon and hydrogen content present in the fuel composition, ie, more carbon content in fuel leads to a rise in soot formation rate and vice versa [98]. Parameters like carbon atoms, double bond, main chain length, aromatic ring, and side-chain length, defining the structure of fuel, also influence the soot formation rate [99]. The results of the studies conducted to determine the role of aromatic rings in soot formation rate showed that particulate formation rate increases with the increasing number of aromatic rings and carbon/hydrogen weight ratio [100]. Particulate matter emitted by the diesel engine poses a serious health hazard to humans, and ultrafine particles released by the engine will get deposited in the pulmonary region of lungs, and smaller size particles can penetrate epithelial tissues and enter bloodstream [101][102][103].

Substantial exposure to diesel engine exhaust is observed to increase the risk of lung cancer and bladder cancer [104]. Soluble organic fraction (SOF) present in the particulate matter is a significant precursor for tumor formation and the presence of mutagenic compounds like 1-nitropyrene [105][106] and benzo[a]pyrene [107] increases the risk of carcinogenicity from diesel exhaust exposure [108]. Metals like iron, calcium, magnesium, etc. present in the particulate matter increase the production of free radicals causing pulmonary disorders and the presence of metals increases the level of epidermal growth receptors in the activated state resulting in cancer-causing mutation of Ras proteins [89].
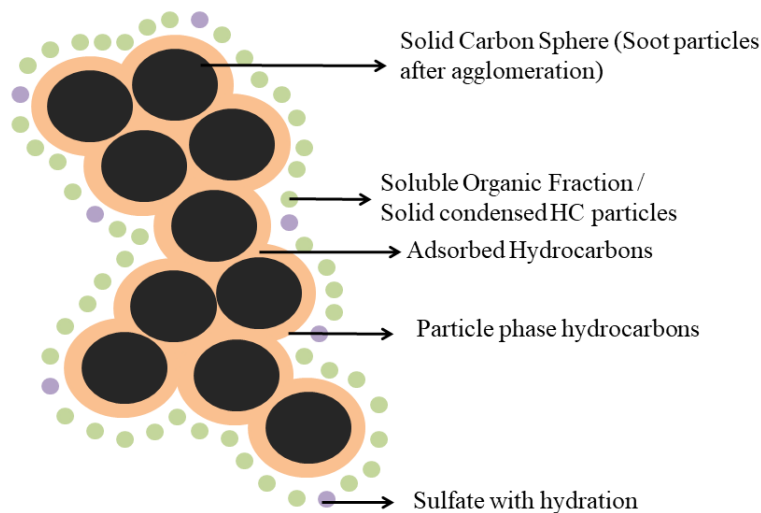
Figure 2.2. Schematic representation of soot particles and soluble organic fraction in particulate matter

2.3 DIESEL OXIDATION CATALYST FILTER (DOC)

DOC is used for oxidation of hydrocarbons, nitrates and soluble organic fraction. It is suitably placed before diesel particulate filter since the oxidation of nitrates can be utilized for passive regeneration of the soot in the particulate filter. Precious metals like platinum, palladium, and rhodium are used mostly as the catalyst. Catalysis can also be performed in two stages, out of which the initial stage involves the reduction of nitrate emissions using rhodium catalysts. The final step is the reduction of carbon monoxide and unburned hydrocarbons by oxidizing them over platinum and palladium catalyst [109]. The expensive nature of precious metal catalysts has led to the doping of non-noble metals into platinum-based catalysts. Huang Jiang et al. 2015 used the impregnation method for preparing a series of Platinum-Vanadium/Cerium-Zirconium oxide (Pt-V/Ce-Zr-O) diesel oxidation catalysts with different Pt/V ratios and the effect of vanadium on sulphur resistance and catalytic activity was investigated in detail. The results of the tests showed that Pt-V/Ce-Zr-O

with only one wt% Pt catalyst showed the highest catalyst performance with vanadium loading of one wt% [110]. Various reactions taking place inside the DOC filter are shown in equation no (1) – (4).

$$2NO \rightarrow N_2 + O_2 \qquad (1)$$

$$2NO_2 \rightarrow N_2 + 2O_2 \qquad (2)$$

$$2CO + O_2 \rightarrow 2CO_2 \qquad (3)$$

$$C_xH_y + \frac{(x+y)}{2}O_2 \rightarrow xCO_2 + \frac{y}{2}H_2O \qquad (4)$$
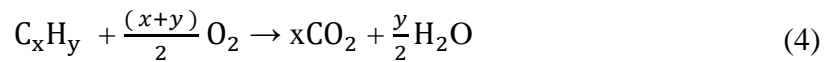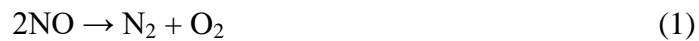
2.3.1 Oxidation of Nitrates for No$_2$ Assisted Passive Regeneration

In DOC, the oxidation of NO was found to reduce with time due to the formation of Pt oxide. The supply of H_2 was proposed to retard Pt oxide formation and improve NO_2 yield [111]. The effect of H_2 was analyzed for four gas mixtures, and a DOC filter with Pt catalyst and Al_2O_3 wash coat was used for evaluation. It was found that for $NO/O_2/CO/C_3H_6$ mixtures, NO_2 yield was increased when the H_2 concentration was 250 ppm. Also, it reduced light-off temperature for C_3H_6 oxidation. There was a temporal enhancement in NO_2 yield due to hydrogen supplementation. Concentrations above 250 ppm were found to reduce NO_2 yield. The effect of hydrogen on the NO oxidation was well known, but it was not concluded whether it is due to the temperature rise caused by hydrogen oxidation or due to its influence on reaction kinetics. Herreros et al. [112] carried out experiments to determine the variation in light-off temperature for different loads of hydrogen, and it was found that the hydrogen effect is due to the combination of various factors rather than hydrogen exothermic effect. But the commercialization of the proposed technique with hydrogen supplementation was not feasible. The

introduction of carbon monoxide and C_3H_6 pulses for the reduction of platinum oxide and oxidation of NO was suggested by Arvajova et al. [113]. The experiments were carried out in an adiabatic lab reactor with synergetic exhaust gas. It was found that the oxidation of NO was higher during the heat-up phase than in the cool-down phase. Catalytic activity was restored by increasing the concentration of carbon monoxide and C_3H_6 pulses during the cool-down phase. Schott et. al [114] designed a laboratory test bench using reactor analytics for evaluating the uniformity and distribution of catalyst coating in the DOC filter since it determines the efficiency of oxidation reactions taking place inside the filter.

2.3.2 CFD Analysis of DOC Filter

CFD analysis has been very much effective in optimizing the designed systems in a virtual environment so that the manufacturing of the optimized design model can be done [115]. It is an effective tool for determining the performance characteristics of designed models before the manufacture of the prototype. Three-Dimensional flow simulations of the flow field in a catalytic converter (DOC) were performed by Fornarelli et. al [76]. Simulation of DOC was carried out, and chemical reactions involved in it were considered for analysis. Monolith was considered as a porous medium, and the values of parameters are determined at three sections. Validation of design was carried out by flow and pressure drop analysis. Results showed that the sudden expansion of diffuser at inlet resulted in the recirculation zone, which would lead to the performance downgrade of the converter. Simulation on the existing exhaust system design of a light commercial vehicle was carried out by Ariara et al. [116]. Designing was done in CATIA V5, and simulation was carried out in the CFX tool. The pressure drop in the converter was determined by simulation. Since it is a validation of the design, no chemical reaction, and no heat exchange were considered for the simulation. The initial

conditions and properties of exhaust gas considered for the simulation were as follows (1) density = 0.5508 kg/m^3, (2) Viscosity = 3.814 × 10^{-4} Pa-second, (3) mass flow rate = 320 kg/hr, (4) Temperature = 520 °C, (5) Pressure at inlet = .212 bar. The results of the simulation showed that there was a total pressure drop of .184 bar in the exhaust system consisting of a muffler, underbody catcon, and close coupled catcon. Hayes et al. [117] developed various single-channel models of the catalytic converter using phoenics software and carried out simulations to determine the effect of changing cell density and wall thickness at constant wash coat loading.

2.4 DIESEL PARTICULATE FILTER (DPF)

The development of a reliable, fast, and cost-effective Diesel Particulate Filter (DPF) is one of the major technical challenges faced by Automotive and other industries. DPF is of two types, namely, flow-through filter (made of ceramic foam or wire mesh or metal wool, filtration efficiency < 60%) and wall flow type filter (Honeycomb monolith, filtration efficiency = 95%). Emission tests carried out in DPF having torturous open channels instead of alternately plugged channels showed that the particle emissions were higher since the filter was open structured, which made it difficult to block particles [118]. Emission tests were carried out based on the EURO steady-state cycle, where the load is increased from 10% to 100% of full load at intervals of 10%. High filtration efficiency of wall-flow filters has made it a standard requirement for diesel vehicles for meeting the emission norms.

2.4.1 History of DPF

The soot removal from the exhaust gas of heavy-duty diesel engines by application of particulate traps with metal fiber mesh was started in 1969 [119]. Particulate traps with ceramic fiber coil were introduced in 1978 [120]. The system consisted of multiple punched metal tubes wound with ceramic

fibers, as shown in Figure 2.3. Diesel oxidation catalyst filter was not used upstream during that time since the sulfur content in fuel was high, and it would lead to sulfur poisoning. Regeneration of accumulated soot particles was carried out by injecting various oxidizing agents like copper chloride, copper perchlorate, and acetylacetone [121]. The research on particulate traps ended in 1994 since engine alterations met the emission norms. As the emission standards got stringent with time, the particulate traps (Ceramic and Metallic DPF) gained attention since the EURO 5b emission norms forced the manufacturers to restrict the particle number emission.
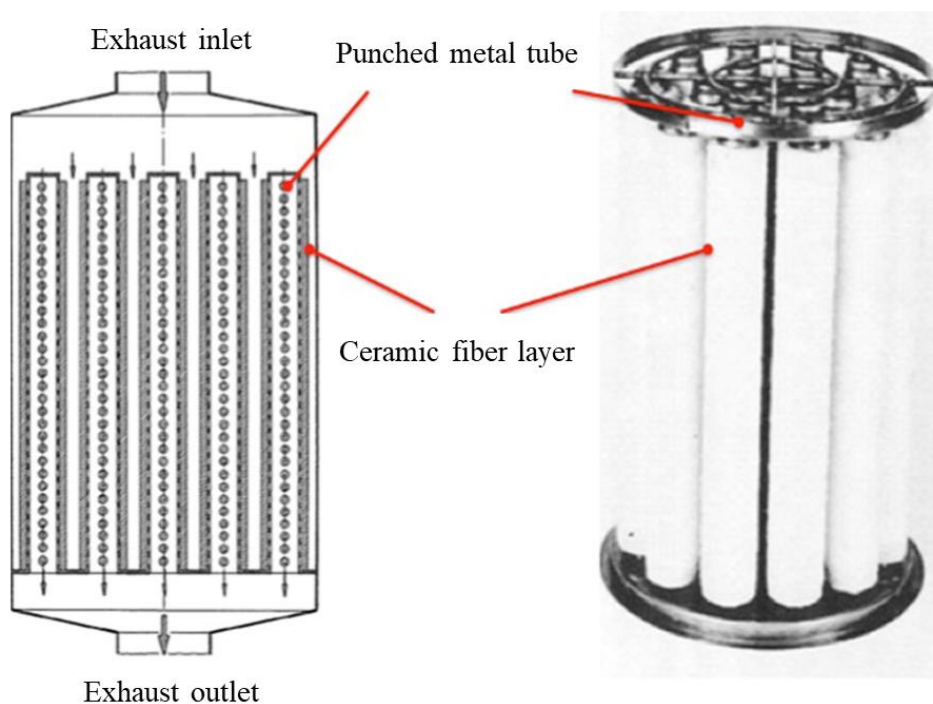
Figure 2.3. Ceramic fiber particulate trap [120]

Declaration of environmental institutes for the regulation of particulate matter based on particle number emissions, in addition to mass concentration, made DPF standard mandatory after-treatment component. Flow-through DPF filters with metallic foam were found to remove only 50% of particulate

matter by mass [115]. Metallic wall flow filters decreased the mass concentration by 50 – 70% and particle number by 50%. Removal of soot, ash deposits, and characteristics of materials used were some of the challenges faced during the development stage of DPF. The availability of low sulfur fuel has also made it possible to place DOC before DPF for enhancing passive regeneration.

2.4.2 Filtration Mechanism of DPF

Wall flow Diesel Particulate Filter consists of alternately plugged channels where the gas enters through open channels in the inlet and finds the other end of these channels closed, forcing it to flow through the porous wall and thus particulate matter gets filtrated. The operating principle of the DPF is detailed in Figure 2.4.
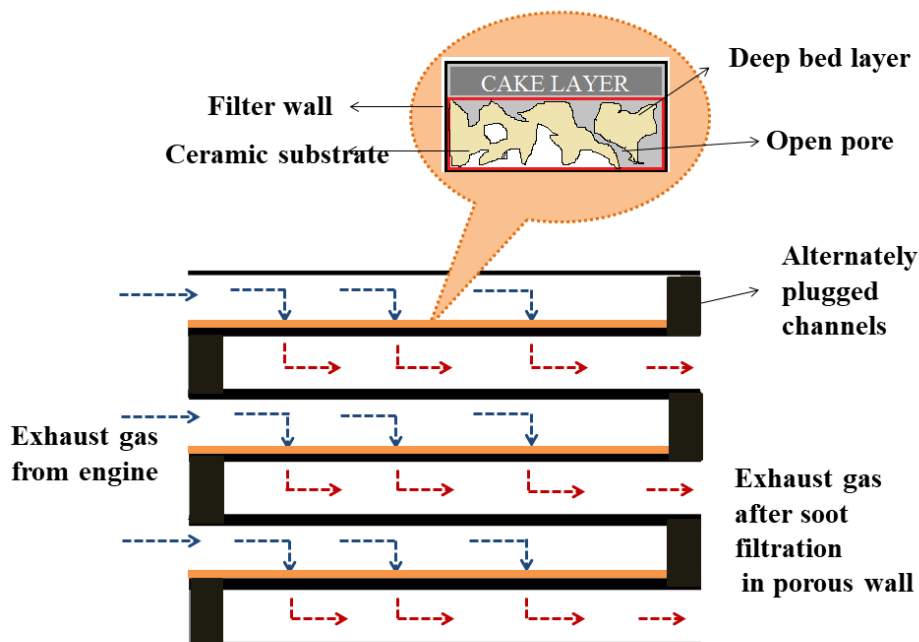
Figure 2.4. Operating principle of wall-flow DPF [78]

The accumulated soot particles lead to a restriction inflow of gas and increase the exhaust backpressure affecting the efficiency of the engine. The accumulated soot particles have to be oxidized periodically for regeneration. The particulate matter emitted by diesel engines consists of particles in accumulation mode (carbonaceous agglomerates) and nucleation mode (volatile organic and inorganic components like sulfates). The filtration in DPF takes place in two stages, namely depth filtration and cake filtration. Initially, the soot particles will get trapped in the porous wall of the filter, which is called as depth filtration. Cake filtration occurs when particle packing density reaches a maximum causing occlusion of pores, and the accumulated particulate matter layer acts as a porous medium to filter the upcoming particles in gas [122]. The transition from depth filtration to cake filtration occurs at a pressure drop range of 700 Pa. The filtration of the soluble organic fraction is not as effective as soot filtration [123]. Regeneration can be carried out by passive and active regeneration methods.

2.4.3 Catalyst Based Passive Regeneration of DPF

Passive regeneration is a continuous regeneration process by application of fuel borne catalyst and NO_2 assisted passive regeneration. Catalyst based regeneration can be carried out by either adding the catalyst to the fuel as organic derivatives or by deposition of catalytic coating to the filter surface. The purpose of the catalyst is to lower the ignition temperature of diesel soot [73]. Fuel borne catalysts will oxidize a part of soot in the combustion chamber and will subsequently improve the soot light-off in DPF. Most commonly used fuel borne catalysts are cerium, iron, and copper-based organic compounds, but it will be collected in the filter as loose ash [124]. Deposition of transition metals (cobalt, copper, and iron) doped with ceria oxide catalysts showed good soot oxidation activity and also reduced the ignition temperature of soot from 550 °C to 180 - 400 °C. Investigation on

catalytic combustion of soot under the CePr active phase was carried out in realistic reaction conditions by Perez et al. [125]. The results showed that ceria-based catalysts are capable of accelerating soot combustion under real conditions. Cerium oxide (CeO_2) based catalytic DPF oxidizes the particulate matter on the ash layer up to the thickness of about 100 μm whereas Platinum/Alumina based DPF promotes oxidation of PM up to ash layer thickness of 50 μm only [70].

Copper-based catalysts were also found to be a suitable alternative for precious metal catalysts owing to its high catalytic activity, nitrogen oxide reduction, and hydrocarbon oxidation [126]. It was found that Copper-based catalysts can be used as an efficient alternative catalyst for the reduction of particulate matter at low temperatures, even at 150 °C. Palma et al. [127] developed an optimized preparation procedure for catalytic DPF and studied the effect of active species load. Catalytic DPF was prepared by repeated impregnation in the solution of catalyst (drying at 60 °C) and calcination at 1000 °C after each impregnation. The preparation procedure supported the deposition of active species on the filter without the wash coat. An increase in NO_x emissions was found in the downstream of catalytic Pt coated Diesel Particulate Filter [128]. The reason for high NO_x emissions from DPF was due to the high content of Pt in coating and low space velocity. The catalytic activity of the Ag-K/CZA with platinum was experimented on the synthetic soot prepared in laboratory conditions, and the results showed that the reactivity of synthetic soot was lower as compared to real soot [75]. Catalyst load in the filter can be increased by modifying the porosimetric characteristics of the filter material so that the particulate matter oxidation temperature and pressure drop can be maintained at lower levels [69]. Catalyst based regeneration techniques are complex phenomena because of the complexity of chemical reactions taking place inside the filter, and it is a slower process since there will be poor contact between soot and catalyst [80].

2.4.4 NO$_2$ Assisted Passive Regeneration of DPF

Post injection and intake throttle valves will have a significant impact on exhaust temperature [67]. Engine exhaust temperature is an essential factor affecting the NO$_x$ emissions, and maximum emissions were found at a temperature range of 300 to 350 °C. NO$_x$ emissions were low when the exhaust gas temperature was below 200 °C and above 400 °C. Continuous regeneration technology in DPF involves initial oxidation of soot by NO$_2$ released as a product of reactions taking place inside DOC and further oxidation of soot by reaction with oxygen [124]. DOC is placed upstream of DPF to enhance the NO$_2$ assisted passive regeneration. Jiaqiang et al. [129] developed a mathematical model for NO$_2$ assisted regeneration, where the results showed that the regeneration speed is optimum when the length of the filter is in the range 200 mm to 250 mm, and the channel thickness is below 0.31 mm. The parameters which influence the regeneration speed of DPF in case of NO$_2$ assisted regeneration are as follows; flow rate of exhaust gas, the temperature of exhaust gas, the concentration of NO$_2$, and mass fraction of NO$_2$ / PM [83].

2.4.5 Commercial Fuel Based Active Regeneration of DPF

Active regeneration methods include non-thermal plasma techniques, ozone injection, application of induction heating, and post fuel injection. Fuel based regeneration method is commercially used for regeneration where a secondary fuel is injected, and it burns the accumulated soot particles, as detailed in Figure 2.5. Fuel-based regeneration affects the durability of DPF and also causes lubricant oil dilution, which results in an increase in engine wear and also increases the frequency of maintenance. The burning of the accumulated soot particles creates overheating spots in the filter, which will damage the system [65]. A single channel model of the DPF filter was used by Sarli et al. [74] for simulating the soot combustion in a DPF. The results of the

simulation showed that the combustion of soot causes a high-temperature rise in the filter, which would affect the durability of DPF. Uncontrolled combustion during fuel-based regeneration will fail DPF by the formation of cracks, melts, and pinholes [55].
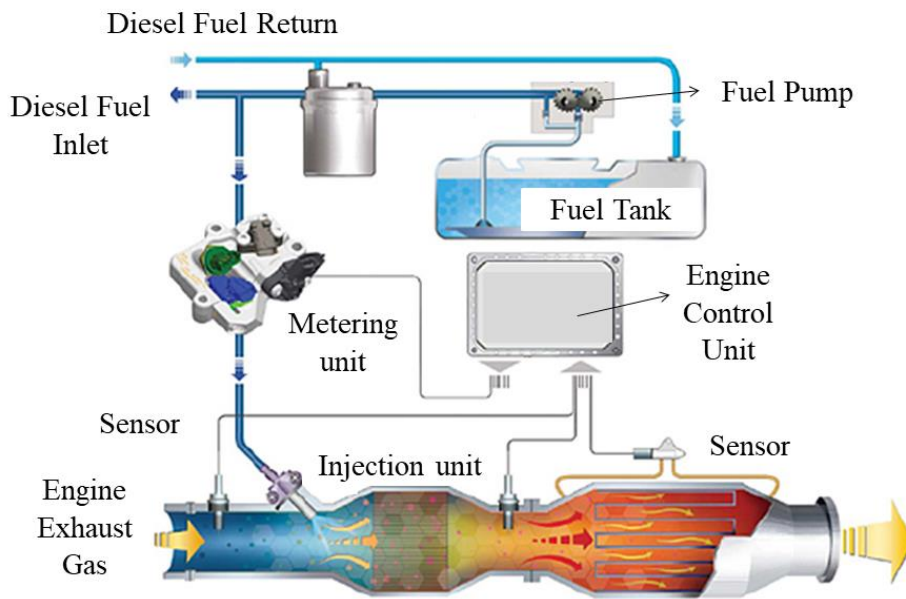
Figure 2.5. Setup for fuel-based regeneration of DPF [130]

Ash formed after regeneration will mix with the soot particles to form a particulate layer causing higher pressure drop. It can be reduced if ash is deposited in the rear part of the inlet channel. Bermudez et al. [72] proposed a novel technique on Pre-DPF water injection where the redistribution of accumulated soot particles was carried out by dragging the particles with the help of water to the end of the inlet channel. But it was observed that the injection of water would reduce the temperature at the inlet and outlet of the DPF. The temperature at the inlet will be recovered instantaneously because of engine operating conditions, while the temperature at the outlet will take some time to recover due to the higher residence time of water. It was also observed that the particle emissions increased during water residence in DPF.

2.4.6 Other Techniques for Active Regeneration of DPF

The application of electric heaters for the regeneration of trapped soot particles was studied by Palma et al. [68]. Lupe et al. developed a semi-analytical model for the analysis of filter behavior during soot loading and regeneration [131]. Oxidation of soot by application of a Non-thermal plasma technique was proposed by Ranji et. al [132]. Diesel exhaust gas is passed through a catalyst bed of metal oxides and a corona plasma reactor where the plasma charge is directed to exhaust gas and catalysts. Catalyst reacts with plasma charge (O_3) to give O and O_2. O is very much reactive, and it oxidizes the soot. Oxidation of soot depends on the ability of the catalyst to absorb O_2 and supply O.
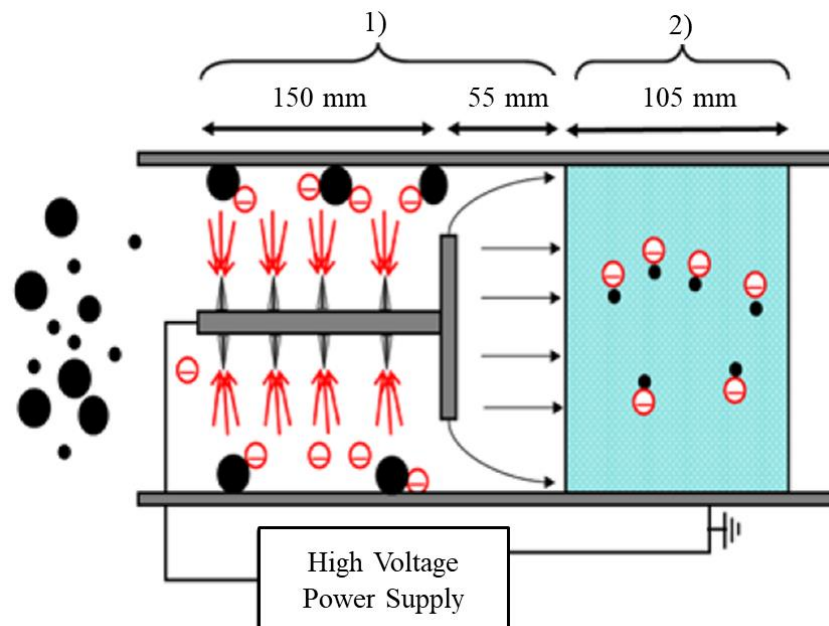
Figure 2.6. Electrostatic filtration system with corona discharge (H.J Kim et al. 2010)

Tuler et al. [133] developed a simple DPF system with a honeycomb monolith (70% sepiolite and 30% silicon carbide) and active species. Catalytic ingredients like cobalt, cerium, barium, potassium, etc. were used to decrease

the temperature of soot combustion. It was found that the monolith with 70% natural clay in its composition had similar characteristics to commercially available DPF monoliths. The pore size of the monolith has to be improved for better filtration efficiency. A combination of flow-through DPF and electrostatic filtration system for improving the filtration efficiency was developed by placing corona chargers upstream of DPF [81]. Corona discharge was placed perpendicular to the direction of exhaust flow, as shown in Figure 2.6. It was found that the filtration efficiency of the flow-through filter improved from 20 - 40% to 40 - 95%, but corona discharge became unstable when the load and speed were increased. A system for regeneration of soot by discharging a capacitor into filter was developed by Graupner et al. [78] where the accumulated soot particles were removed by the formation of shock in the surrounding air. The regeneration took place in three stages where the first one involves the application of high voltage pulse to the filter to initiate resistive current flow, the second stage is the occurrence of micro discharge to erode the soot layer, and the final stage involves underdamped LC oscillations by elements. The cake layer in the filter walls was removed completely, but it was found that the third stage of regeneration is leading to the formation of pinholes and ringing in the substrate.

2.4.7 Microwave Assisted Active Regeneration of DPF

Microwave energy is considered as the best alternative for the regeneration of DPF because of its ability to penetrate instantaneously into the filter without heating the exhaust gases [79]. Microwave radiations also enhance rapid and uniform heating of the filter by resistance heating. Microwave based regeneration will reduce energy consumption by replacing secondary fuel injection, and it is independent of the engine operating conditions [134]. Properties of the microwave, which makes it suitable for regeneration purpose includes instantaneous penetration into filter body, selective absorption of the

microwave by soot layer, and good dielectric property of the filter material. The material of the particulate filter must have good permeability (like ceramic, silicon carbide, etc.), which will allow the microwaves to pass through it without heating the exhaust gases. The dielectric properties of a material determine its ability to get heated by microwaves. The dielectric constraints consist of real and imaginary components, as shown in equation number 5.

$$\varepsilon' + j\varepsilon'' = \varepsilon \qquad (5)$$

Table 0.2. Dielectric properties of materials

Material	Dielectric constant (ε')	Dielectric loss factor (ε'')
Diesel soot	10.70	3.60
Cordierite	2.90	0.140
Alumina ceramic	8.90	0.009
Quartz	3.80	0.0001

When the trapped soot particles are subjected to microwave radiations, it gets heated up directly by the microwaves, while the cordierite material will get heated up only by conduction or by convection of heat from soot. The values of dielectric constant for different materials are given in Table 2.2. Microwave radiations heat the soot particles by the interaction between the high-frequency electromagnetic field and soot. Design of the oven cavity, where a magnetron introduces the microwave radiations must be done by considering the parameters like dimensions, resonant properties of the oven cavity, and energy density in the cavity [135]. The oven cavity should have a good heating pattern and also should present the proper load to the magnetron. Microwave radiations produced by Vector Network Analyzers (VNA) were

used by Feulner et al. [66] for determining the soot loading in the DPF, as shown in Figure 2.7. The electromagnetic field is impressed to the filter housing, which acts as a resonator through one or two ports. The electric and magnetic field is induced inside the resonator depending on the frequency and properties of material inside the filter housing. The amount of soot loading in the filter can be determined by the value of the transmission factor measured at ports.
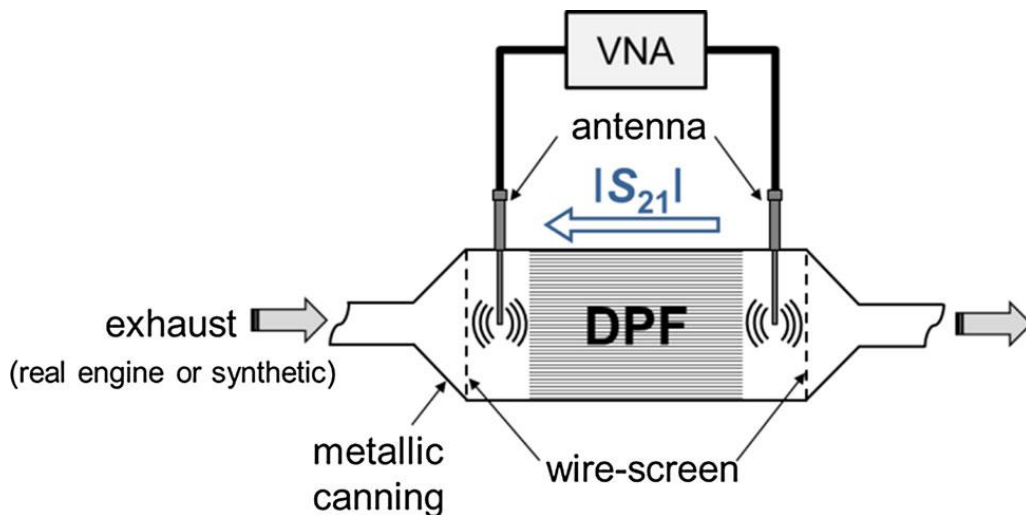
Figure 2.7. Application of microwaves for determining soot load in DPF [66]

2.4.8 Composite Regeneration of DPF

Composite regeneration is the combination of active and passive regeneration techniques where catalyst based regeneration (either by mixing in fuel or by deposition on filter substrate) and thermal-based regeneration (post fuel injection, microwave-based, heaters, etc.) is used simultaneously. In DPF, there is a mutual contradiction between filtration efficiency and pressure drop. Multidisciplinary optimization models were used for systems whose performances could conflict with each other. Zhang et al. [136] developed a multidisciplinary optimization model on objective functions, namely pressure drop, regeneration performance, microwave energy consumption, and thermal

shock resistance. Zuo et al. [77] developed a three dimensional model of a particulate filter to evaluate the performance of composite regeneration by coupling cerium based catalyst and microwave radiations using a multi-field synergy principle. Microwave radiations will enter the filter in the form of a traveling waveguide and burns the trapped soot particles. The development of an alternative regeneration technique using electromagnetic waves in the microwave region is the only possible solution for improving the durability of DPF and also for meeting the emission norms.

2.5 RESEARCH GAPS FROM LITERATURE SURVEY

The emission norms by environmental protection agencies have become stringent to reduce the toxicity levels of engine emissions to acceptable limits. The review of the emission control system techniques using diesel oxidation catalysis and diesel particulate filtration has brought us substantial information about its working principle and also on the major research challenges faced by these techniques. Fuel-based traditional regeneration of Diesel Particulate Filter is leading to uncontrolled combustion inside the filter substrate affecting the durability of the filter substrate. The failure caused in the DPF substrate due to regeneration process is caused by pinhole defects, melt defects and cracking defects. The development of an innovative alternate regeneration system for the effective operation of the particulate filter is the major technical challenge. Results of the alternate regeneration techniques by application of electric heaters, corona discharge, pulsed discharge, etc. failed to improve the durability of the filter.

The application of microwave energy for the regeneration of DPF is considered as a possible alternative. Microwave radiations can penetrate the filter instantaneously to burn the deposited particles by selective absorption owing to its good dielectric properties. It has been concluded from the literature study that emission control systems play an important role in the

roadmap to reduce carbon emissions. Various challenges faced by diesel particulate filtration systems have been addressed and an effective system with alternate regeneration technique with the application of microwave energy has been proposed. Composite regeneration technique involving microwave energy-based active regeneration and DOC assisted passive regeneration has been proposed for selective burning of the accumulated soot particles.

CHAPTER 3. MATERIALS AND METHODS

An emission control system, which is a combination of Diesel oxidation catalyst filter and Diesel Particulate filter with microwave-assisted regeneration, has been proposed in this work. Microwave energy has been considered to be used for regeneration purposes. The material of the particulate filter must have good permeability like ceramic, silicon carbide, etc. which will allow the microwaves to pass through it without heating the exhaust gases. All experiments were conducted by retrofitting the developed emission control system to a multi-cylinder compression ignition engine, as shown in Figure 3.1, and specifications of the engine are detailed in Table 3.1.
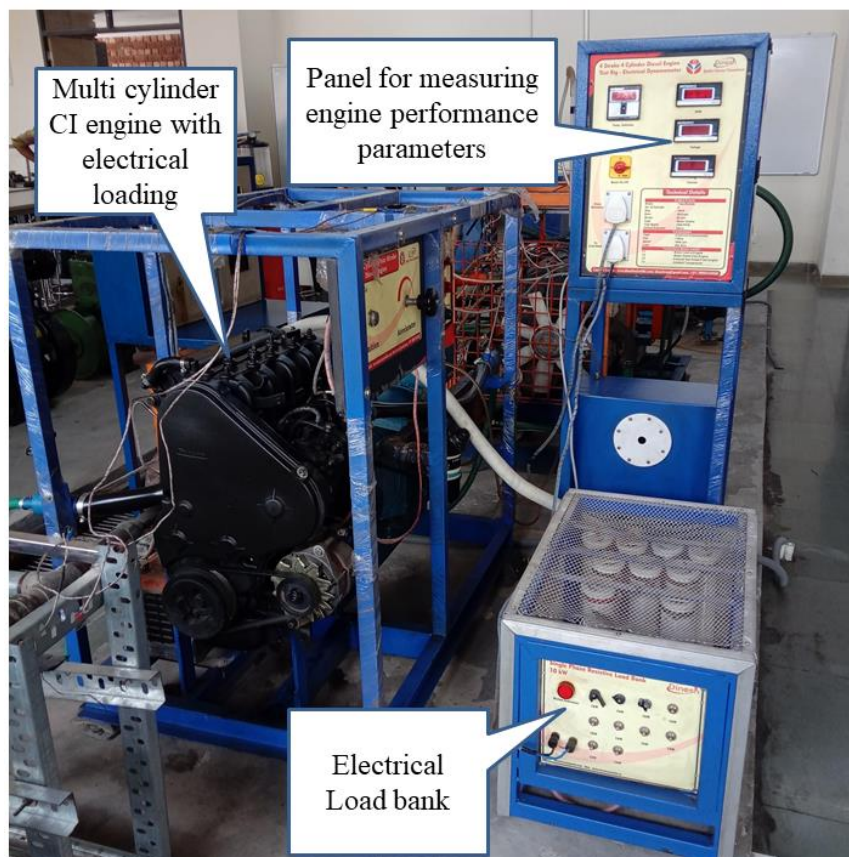
Figure 3.1. Multi-cylinder diesel engine setup with electrical dynamometer loading

. Specifications of the DOC and DPF substrate used in this study are described in Table 3.2. The line diagram for the proposed emission control system is shown in Figure 3.2. The gaseous emissions were sampled from raw exhaust using AIRREX HEPHZHIBA (HG 540) gas analyzer for measuring hydrocarbon, carbon monoxide, carbon dioxide, and oxygen concentrations simultaneously. Specifications of the analyzer are detailed in Table 3.3. Details of the instruments used for measuring various parameters are described in Table 3.4. The pressure drop across the diesel particulate filter substrate was monitored by using a differential pressure sensor (MPX10DP) with a measurement range of 0 to 10 kPa. Particle number emissions were measured using sensor module (Shinyei DSM 501A) which works by particle counter mechanism with high sensitivity to particles greater than 1 μm in size. The differential pressure sensor (MPX10DP) and particle number sensor (DSM 501A) were interfaced with Arduino Uno (microcontroller board) by encoding the C program in Arduino software as shown in Appendix I (S1.1). Uncertainty analysis has been carried out for the experimental data to determine the error involved and accuracy of measurements as detailed in Appendix II (S2.2)

Table 3.1. Specifications of Engine Setup

Sl. No	Parameter	Feature/Value
1	Engine Type	Four cylinder, water-cooled CI Engine
2	Bore (mm)	69.9
3	Stroke (mm)	82
4	Orifice diameter (mm)	20
5	Loading device	Electrical Dynamometer
6	Max Load	20 A
7	Max Power	7.5 kW / 10 hp
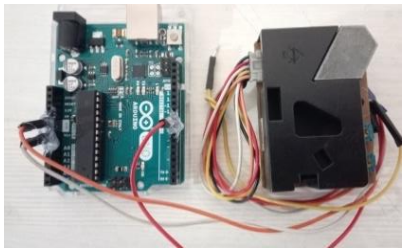
Table 3.2 Specifications of DOC and DPF substrate

Sl. No	Specifications	Metallic DOC (300 cpsi)	Ceramic DOC (300 cpsi)	Ceramic DOC (300 cpsi)	Ceramic DOC (400 cpsi)	Ceramic DPF (200 cpsi)
1	Length (mm)	160	152.4	152.4	152.4	80
2	Diameter (mm)	100	100	100	100	80
3	Cell Density (cpsi)	300	300	300	400	200
4	Catalyst loading (g/cub.ft)	20	20	35	35	Nil
5	Ratio (Pt:Pd)	1:1	1:1	5:1	5:1	Nil
6	Material	Steel	Cordierite	Cordierite	Cordierite	Cordierite

Table 3.3. Specifications of emission analyzer

Sl. No.	Parameter	Feature/Value
1	Manufacturer	Hephzibah Co. Ltd (HG 540)
2	Measuring items	HC, CO, and CO_2
3	Measuring method	NDIR (Non-Dispersive Infrared)
4	Measuring range/resolution (HC)	0 to 15000ppm / 1ppm
5	Measuring range/resolution (CO)	0 to 9.999% / 0.001%
6	Measuring range/resolution (CO_2)	O to 20% / 0.01%
7	Repeatability	Less than ±2% FS
8	Flow rate	2 – 4 l/min

Table 3.4. Specifications of the instruments used

Sl. No.	Parameter	Instrument	Specifications/Working principle /Image
1	Pressure drop	MPX10DP	Monolithic silicon pressure sensor (piezoresistive transducer) Range: 0 to 10 kPa Interface: Arduino Uno
2	Particle number	DSM 501A	Aerosol particle sizer Light chamber with a photo-diode detector, light-emitting diode and particle counter Sensitivity: >1 micron Interface: Arduino Uno
3	Microscopic imaging	Nikon-ECLISPSE MA200	Inverted Metallurgical Microscope

4	Particle size	Malvern ZEN1690	Particle Size Analyzer
5	Functional groups	Perkin Elmer, Frontier FT-IR/FIR	Fourier Transform Infrared Spectroscopy
6	Gaseous emissions	Hephzibah Co. Ltd (HG 540)	NDIR (Non-Dispersive Infrared)

3.1 DESIGN OF EXPERIMENTS

Dependent variables are particle number, flue gases (CO, NO, and hydrocarbons) concentration, etc. Independent variables are substrate dimensions, cell density, etc. Emission tests will be performed based on the steady-state cycle which is mostly used for experimentation purpose [137]. The steady-state cycle applied in this study is a five-mode cycle, where the exhaust emissions from the engine are measured at different engine loads, and the engine is loaded with the help of an electrical dynamometer and load bank [138][137]. The engine speed will be kept constant at 1400 rpm with a tolerance of ±50 rpm. Engine emissions will be measured at five steady-state loads (0%, 25%, 50%, 75% & 100%) which corresponds to electrical loads (0 kW, 1 kW, 2 kW, 3 kW & 4 kW). Emissions are measured once the engine is steady at each loading condition hence it called as a steady state cycle. The total load applied is classified as a percentage of maximum loading capacity while carrying out the experimentation. The brake power of the engine is varied from 0 to 10 hp, and current is varied from 0 to 20 A at a constant speed of 1400 rpm (The engine setup used for the experimentation purpose is coupled with electrical dynamometer, and maximum loading capacity of the setup is dependent on electrical loading capacity of the dynamometer). The engine can be loaded as per the maximum loading capacity of the coupled dynamometer. The maximum loading capacity of the engine setup is brake power of 10 hp at a maximum current of 20 A (speed 1400 rpm).The quality of the exhaust gas depends on engine loading and control of engine emissions at lower load conditions is one of the significant challenges faced by the automotive industry [139][140][141]. The performance of the engine is better at full load conditions, and with improvement in performance, the quality of exhaust gas improves; especially particle number emissions and unburnt hydrocarbon emissions are reduced (and the experiments will be conducted similarly).
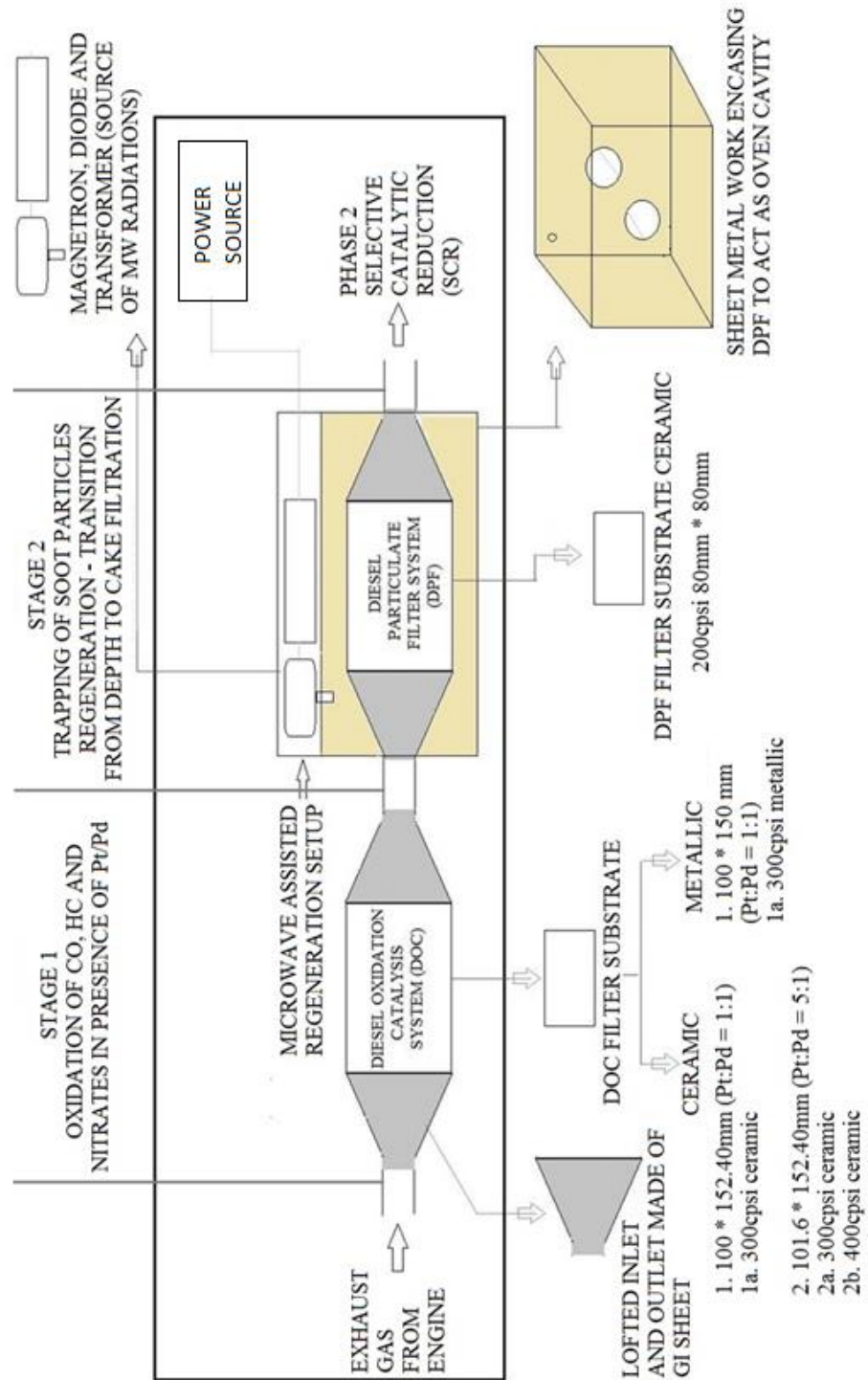
Figure 3.2. Line diagram of the proposed emission control system

44

Moreover, the concern on emissions is on the low load side rather than that on the higher loading. The parameter which varies with the higher load is the temperature of exhaust gas. With the increase in exhaust gas temperature, oxidation reactions in the DOC system will improve, and the conversion efficiency of DOC also increases [142][143]. The catalyst light-off temperature for platinum catalyst in the DOC system is 150 °C, which would be achieved in the loading conditions considered for experiments. Exhaust gas after the treatment in the DOC system is directed to diesel particulate filtration system where the particulate matter is trapped, and the major focus of the study is on the soot filtration and regeneration. The performance characteristics of the engine were evaluated by using equations as detailed in Appendix II (S2.1).

3.1.1 Experiment to Determine Conversion Efficiency of DOC

Interpretation and analysis of experimental results concerning the data captured in Table 3.5.

Table 3.5. Format for raw data entry in conversion efficiency experiment with sample readings (50 % engine loading conditions)

DOC	Load	Speed (rpm)	The concentration of flue gases (Vol.)					PN	η_{DOC} (HC, CO & PN)
			CO %	NOx ppm	HC ppm	CO_2 %	O_2 %		
No DOC	50 %	1400	.049	49.25	60	4.78	14.2	172500	--
Ceramic 300cpsi (1:1)	50 %	1400	.042	61	30.5	3.95	15.2	96450	49.2% 14.8% 44.1%

45

Metallic 300cpsi (1:1)	50 %	1400	.043	70.5	33	4.20	14.7	120000	45% 12.8% 30.4%
Ceramic 300cpsi (5:1)	50 %	1400	.036	68.25	25	4.09	14.8	92225	58% 27% 46.5%
Ceramic 400cpsi (5:1)	50 %	1400	.034	73	29	4.11	14.9	70000	52% 31% 59%

1. The conversion efficiency of each DOC (ie, change in concentration of gases with and without DOC) was calculated using equation no. 6 [144].

$$\eta_{doc} = \frac{gas\_conc_{before} - gas\_conc_{after}}{gas\_conc_{before}} \times 100 \tag{6}$$

2. Comparison of metallic and ceramic DOC (effectiveness)

3. Effect of catalyst loading on conversion efficiency (Case1. Pt : Pd =1:1 & 20 g/cubic feet and Case 2. Pt : Pd = 5:1 & 35 g/cubic feet)

4. Variation in concentration of flue gases with load in each DOC (Determination of optimum engine load for lower emissions)

5. The DOC with the lowest emission was considered for the next experiment.

3.1.2 Experiment to Determine Filtration Efficiency and Soot Accumulation Rate in DPF

Interpretation and analysis of experimental results will be conducted concerning the data captured in Table 3.6.

Table 3.6. Format for raw data entry in filtration efficiency and soot accumulation experiment with sample readings (50% engine loading)

DOC	DPF	Load (kW)	The concentration of flue gases (Vol.)				ΔP kPa	PN	Inc in Wgt. g	Soot accu. rate g/kWh
			CO %	CO$_2$ %	HC ppm	O$_2$ %				
Nil	DPF	50%	.043	4.8	30	14.2	0.12	13486	0.53	0.156
DOC	DPF	50%	.034	4.73	24	14.3	0.12	13190	0.09	0.025

a) Filtration efficiency of DPF (PN emission with and without DPF)

$$\text{PM trapping efficiency} = \eta_{doc} = \frac{gas\_conc_{before} - gas\_conc_{after}}{gas\_conc_{before}} \times 100 \qquad (7)$$

Where,

C_{before} = particle number in exhaust gas (without DOC/DPF)

C_{after} = particle number in exhaust gas (with DOC/DPF)

b) Soot accumulation rate (with variation in load and DOC)

Soot accumulation rate = (Inc in weight of substrate/time)

c) Effect of DOC assisted continuous regeneration on soot accumulation rate in DPF

d) Effect on engine load and soot accumulation rate on the pressure drop across the DPF

3.1.3 Experiment to Determine Soot Loading and Regeneration Rate in Microwave Regeneration Based DPF

Interpretation and analysis of experimental results concerning the data captured in Table 3.7.

a) Soot regeneration rate of DPF at different power levels.

b) Time taken for regeneration by magnetron and energy consumed for regeneration.

c) Determine the power level for effective regeneration.

Table 3.7. Format for raw data entry in soot regeneration experiment with sample reading (at 50% power levels)

DPF	Soot loading (g)	Power levels (W)	Regeneration time (sec)	Reduction in loading (g)	Regeneration rate (g/min)
DPF	6.04	336	30	0.1043	0.2086

3.1.4 Expected Results

a) Improvement in regeneration efficiency of DPF by active regeneration.

b) Reduction in emission of exhaust gases like carbon monoxide, hydrocarbons, and soot particles.

c) Reduction in DPF soot accumulation rate by combined application of microwave energy and DOC assisted continuous regeneration.

The experiments were conducted as per the design of experiments. The CFD analysis and experimental study were conducted on the DOC system in chapter 4. The conversion efficiency of four different DOC substrates was experimentally evaluated to determine the one with the best performance. Based on the achieved results DOC substrate with best conversion efficiency was used for conducting studies in chapter 5, where the filtration efficiency of the integrated DOC-DPF system was investigated. Soot layer modelling, flow analysis, and soot accumulation rate in the DPF was also covered in this chapter. The modelling, computation study, fabrication and experimentation on microwave assisted composite regeneration system were carried out in chapter 6.

CHAPTER 4. MODELLING AND EXPERIMENTAL STUDY ON DIESEL OXIDATION CATALYSIS (DOC) SYSTEM

The diesel oxidation catalysis system consists of a monolith substrate with a layer of wash coat in which the precious metal catalyst (platinum group) is impeded [123][145]. Investigations on the application of catalysts for exhaust emission control were initiated after the introduction of the clean air act 1970 when the engine modifications failed to meet the emission limits [146]. Poor thermal durability and sensitive nature of transition metals led to the application of precious metals like platinum and palladium for catalysis purposes owing to its good oxidation capability and durability [125][147]. Oxidation performance of the DOC system also depends on its distance from the engine since it has a direct impact on the catalyst light-off temperature and hence in most cases, it is placed as the first component in the exhaust train after engine [148][149][150]. The function of the DOC system includes oxidation of hydrocarbons, nitrates and carbon monoxide, and exothermic nature of nitrate oxidation reaction supports continuous regeneration of diesel particulate filtration system [151][152].

At initial stages of product development, the DOC systems used in automotive applications were made of pellets which are packed inside a canister whereas the mobile nature of the vehicles affected the performance of the system due to the disintegration of the packed pellets [153]. DOC systems used currently consist of metallic or ceramic monolith substrate with a layer of alumina washcoat in which the precious metal catalysts are dispersed as shown in Figure 4.1. Washcoat layer increases the exposed surface area and the number of precious metal sites for oxidation reactions [154]. Alumina, zirconium, and zeolite-based components are mostly used as a wash coat layer [112]. Thermally treated alumina wash coat layer is found to provide higher

surface area and larger pore size which helps to increase the number of catalyst sites after dispersion leading to good oxidation performance [155]. The surface area of the zirconium wash coat layer was found to be smaller than that of alumina whereas, in the case of propane oxidation, the zirconium wash coat layer is found to exhibit better oxidation characteristics [156]. Zeolite can adsorb hydrocarbons during cold start conditions but it is also found to release hydrocarbons at higher operation temperature which reduced its overall performance as a wash coat layer [157].

Alumina washcoat layer is found to reduce the chances for the formation of platinum oxides which affects the oxidation activity of exhaust gases as compared to other washcoat layers which are made of less acidic components [158]. Precious metal catalysts commonly used in DOC systems include platinum, palladium, and rhodium [159]. These precious metals act as an active site for hydrocarbon oxidation depending on its oxidation states [160]. Platinum exhibits good oxidation activity at normal operating temperature and has good resistance to sulfur poisoning, whereas its performance reduces at conditions of extreme temperature during regeneration [161]. Exposure of catalysts to excessive oxygen and nitrogen will also lead to the formation of platinum oxides which reduces the hydrocarbon oxidation. Sulfur poisoning is found to be high at palladium-based active sites compared to that of platinum-based active sites [162]. The advantage of palladium-based catalysts is that it has a high resistance to sintering at high temperatures compared to platinum [163]. In order to take advantage of the desirable properties of each catalyst, usually, a catalyst mixture is dispersed in the wash coat layer instead of a single catalyst [164]. It can be achieved either by dispersing an alloy of platinum and palladium in the wash coat layer which will separate at reaction temperatures or by dispersing the catalyst as separate components in the form of the bimetallic cluster [118].
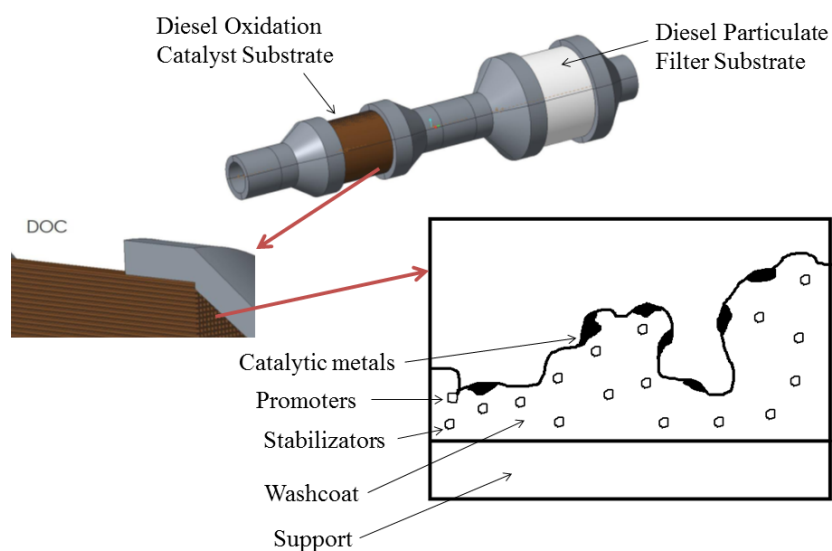
Figure 4.1 Structure of the emission control system with monolith DOC substrate

The proportion of palladium in the mixture is kept high to reduce the overall cost of the DOC systems. DOC system with 3:1 (Pt : Pd) catalyst ratio showed a lower hydrocarbon slip but it experienced an extinction in reaction at temperatures below 250 °C [165]. In this chapter experimental study has been conducted to determine the conversion efficiency of diesel oxidation catalysis filter substrate for varying loads at a constant speed of 1400 rpm in a multi-cylinder compression ignition engine.

4.1 MECHANISM OF OXIDATION REACTIONS IN DOC SYSTEM

Interaction of the catalysts and reactants with the available oxygen is an important factor for the occurrence of the oxidation reactions in the DOC system. Oxidation of carbon monoxide occurs by simple reaction but the oxidation performance will be affected by a low-temperature range of exhaust gas. Adsorption of carbon monoxide occurs by the bonding of carbon atom to the platinum atom while the oxygen atom will be away from the latter [114]. The conversion rate of carbon monoxide to carbon dioxide can be achieved by increasing the temperature of the catalyst to that of the desorb surface. Earlier

studies have shown that the oxidation of carbon monoxide in the presence of platinum catalyst occurs by Langmuir-Hinshelwood dual-site mechanism where the rate of reaction depends on the reaction between oxygen and carbon monoxide adsorbed by the catalyst layer [162]. A term for resistance has to be considered in the calculations for the oxidation rate of carbon monoxide to account for inhibitory effects of carbon monoxide, nitrates, and propylene which is not dependent on the number of sites [166]. Carbon monoxide migrates to the oxygen atoms adsorbed in the surface owing to its mobile nature for oxidation reaction as shown in equation no. 8 to 10 [167]. Self-inhibition of oxidation reactions might take place in cases when the adsorption of carbon monoxide will block the adsorption of oxygen whereas an increase in temperature will reduce the chances of self-inhibition.

$$CO + [*] \leftrightarrow [CO*] \tag{8}$$

$$O_2 + 2[*] \leftrightarrow 2[O*] \tag{9}$$

$$[O*] + [CO*] \rightarrow CO_2 + 2[*] \tag{10}$$
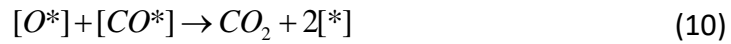
Incomplete combustion of fuels in the engine leads to the emission of hydrocarbons from engine exhaust [159]. Hydrocarbons of different functional groups like aromatics, unsaturated and saturated will be present in the exhaust emissions [168]. The rate of oxidation reactions in DOC varies according to the mixture of hydrocarbon in the exhaust. Hydrocarbon oxidation in the DOC system fits good with the Mars-van Krevelen mechanism as shown in equation no 11 to 13 [169], where $*$ and $\otimes$ represents reaction sites. Oxidation of nitric oxide is an important step in the abatement of NO_x in the exhaust emissions. Oxidation of nitric oxide takes place generally by adsorption reactions as detailed in equation no 14 to 17 [170].

$$O_2 + [*] \rightarrow [O_2^*] \rightarrow 2[O^*] \tag{11}$$

$$HC + [\otimes] \leftrightarrow [HC^{\otimes}] \tag{12}$$

$$[HC^{\otimes}] + [O^*] \rightarrow CO_2 + [*] + [\otimes] \tag{13}$$

$$NO + * \rightarrow NO^* \tag{14}$$

$$NO_2 + 2* \leftrightarrow NO^* + O^* \tag{15}$$

$$O_2 + * \rightarrow O_2^* \tag{16}$$

$$O_2^* + * \rightarrow 2O^* \tag{17}$$
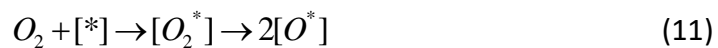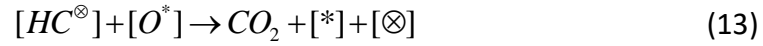
4.2 GEOMETRICAL MODELLING OF THE DOC SYSTEM

4.2.1 CAD Modelling

Modelling of the lofted inlet and outlet for the monolith substrate was done in SolidWorks 2010. The angle of the loft is an important parameter deciding the pressure drop and also the flow uniformity of the gases into the cylinder. Nine models with different loft angles were made using SolidWorks. Details of these models are given in Table 4.1.

4.2.2 CFD Analysis

Computational Fluid Dynamics (CFD) analysis of the Diesel Oxidation Catalysis (DOC) system was carried out to determine the characteristics of a model in a virtual environment before manufacturing the prototype [116]. Taibani et al [2012] conducted CFD simulations to analyze the performance of the catalytic converter, where the species concentration before and after the catalytic converter was measured. The results of the simulation showed that radial flow catalytic converter has better performance as compared to axial flow catalytic converter owing to higher residence time. In this work, CFD analysis was used to determine the pressure drop and flow uniformity of the exhaust gases through the filter for different loft angles.

Table 4.1. Specifications of designed models.

Model No	Length (mm)	Loft angle (degree)	Taper Length (mm)
1	50	63	112
2	55	61	114
3	60	59	117
4	65	57	119
5	70	55	122
6	75	53	125
7	80	51	128
8	85	49	131

Table 4.2. Initial and boundary conditions

Type	Pressure based
Time	Steady
Velocity formulation	Absolute
Model	K-epsilon
Fluid	Exhaust gas
Fluid density	0.5508 kg/cubic meter
Fluid viscosity	0.00003814 Pascal second
Substrate	Porous zone
Viscous resistance	Direction 1: 3.846e+07 (m^{-2}) Direction 2: 3.846e+10 (m^{-2}) Direction 3: 3.846e+10 (m^{-2})
Inlet	Velocity inlet
Inlet velocity	22.6 m/s
Outlet	Pressure outlet
Outlet pressure	101325 pa
Surface	Wall
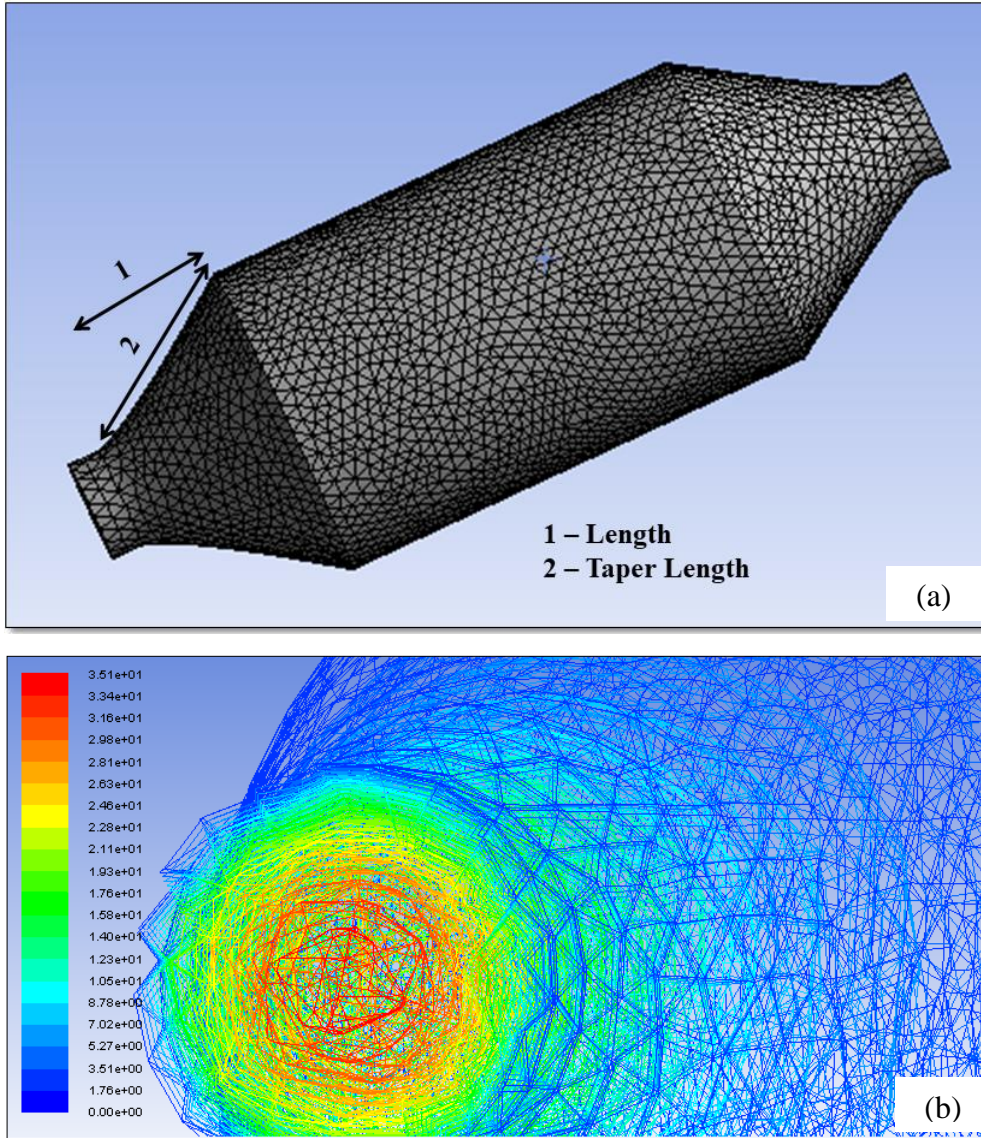
Figure 4.2 (a) Meshed model of the DOC system (b) Contour of velocity magnitude at the inlet section of the DOC system

Models designed in SOLIDWORKS were imported to ANSYS Workbench as an IGES file. Monolith substrate was considered a porous medium and it was also considered to be impermeable in other directions. Inlet and outlet sections of the model will have turbulent flow while the substrate will be having laminar flow. The structured mesh was generated in the model with fine relevance as shown in Figure 4.2 (a). The meshed model was then

imported to ANSYS FLUENT for carrying out simulations. The model was scaled in millimeter and the quality of the mesh was also checked. Minimum orthogonal quality and maximum ortho skew of the mesh in all models were found to be in the acceptable region. Pressure based type solver with absolute velocity formulation was used for analysis and time was considered as steady. K-epsilon turbulence model was used where the first variable is the turbulent kinetic energy and the second variable is the dissipation rate of kinetic energy. This model is commonly used for flows with small pressure gradients and also in cases where Reynold stresses are important. The details of the initial and boundary conditions are given in Table 4.2. Fluid flowing through the filter was assumed to be exhaust gas by providing its density and viscosity. The ceramic substrate was considered as the porous zone with the laminar flow by providing the viscous resistance and inertial resistance in three directions. The inlet was assumed as velocity inlet and outlet as a pressure outlet.

4.2.3 CFD Simulation Results

Calculations were carried out for different models of the Diesel Oxidation catalyst filter and the simulation started from the inlet of the DOC with provided initial and boundary conditions.

Pressure drop across DOC: The exhaust gases from the engine are directed to the inlet of the DOC filter and there will be a drop in its pressure due to lofted inlet and also due to the flow through the monolith porous substrate. The filter with the lowest pressure drop will be considered to be the most suitable one for this application since these gases will be directed for further treatment to Diesel Particulate Filter (DPF). The calculations were carried out for each model with different lofts until the results are converged and contour of velocity magnitude generated from results are as shown in Figure 4.2 (b). Contours of the pressure coefficients and static pressure were generated using

the results obtained from ANSYS FLUENT as shown in Figure 4.3 (a) and (b).
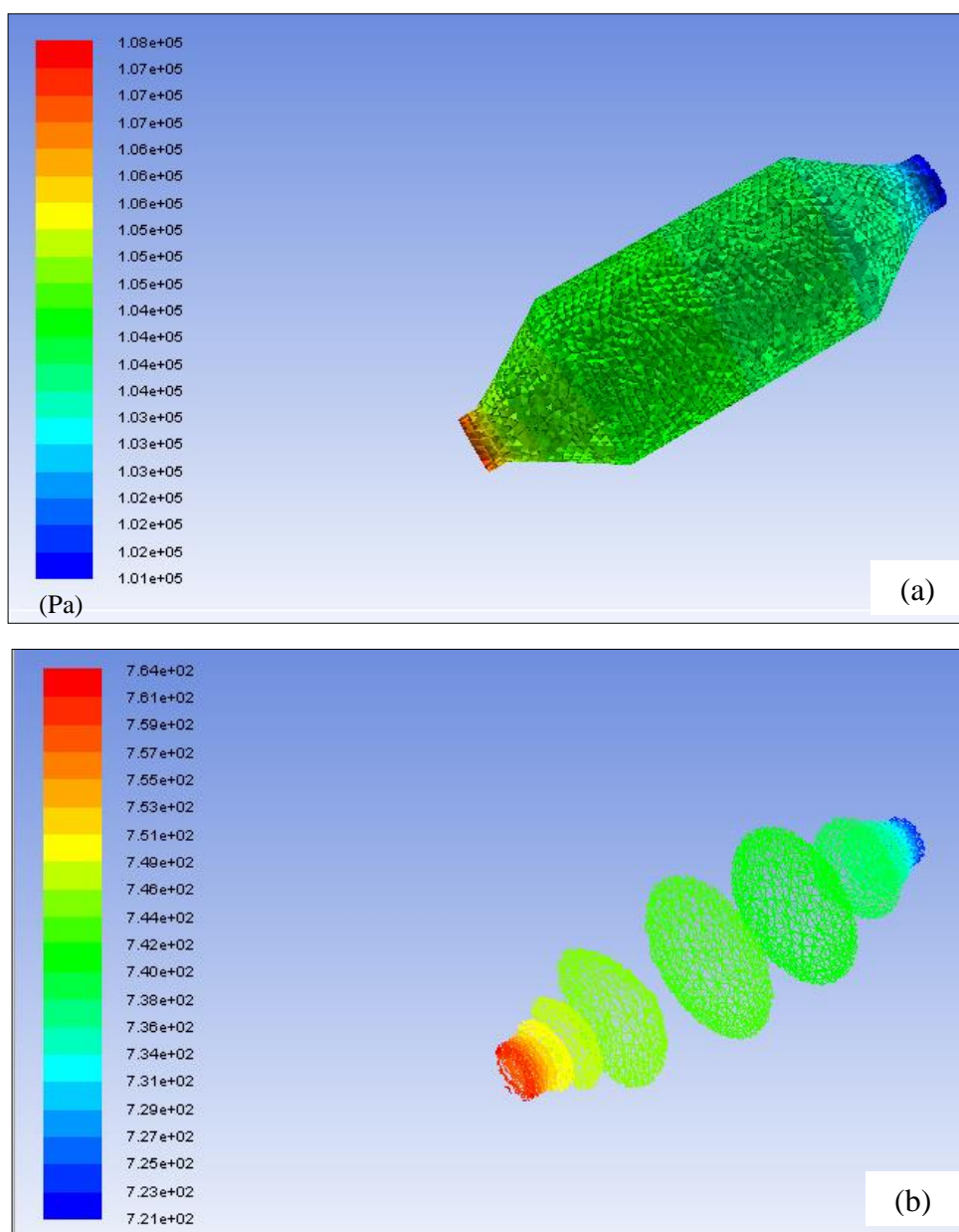
Figure 4.3. (a) Contour of static pressure (b) Contour of pressure coefficient at different sections

57

From the contours, it can be seen that there was a substantial fall in the pressure as the gas flows from the inlet to the outlet. The pressure on the inlet side was at a higher-end as indicated by red color and at the outlet, was at the lower end as indicated by blue color. The values of the pressure at the inlet, interior solid and the outlet were derived from the report generated after the simulation.

A graph was plotted to determine the variation in the static pressure and pressure coefficient with different models as shown in Figure 4.4 (a) and (b). The pressure drop in each case was then calculated using the obtained results and a graph was plotted between the length of loft and difference in pressure at the inlet and outlet of the DOC as shown in Figure 4.5 (a). From Figure 14, it can be seen that the pressure drop increases from 5400 Pa to 6000 Pa when the loft length increases from 45 mm to 50 mm. Then there was a sudden reduction in pressure drop when the loft length was about 55 mm. From this point, the pressure drop was found to increase as the loft length increases up to 75 mm and then there was a sudden drop and rise when the loft length was increased to 80 mm and 85 mm.

From the results, it could be seen that the loft length of 55 mm with a loft angle of 61˚ is more suitable for the fabrication of the DOC since it has the lowest pressure drop and also due to its stability in the manufacturing point of view. Even though the model with a loft length of 45 mm had a lower pressure drop, the structural stability of the model was very low.

Flow uniformity index: Level of uniformity or how uniform is the flow through the model was determined by the uniformity index. The model with a more uniform flow was considered to be more suitable for this application. The uniformity index for all the models was derived after CFD simulation and a graph was drawn as shown in Figure 4.5 (b) to study the variation in the uniformity index as the loft length of the model increases.
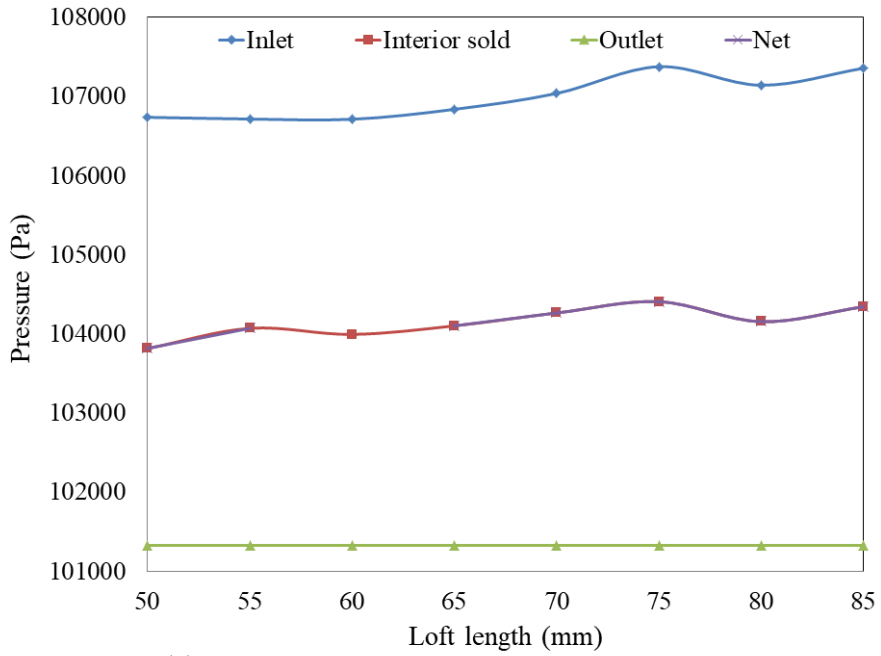
(a)
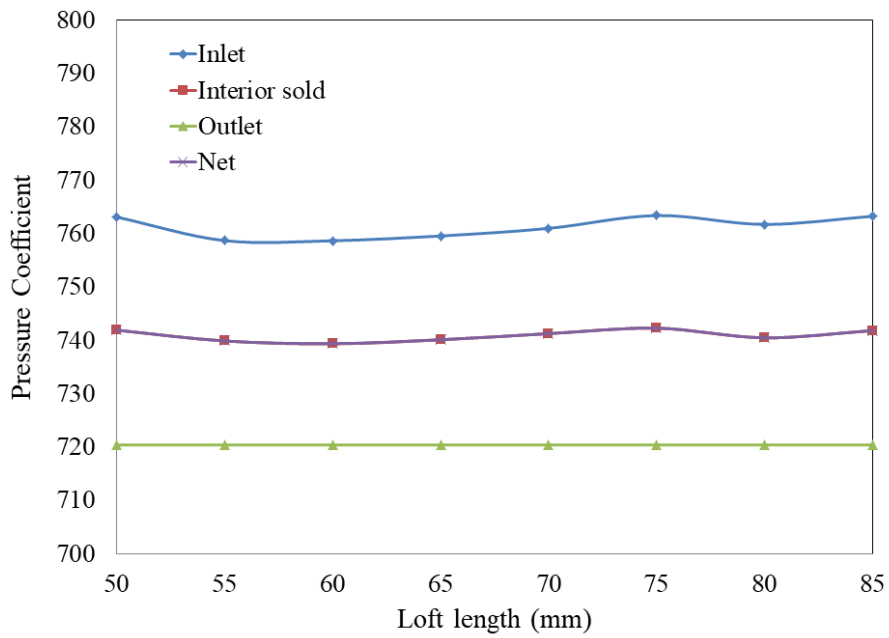
(b)

Figure 4.4. Effect of the loft length on (a) static pressure (b) pressure coefficient.
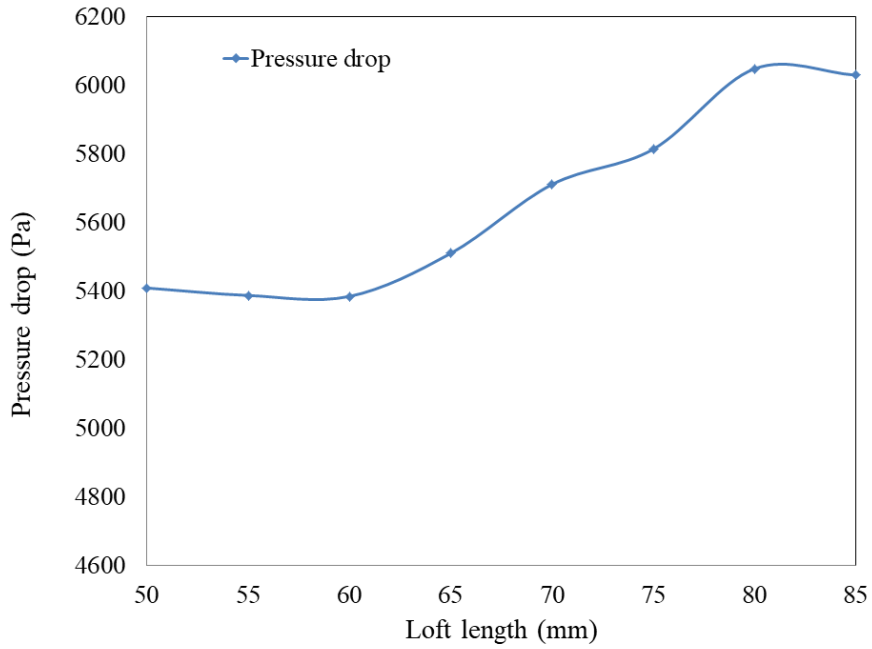
(a)
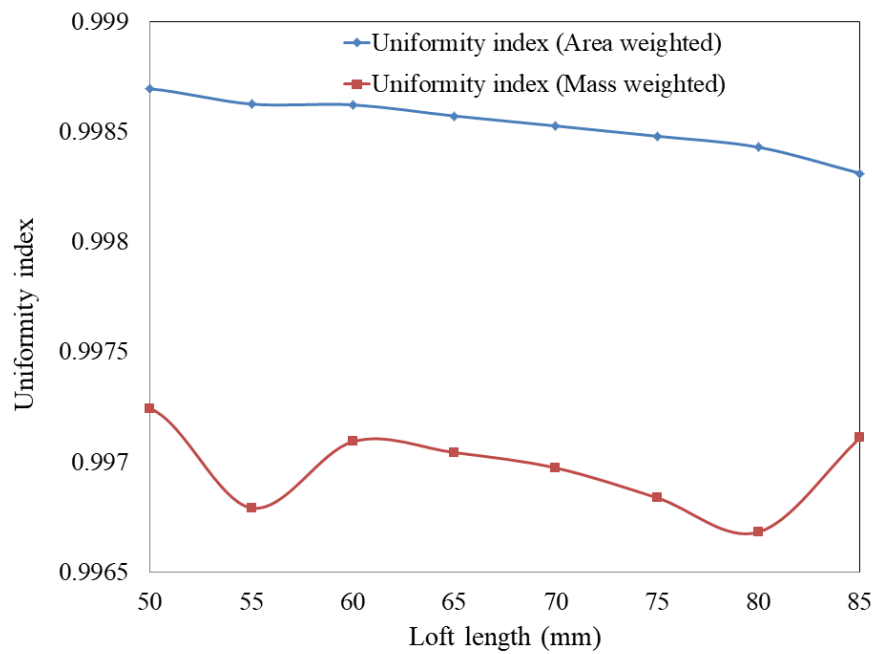
(b)

Figure 4.5. Variation in (a) pressure drop and (b) uniformity index with loft length.
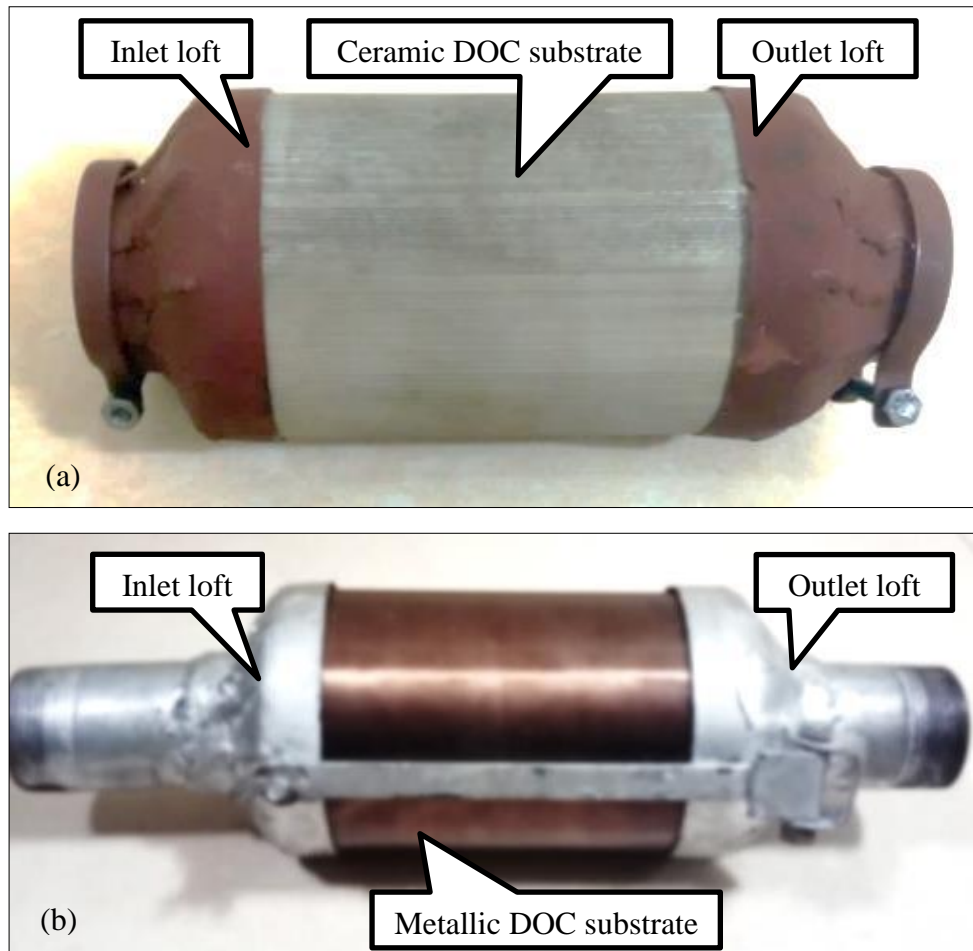
Figure 4.6. Fabricated (a) Ceramic and (b) Metallic DOC system with inlet and outlet lofts

From the plots, it can be seen that the area-weighted uniformity index decreases as the loft length increases and the mass-weighted uniformity index also shows a similar pattern as an average. The changes in the uniformity index were very low and hence the same was neglected.

Analysis of the simulation results: The results of the simulations were plotted and from the Figure 4.5 (a), it was evident that the lowest pressure drop was achieved in the third case where the loft length is 55 mm. Therefore it was suggested to fabricate the DOC filter with a loft length of 55 mm for flow with

61

the lowest pressure drop. The uniformity index of the model with the loft length of 55 mm was also in the acceptable range from Figure 4.5 (b) and the lofts were fabricated with observed results as shown in Figure 4.6.

4.3 EXPERIMENTAL ANALYSIS: CONVERSION EFFICIENCY OF DOC SYSTEM

Engine test bench with post-treatment system comprising of diesel oxidation catalysis system is presented in Figure 4.7. The specification of the diesel engine test bench is shown in Table 3.1. Hephzibah (Airrex HG 540) emission analyzer was employed for raw exhaust gas sampling to measure hydrocarbon, carbon monoxide and carbon dioxide emissions. Specifications of the emission analyzer are detailed in Table 3.3. Dust sensor module (DSM 501) with sensitivity to particles greater than 1 μm in size was used for the measurement of particle number emissions. Three types of DOC substrates were used for the experimental study and its specifications are detailed in Table 3.2.

Emission tests were conducted in steady state test modes at five engine loading conditions (0%, 25%, 50%, 75%, and 100%) using electrical load bank and engine was coupled with electrical dynamometer to facilitate electrical loading and performance characteristics of the engine at different loading conditions are as shown in Figure 4.8 (a). The effect of the DOC system on diesel engine exhaust emissions is as shown in Figure 4.8. Hydrocarbon emissions had an increasing trend with the engine load as shown in Figure 4.8 (b) and DOC system had an average conversion efficiency of 51% (ceramic; 300 cpsi; 35 g/cub ft) , 54% (ceramic; 400 cpsi; 35 g/cub ft), 48% (metallic; 300 cpsi; 20 g/cub ft) and 48% (ceramic; 300 cpsi; 20 g/cub ft). The maximum conversion efficiency of 60% was observed at higher loading conditions in the case of a 400 cpsi DOC system.
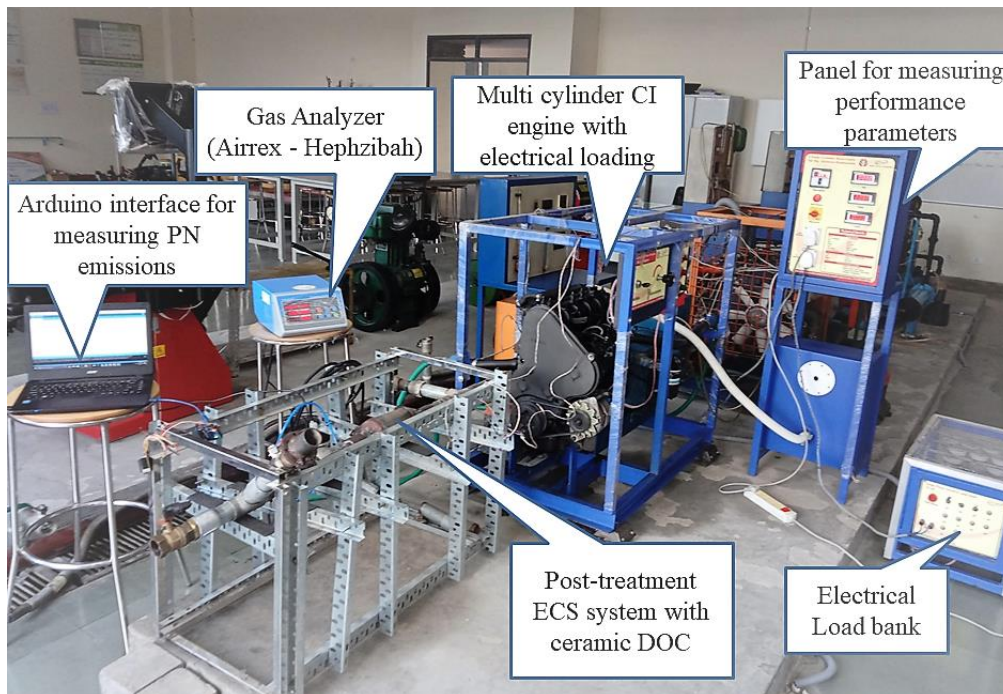
Figure 4.7. Engine setup with after-treatment DOC system

Carbon monoxide is a product of the incomplete combustion of fuel in the cylinder and DOC system had an average conversion efficiency of 32.4% (ceramic; 300 cpsi; 35 g/cub ft), 27% (ceramic; 400 cpsi; 35 g/cub ft), 19% (metallic; 300 cpsi; 20 g/cub ft) and 24% (ceramic; 300 cpsi; 20 g/cub ft) for carbon monoxide emissions as shown in Figure 4.9 (a). An increase in the conversion of hydrocarbon emissions will result in a rise in carbon monoxide and carbon dioxide emissions since these are the byproducts released during the oxidation of hydrocarbon. Particle number emissions had a decreasing trend with engine load as shown in Figure 4.9 (b). The concentration of oxygen gas in the exhaust emissions will have a decreasing trend with engine load due to more fuel consumption and combustion resulting in higher consumption of oxygen as shown in Figure 4.10 (a).

(a)

(b)
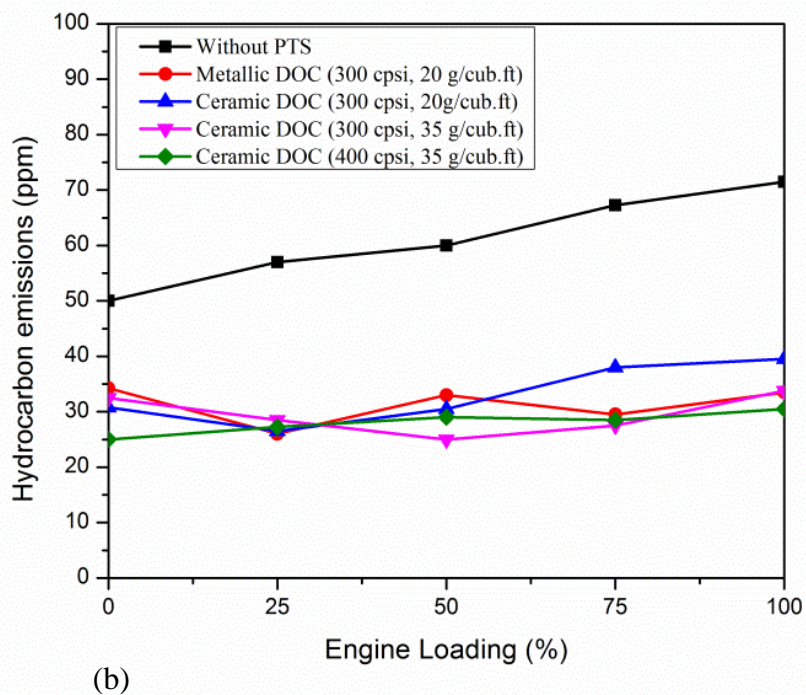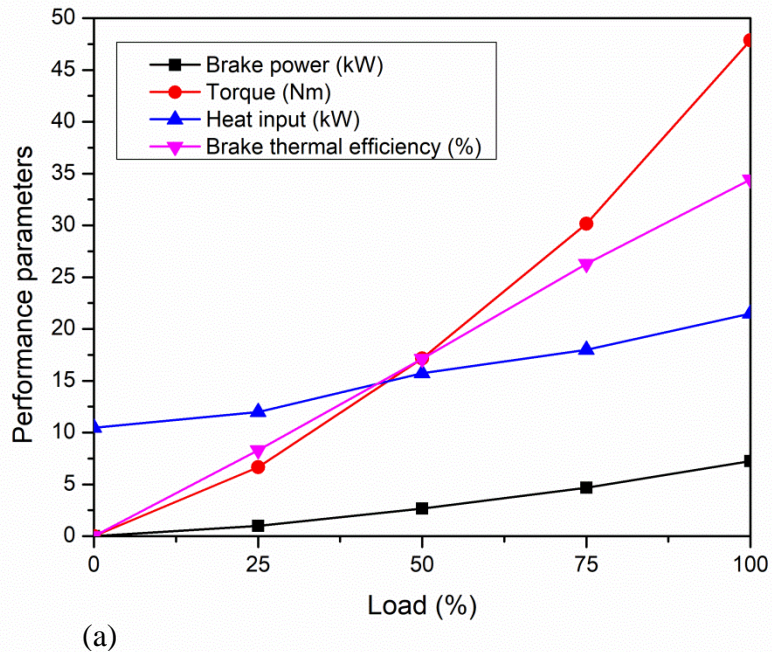
Figure 4.8. (a) Performance characteristics of the engine at different loading
conditions; (b) Effect of post-treatment system with DOC on hydrocarbon emissions

(a)

(b)
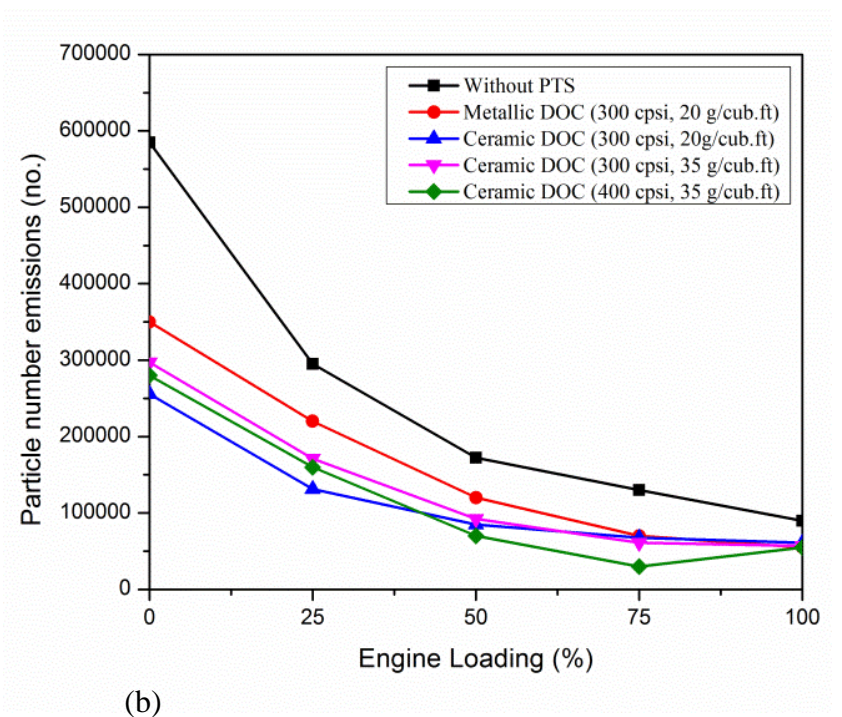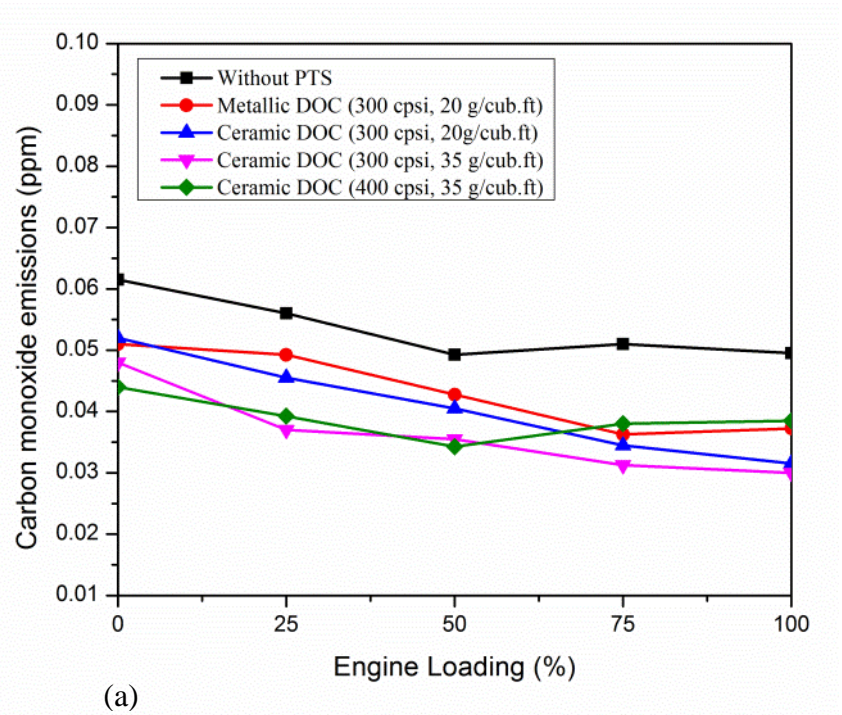
Figure 4.9. Effect of PTS with Diesel Oxidation catalysis System on (a) Carbon
monoxide emissions; (b) Particle number emissions
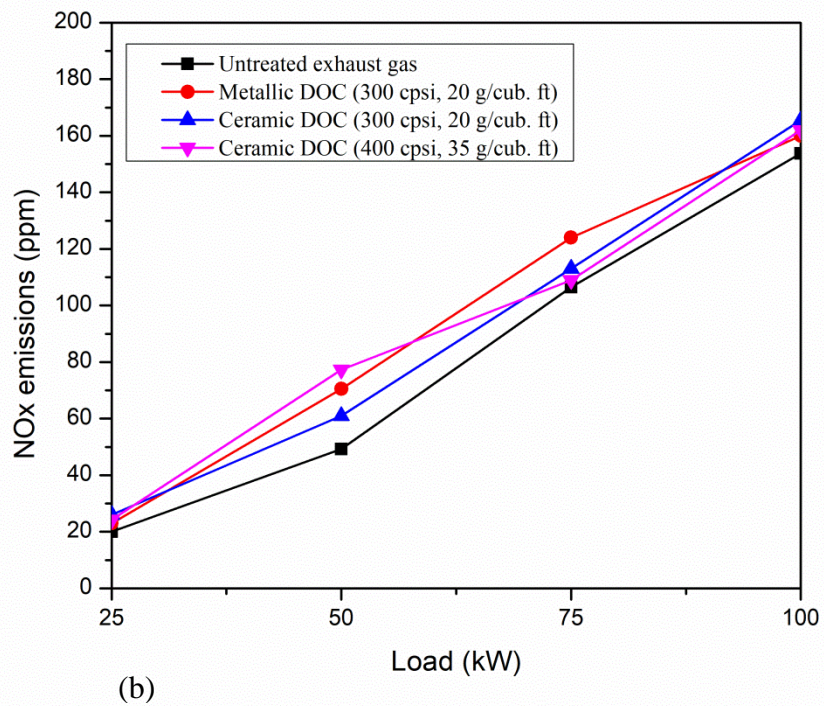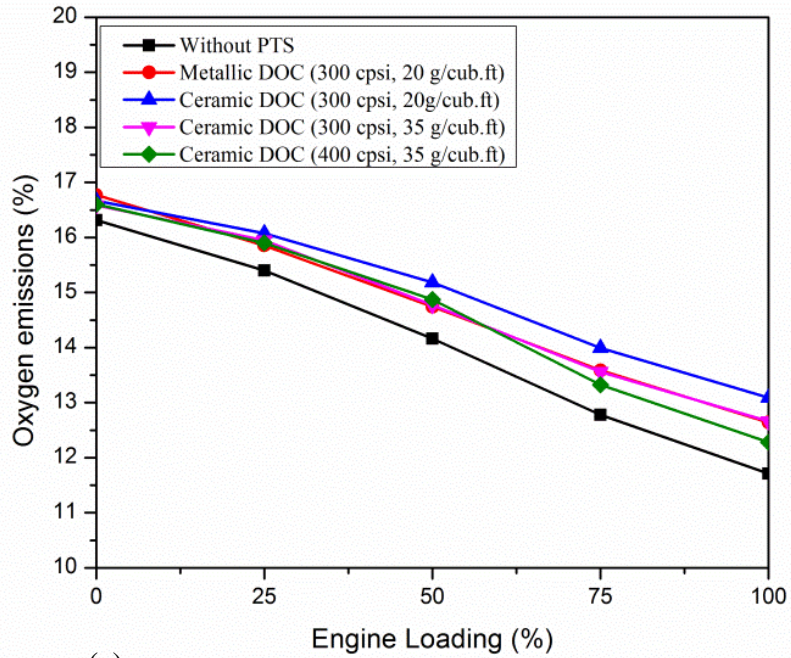
Figure 4.10. Effect of PTS with Diesel Oxidation Catalysis System on (a) oxygen and
(b) nitrogen oxide emissions
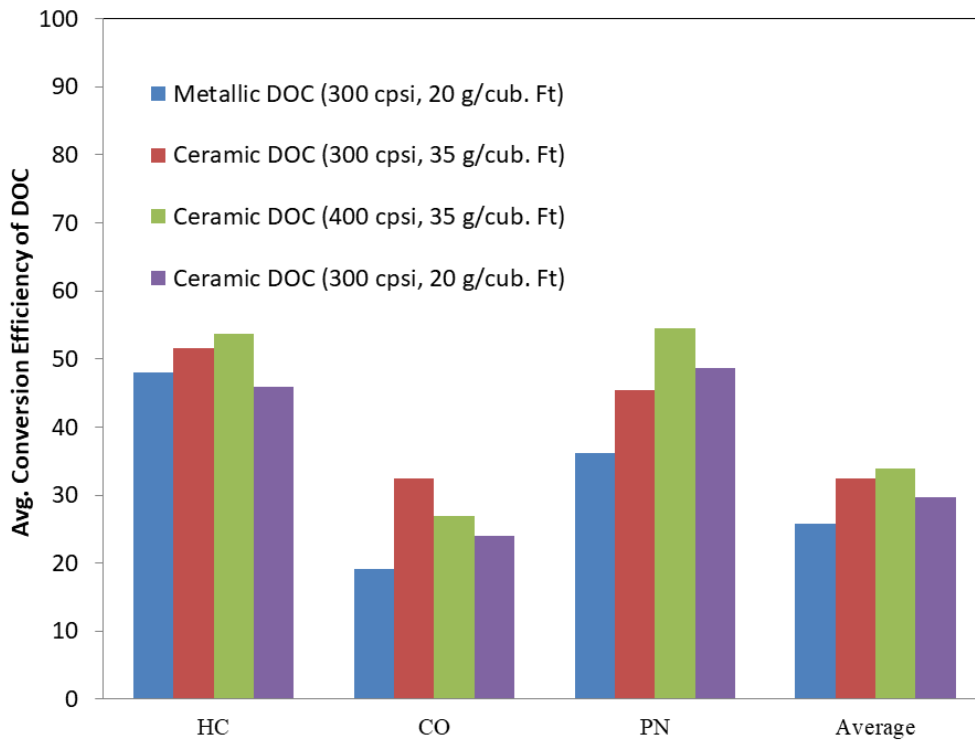
Figure 4.11. Average conversion efficiency of the DOC system

In the case of the DOC system, the oxygen gas in the exhaust stream was found to increase by approximately 4-6%, due to the reduction reaction involving conversion of nitrogen dioxide to nitrogen monoxide as shown in Figure 4.10 (b). Average rise in the concentration of oxygen gas in the exhaust stream was around 4.75% (ceramic; 300 cpsi; 35 g/cub ft), 3.83% (ceramic; 400 cpsi; 35 g/cub ft), 4.8% (metallic; 300 cpsi; 20 g/cub ft) and 6.94% (ceramic; 300 cpsi; 20 g/cub ft). In the exhaust gas stream, more than 80% of the nitrate emissions are nitrogen monoxide and hence nitrogen monoxide emissions are measured in the emission analyzer. In the DOC system, the reduction of nitrogen dioxide takes place resulting in the formation of nitrogen monoxide and hence there will be a rise in nitrogen monoxide emissions after the exhaust gas treatment in the DOC substrate. Average rise in the concentration of nitrogen gas in the exhaust stream was around 22% (ceramic;

300 cpsi; 35 g/cub ft), 21% (ceramic; 400 cpsi; 35 g/cub ft), 19.6% (metallic; 300 cpsi; 20 g/cub ft) and 17% (ceramic; 300 cpsi; 20 g/cub ft). The results of the experimental study showed that 400 cpsi ceramic DOC (35 g/cub. ft) has better conversion efficiency and performance among the DOC substrates considered in this work as shown in Figure 4.11. Hence 400 cpsi DOC was considered for further experimental study for the composite regeneration system with DPF.

4.4 CHARACTERIZATION OF DOC SUBSTRATE

Inverted Metallurgical microscope (Nikon-ECLIPSE MA200) imaging was used for capturing the uniformity of catalyst coating in the DOC substrate The variation in functional groups of the DOC substrate after application in the engine test bench was evaluated using Fourier transform Infra-red Spectroscopy (FTIR, Perkin Elmer). FTIR analysis was conducted to determine the molecular composition of the sample by decoding the spectrum of infra-red radiations absorbed by the sample.

FTIR sample was prepared using the standard procedure by preparing KBr (Potassium bromide) pellet with a substrate sample [171][172]. The intensity of particle size distribution in the DOC substrate before and after application in the engine test bench was determined using Particle Size Analyzer (Malvern ZEN1690). Particle size analyzer works by the principle of dynamic light scattering and has a measurement range of 0.3 nm to 5 microns. The sample for PSA analysis was prepared by dispersing the substrate in ethanol solution by using an ultrasonicator. The uniformity of the catalyst coating in the monolith substrate of the oxidation catalysis system was analyzed using an inverted metallurgical microscope.
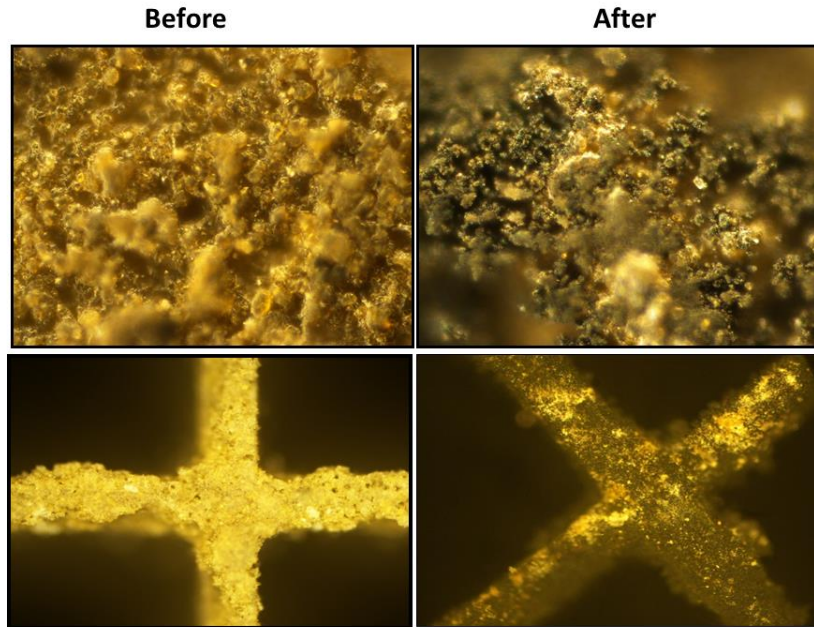
Figure 4.12. Microscopic images of 400 cpsi DOC substrate before and after
application in engine exhaust
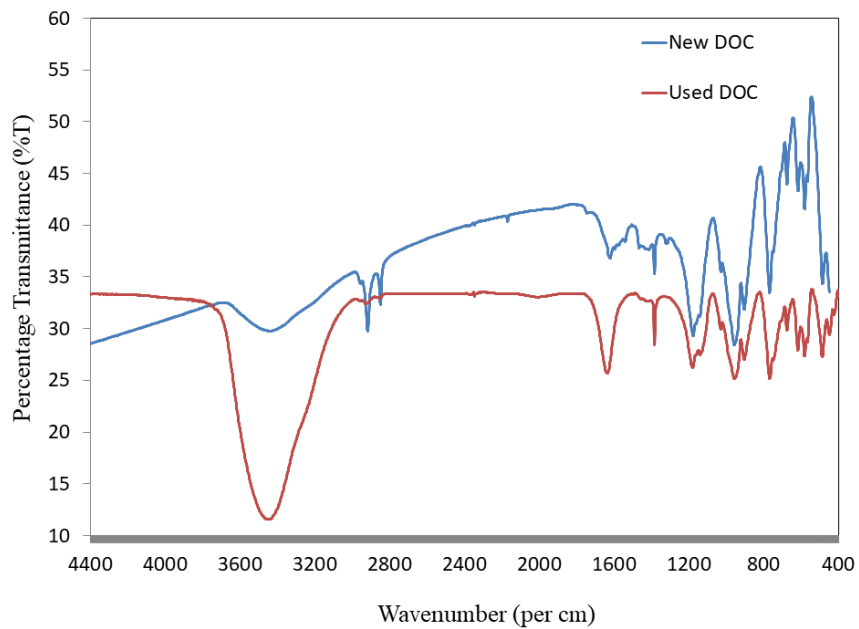
Figure 4.13. FTIR analysis of DOC substrate (35 g/cub ft) before and after
application in engine exhaust
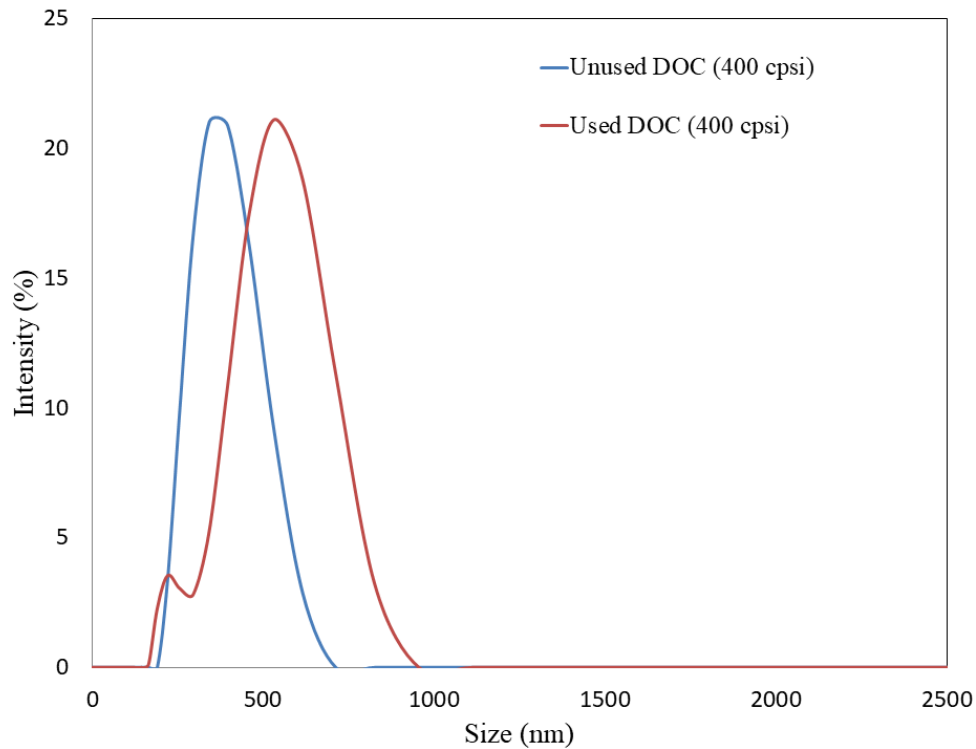
Figure 4.14. Particle size analysis data for average particle size distribution in DOC substrate, before and after application in the engine exhaust stream

The catalyst coating of the new (unused) DOC substrate is as shown in Figure 4.12, where the precious metal coating in the alumina washcoat layer can be observed. After application in the diesel engine, some patches of the platinum poisoning and carbon deposition were observed in the microscopic image of the DOC substrate, as shown in Figure 4.13.

Anatase functional group detected in the DOC substrate indicates the formation of oxides due to the poisoning of catalysts as shown in Figure 22. The intensity of the size distribution for particles in the DOC substrate after application in the emission control system was analyzed using particle size analyzer (Malvern ZEN1690) as shown in Figure 4.14. The results of the study showed that the intensity of particle size distribution was increasing in

the case of DOC, indicating the occurrence of catalyst poisoning by the formation of oxides.

The CFD analysis and experimental study were conducted on the DOC system in this chapter. The conversion efficiency of four different DOC substrates was experimentally evaluated to determine the one with the best performance. Based on the achieved results DOC substrate with best conversion efficiency was used for conducting studies as discussed in chapter 5, where the filtration efficiency of the integrated DOC-DPF system was investigated.

CHAPTER 5. MODELLING AND EXPERIMENTAL STUDY ON DIESEL PARTICULATE FILTRATION (DPF) SYSTEM

Among all these emission control strategies, diesel particulate filtration (DPF) system is most effective in terms of cost and soot trapping efficiency [173][174][175]. Implementation of diesel particulate filtration (DPF) system is the best possible way of reducing particulate matter emissions from the in-use vehicles [176]. The results of the Swiss retrofitting program proved the technical, economic, and operational feasibility of DPF systems in reducing the PM emissions to meet the stringent emission norms [177][178]. DPF system has a monolith substrate with alternately plugged channels which forces the exhaust gas to flow through the porous wall [87]. The soot particles get trapped in the porous wall by depth filtration as shown in Figure 5.1. The thickness of the soot layer increases with time resulting in pressure drop across the system and for sustainable flow through the system, backpressure must be minimized [122].

The transition from depth filtration (porous wall) to cake filtration (soot layer) will occur when the soot layer thickness increases beyond a certain limit affecting a rise in backpressure [83][129]. The average range of pressure drop during the transition stage will be around 700 Pa [179]. The accumulated soot particles have to be regenerated at regular intervals to avoid the backpressure rise in the system [136][180]. Commercially available fuel-based regeneration is leading to catastrophic failure of the system due to uncontrolled combustion [119][181]. The major challenge in the implementation of the DPF system is the need for the development of an alternate regeneration technique [182][183].
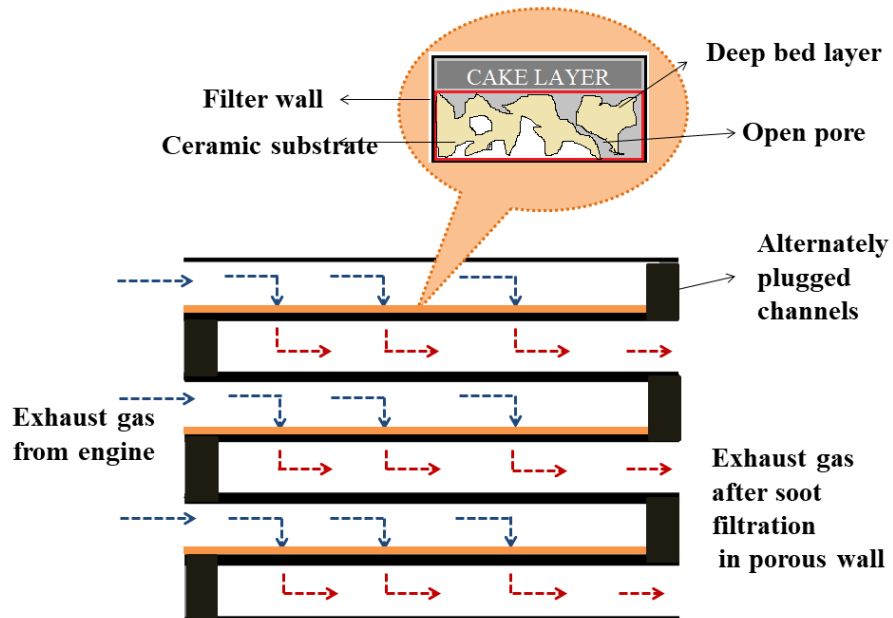
Figure 5.1. Filtration mechanism of DPF

5.1 SINGLE CHANNEL FLOW ANALYSIS

Pressure drop is the major parameter determining flow across the system and a major drop of pressure occurs in the DPF substrate. To study in detail about the pressure drop across DPF, simulations were carried out in a single pair of adjacent DPF channels. The properties of exhaust gases and the other parameters considered in initial and boundary conditions are extracted from [116], where flow analysis of the exhaust system in light commercial vehicles was carried out. Simulation parameters are detailed in Table 5.1. The mass flow rate of exhaust gas for different temperatures was calculated and the simulations were carried out for each case. Since the only single-channel flow is considered in this case, the flow rate in each cell is calculated by assuming that there is uniform flow. Variation in the density of the exhaust gas with temperature is plotted in Figure 5.2 (a).

Table 5.1.Simulation parameters

Parameter	Value
Turbulence Model	K – epsilon
Fluid	Exhaust gas
Fluid density	0.5508 kg/cubic meter
Fluid viscosity	0.00003814 Pa.s
Viscous coefficient	$3.236\ e^7\ m^2$
Pressure jump coefficient	$20.015\ m^{-1}$

Exhaust gas mass flow rate was calculated by considering the parameters of an engine with 1.5 l of combustion chamber volume and speed of 1500 rpm. A single pair of filter channels intake only a small amount of the whole flow. The ratio of the cell area to the area of the whole filter is calculated to determine the amount of flow that is going inside the channel by assuming that the flow is uniformly distributed. The calculated values of exhaust flow rate and cell flow rate at different temperatures are mapped in the graph as shown in Figure 5.2 (b).

The porous medium is applied to the white stripe as shown in Figure 5.3. The porous medium induces a velocity drop when exhaust gas flows through it. Velocity drop is about 25% as compared to that of the flow without a porous medium. There is no leakage and mass flow rate is constant, which is evident from Figure 5.4 (a) and (b) where the contours of velocity at the inlet and outlet side are plotted. Simulations were carried out without considering porous medium initially to highlight the phenomenon non-linked to the porous cause. The pressure drop due to shape and geometry can be determined from these results.
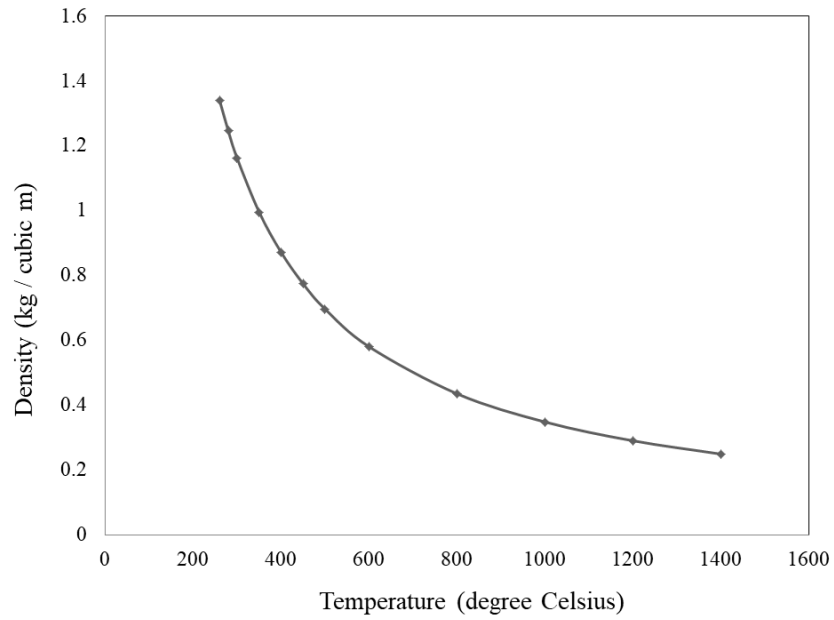
(a)
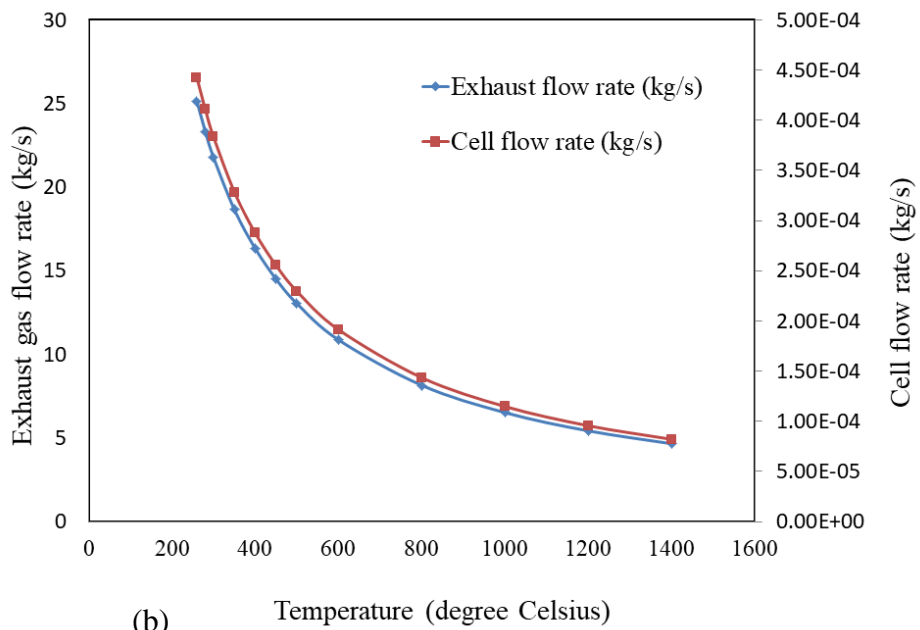
(b)

Figure 5.2. (a) Variation in density of exhaust gas with temperature and (b) Variation
in exhaust flow rate with temperature

Various factors contributing to the total pressure drop (ΔP_{Total}) across the DPF is detailed in equation no 18, where ΔP_{cont} is the local pressure drop due to contraction in the outlet loft side of the filter, $\Delta P_{\exp}$ is the local pressure drop due to expansion in the inlet loft side of the filter, $\Delta P_{in\_channel}$ is the pressure drop along the inlet channel, $\Delta P_{out\_channel}$ is the pressure drop along the outlet channel, ΔP_{wall} is the pressure drop along the filter wall, ΔP_{ash} is the pressure drop due to ash layer in the inlet channel and ΔP_{soot} is the pressure drop due to presence of soot layer in the inlet channel of DPF.

$$\Delta P_{Total} = \Delta P_{cont} + \Delta P_{\exp} + \Delta P_{in\_channel} + \Delta P_{out\_channel} + \Delta P_{wall} + \Delta P_{ash} + \Delta P_{soot} \qquad (18)$$

For pressure drop analysis, simulations were carried out for different mass flow rates and the results were plotted in a graph as shown in Figure 5.5. From the results, it was found that the pressure at inlet and outlet has direct proportionality with the mass flow rate. Pressure drop is found to increase with the mass flow rate of the fluid which proves Darcy's law for flow through the porous medium as shown in equation no 19 [184], where 'u' is fluid velocity, 'K' represents the permeability of medium, 'μ' is dynamic viscosity of fluid, 'L' is the length of filter substrates and '(p₁ - p₂)' is pressure drop across the filter.

$$u = \frac{K(p_1 - p_2)}{\mu L} \qquad (19)$$

(a)

Open alternate channels

Alternately Plugged channels

(b)
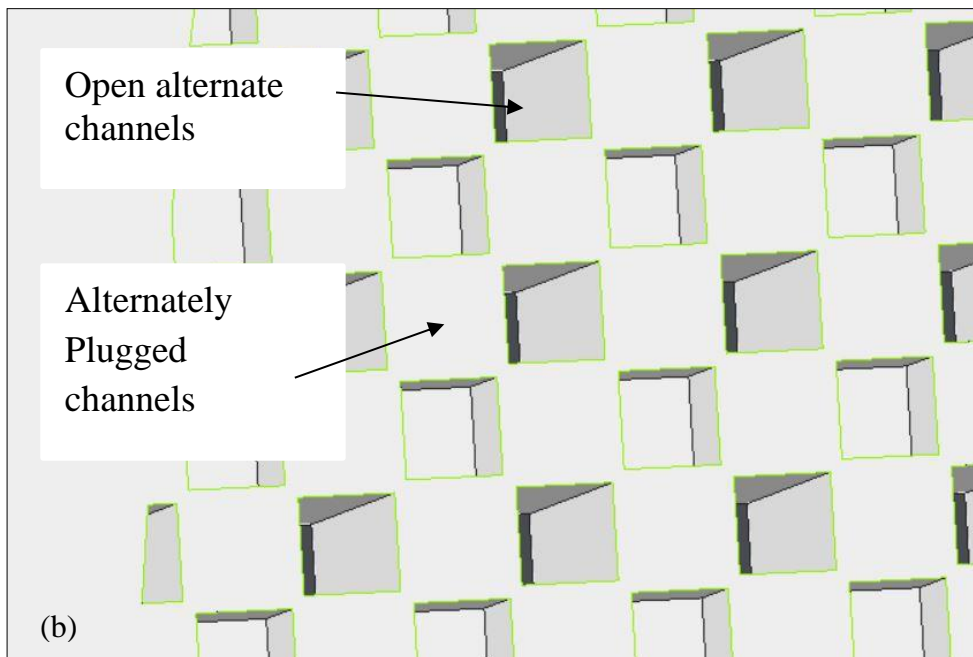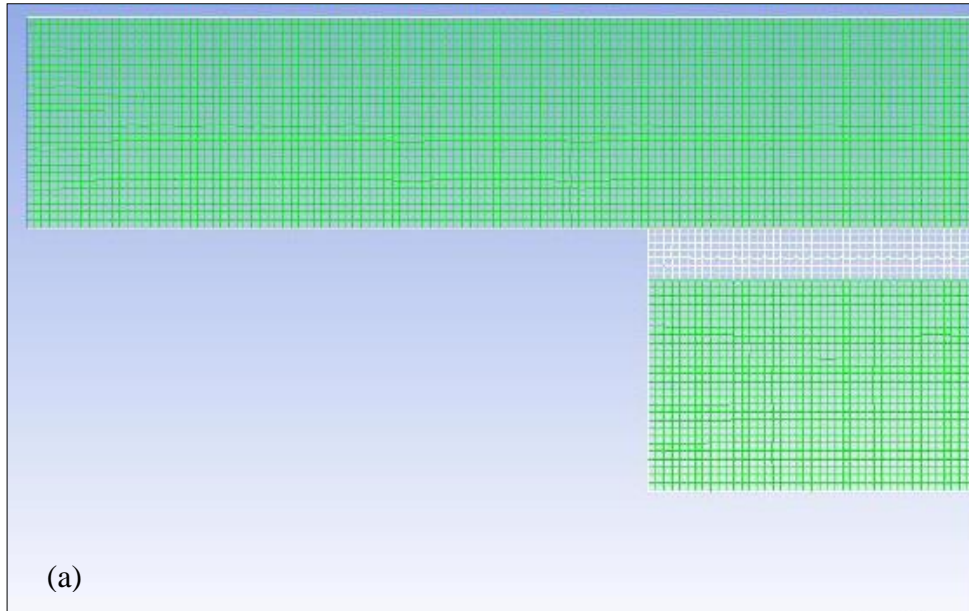
Figure 5.3. (a) Filter wall with Porous medium and (b) Alternately plugged channels of DPF
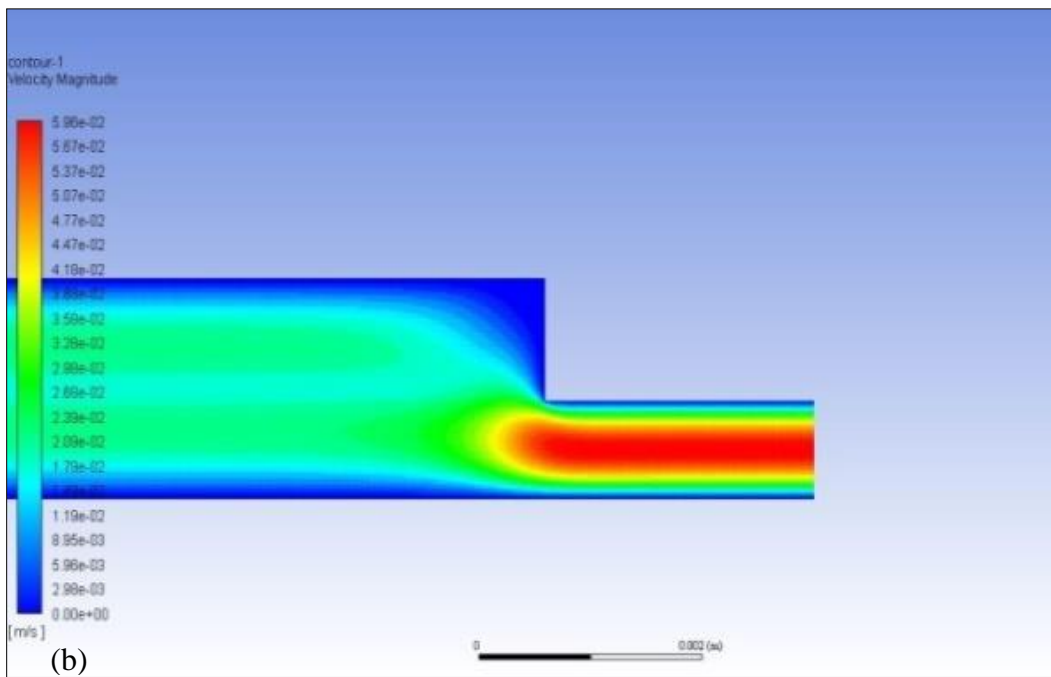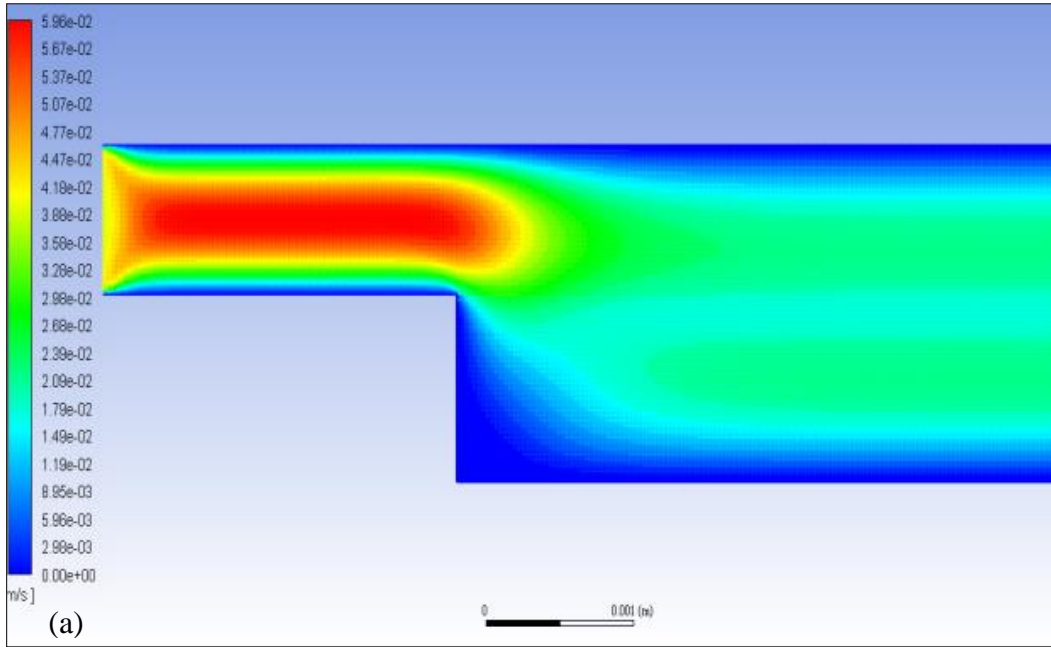
Figure 5.4. (a) Velocity contour at the inlet side of the channel with porous medium
and (b) Velocity contour at the outlet side of the channel with porous medium

Single-channel flow analysis of the designed DPF substrate was done in ANSYS FLUENT software (version 16.0). Simulations were carried out for different mass flow rates of exhaust gas both in the case of DPF channel with porous medium and without the porous medium. The results of the simulation showed that the presence of the porous medium is causing a pressure drop of around 60%. Also, the results showed that the mass flow rate has direct proportionality with the inlet and outlet pressure.
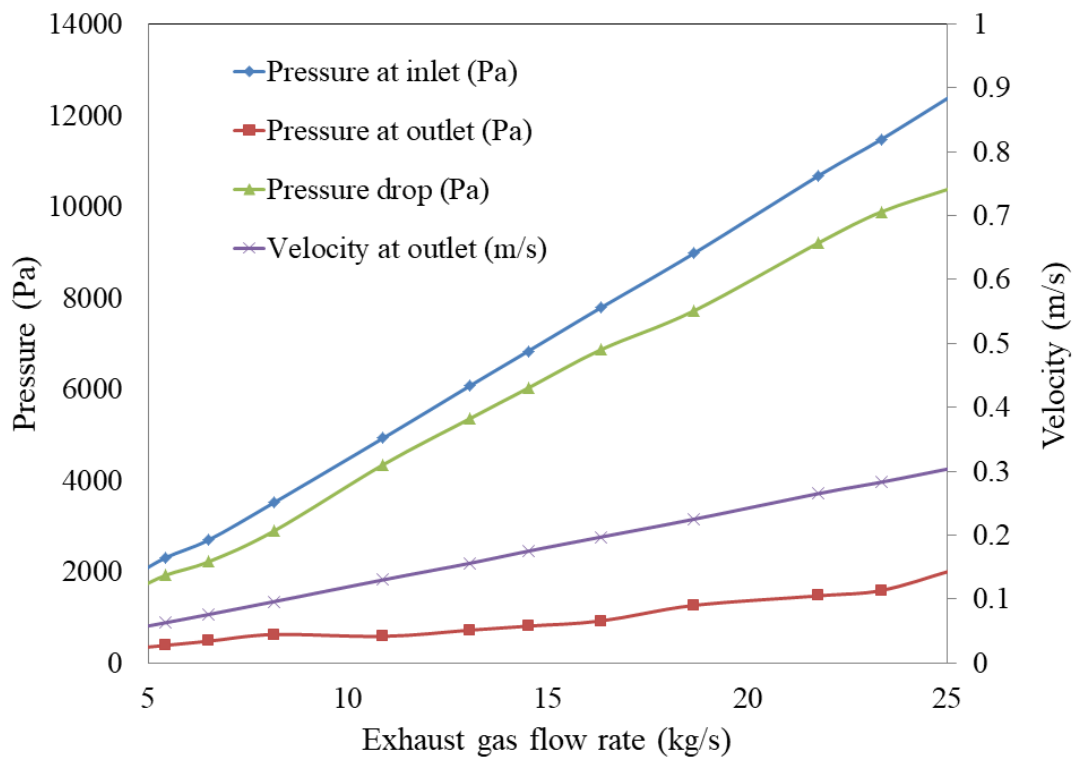
Figure 5.5. Flow behavior of a single DPF channel

5.2 MODELLING OF SOOT DEPOSITION IN FILTER CHANNELS

5.2.1 Soot Accumulation Modelling

Single-channel flow analysis and soot layer formation in pair of filter channels were modeled using COMSOL Multiphysics. The study examines the

deposition of the soot particles in the walls of the filter substrate during the flow of exhaust gas stream and the exhaust gas stream was assumed to behave as an ideal gas. The computational domain of the filter channels consisting of the inlet, outlet and porous wall, which was developed for analysis purpose is as shown in Figure 5.6 (a) and the fine mesh was generated in the model as shown in Figure 5.6 (b). Moving mesh interface was used by the space-dependent model to consider the shape change during soot layer build up in the filter wall. The geometrical specifications of the developed model are detailed in Table 5.2. Equations governing the flow through the filter channels include continuity equation, momentum equation and species conservation as shown in equation no. 20 to 22.

$$\frac{\partial(\phi\rho)}{\partial t} + \vec{\nabla}.(\rho\vec{V}) = S_\rho \tag{20}$$

$$\frac{\partial(\phi\rho\vec{V})}{\partial t} + \vec{\nabla}.(\phi\rho\vec{V}\vec{V}) = -\vec{\nabla}P + \vec{\nabla}.(\overline{\overline{\tau}}) - \frac{\mu}{\alpha}\vec{V} \tag{21}$$

$$\frac{\partial(\phi y_i)}{\partial t} + \vec{\nabla}.(\phi\vec{V} y_i + \vec{J_i}) = S_{y_i} \tag{22}$$

Table 5.2. Geometrical specifications of the filter channels

Parameter	Value
Filter length (mm)	80
Height of inlet and outlet channels (mm)	1
Thickness of filter porous wall (mm)	0.38
Inlet velocity, (m/s)	3
Oxygen concentration (mol. %)	15
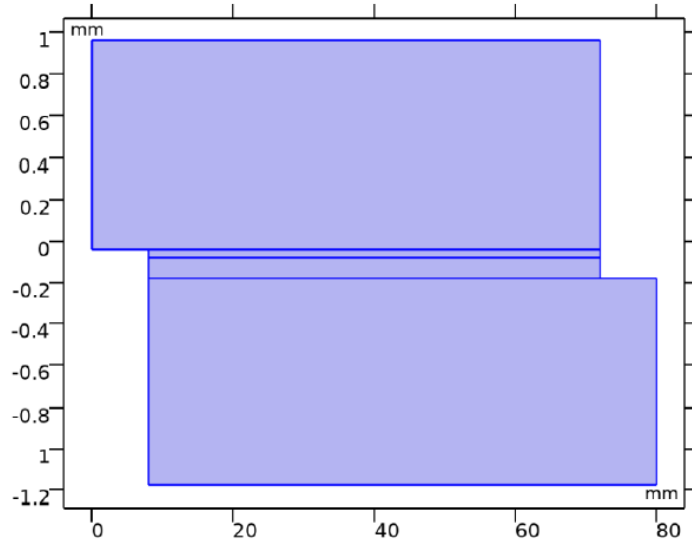
(a)
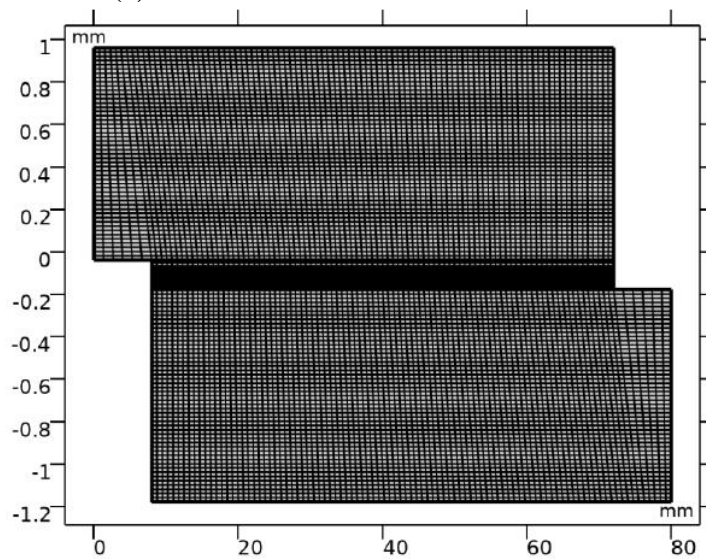
(b)

Figure 5.6. (a) Two-dimensional computational domain for a single pair of DPF filter channel (b) Meshed model of a single pair of DPF filter channels

5.2.2 Soot Layer Formation

The model for soot layer formation was developed in the COMSOL MULTIPHYSICS CFD platform by coding the porous medium model and implementing the properties of components using user-defined subroutines.

Soot conservation equation was coupled with the fluid flow equations by specifying local soot concentration as a user-defined scalar. Rise in the thickness of the soot layer with respect to time was determined by conducting simulations for a total period of 1500 seconds.

(a)

(b)
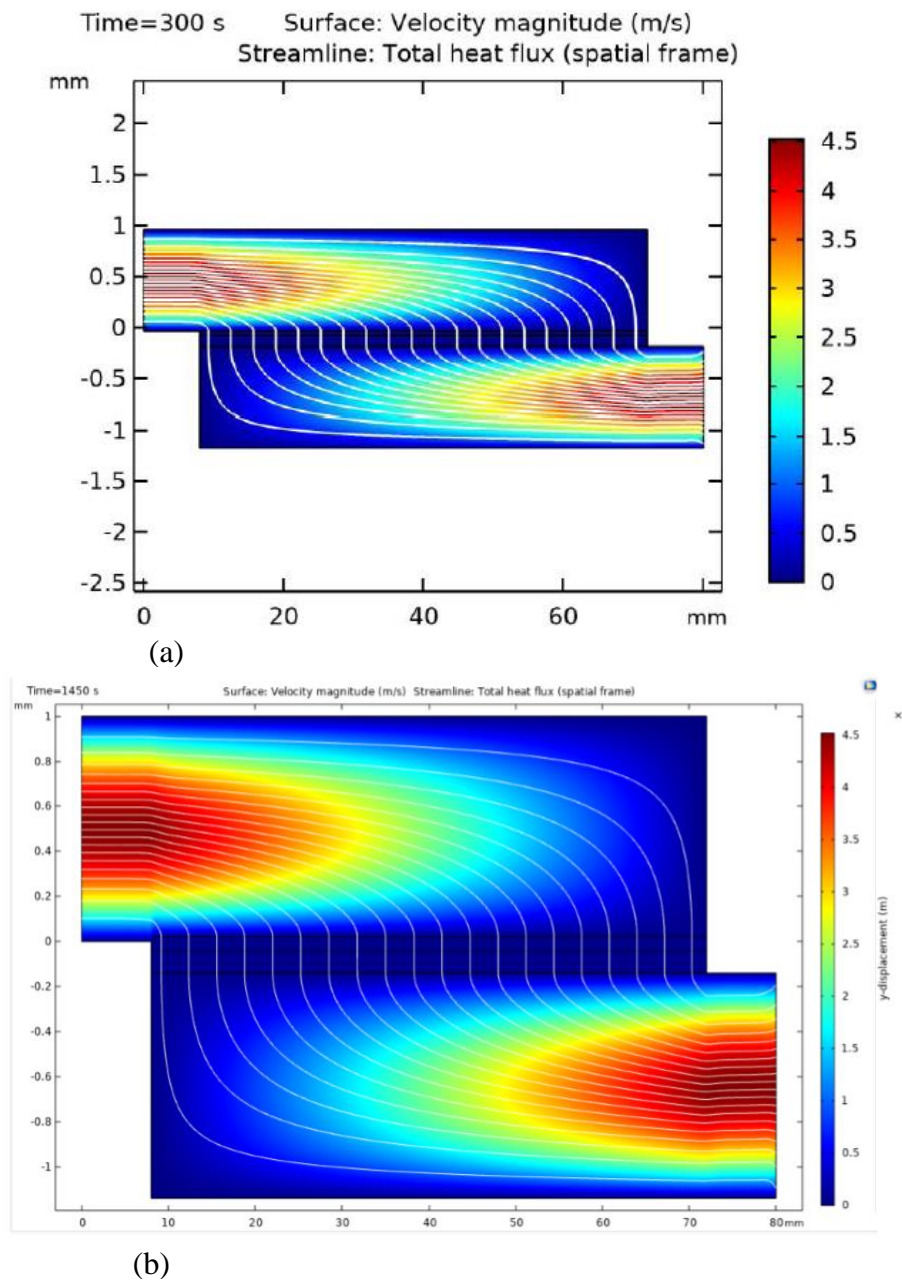
Figure 5.7. Contour map of the surface velocity contour in the filter channel after (a) 300 s and (b) 1500 s of engine operation

The contour of surface velocity magnitude along the filter channels after 300 and 1500 seconds are as shown in Figure 5.7. The rising trend of the soot layer thickness after 1500 seconds of engine operation is as shown in Figure 5.8, where it can be seen that the thickness of the soot layer was raised to 0.2025 mm.
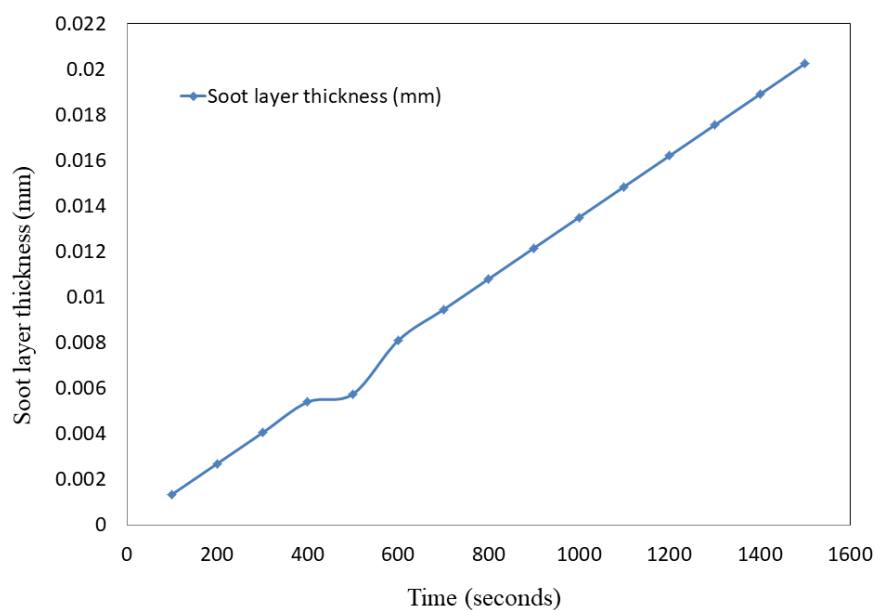
Figure 5.8. Trend of soot layer deposition and rise in the thickness for 1500 seconds

5.3 GEOMETRIC DESIGN VALIDATION AND FABRICATION OF DIESEL PARTICULATE FILTRATION SYSTEM

5.3.1 Cad Modelling

Modelling of the lofted inlet and outlet for the DPF monolith substrate was done in CATIA software (version 6). The actual dimensions of the substrate and fabricated loft were considered for the modelling purpose to validate the geometric design of the developed system. Different views of the DPF system modeled in CATIA software are as shown in Figure 5.9.
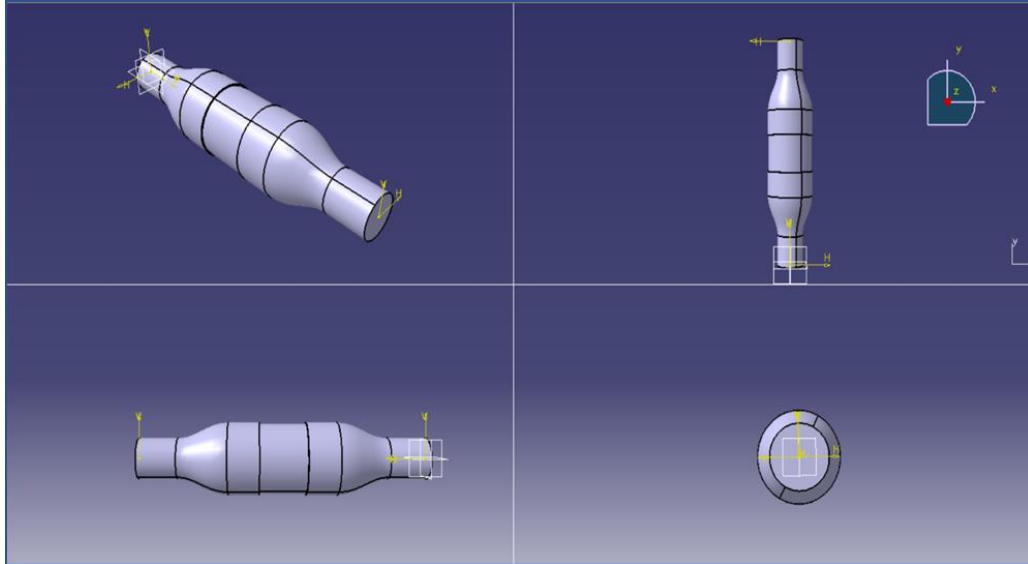
Figure 5.9. Model of the DPF system with inlet and outlet lofts

5.3.2 CFD Analysis

The solid DPF designed on CATIA V5 was imported to ANSYS fluent for carrying out a simulation process for the flow analysis in this particular product. Computational Fluid Dynamics study was done in ANSYS 2019 version R1 to test for the flow behavior inside the filter and examine its physical properties. Pressure based type solver with absolute velocity formulation was used for analysis and time is considered as steady. K-epsilon turbulence model was used where the first variable is the turbulent kinetic energy and the second variable is the dissipation rate of kinetic energy. This model is commonly used for flows with small pressure gradients and also in cases where Reynold stresses are important. Fluid flowing through the filter was assumed to be exhaust gas by providing its density and viscosity. The ceramic substrate was considered as the porous zone with the laminar flow by providing the viscous resistance and inertial resistance in three directions.

5.3.3 CFD Simulation Results

Pressure: The simulation results of total pressure analysis showed that there was a decrease in pressure at the outlet section as compared to the inlet, obeying the continuity laws. The gradual decrease in the pressure is due to the diverging and then converging section of the filter which helps in increased velocity at the outlet section. The contour of total pressure and pressure coefficient are as shown in Figure 5.10 and 5.11. DPF system with inlet and outlet lofts were fabricated with inference from the simulation results as shown in Figure 5.12.
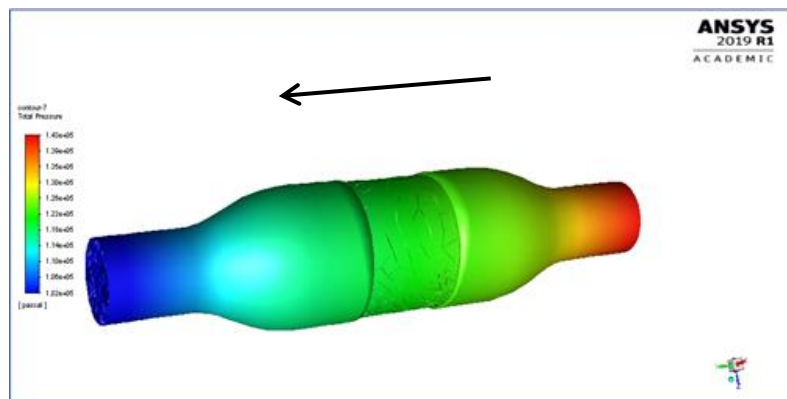
Figure 5.10. Contour of total pressure with flow direction
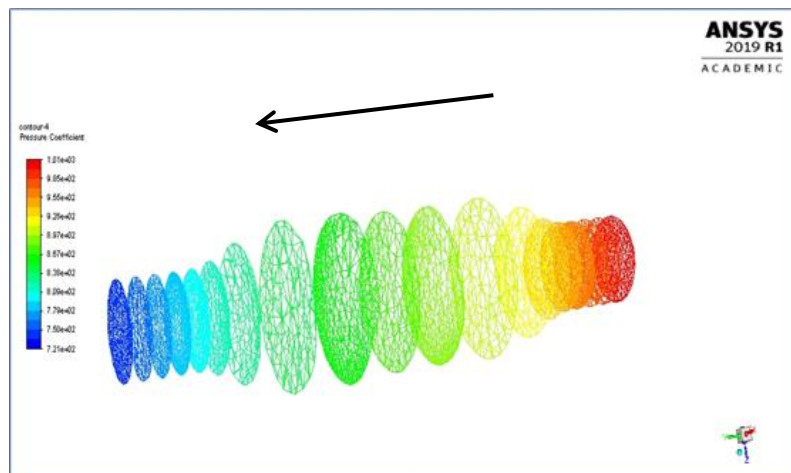
Figure 5.11. Contour of total pressure with flow direction
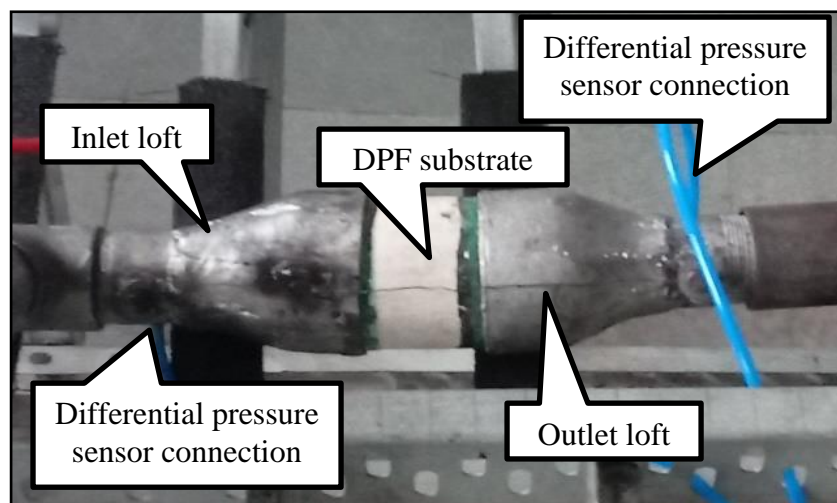
Figure 5.12. Fabricated ceramic DPF system

5.4 EXPERIMENTAL ANALYSIS: SOOT DEPOSITION AND EMISSIONS IN DPF AND INTEGRATED DOC-DPF SYSTEM

The engine test bench coupled with integrated DOC-DPF post-treatment system is shown in Figure 5.13 and engine specifications are detailed in Table 3.1. The gaseous emissions were sampled from raw exhaust using AIRREX HEPHZHIBA (HG 540) gas analyzer measuring hydrocarbon, carbon monoxide, carbon dioxide, and oxygen concentrations simultaneously. Specifications of the analyzer are detailed in Table 3.3. Particle number emissions were measured using sensor module (Shinyei DSM 501A) which works by particle counter mechanism with high sensitivity to particles greater than 1 µm in size. The pressure drop across the diesel particulate filter substrate was monitored by a differential pressure sensor (MPX10DP) with a measurement range of 0 to 10 kPa. The steady-state cycle was followed for conducting experiments and engine operation parameters were varied by control panel for dynamometer
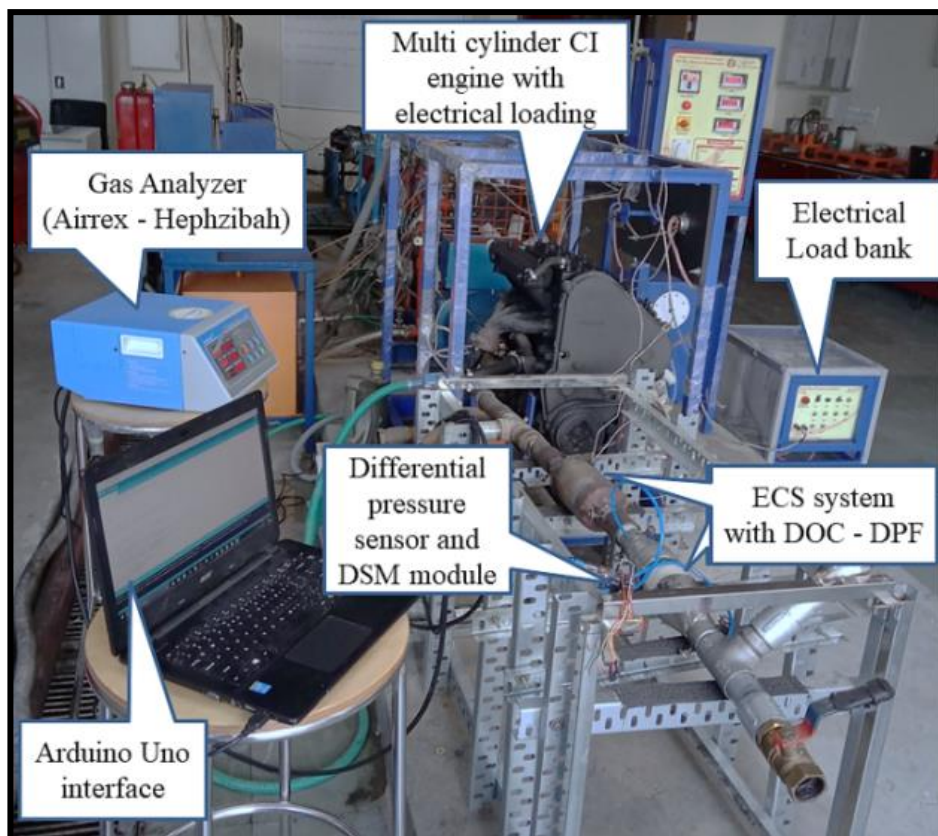
Figure 5.13. Engine setup with coupled DOC – DPF post-treatment system

Table5.3. Specifications of DOC and DPF substrate

Sl. No	Parameter	DOC	DPF
1	Substrate	Cordierite	Cordierite
2	Cell density (cpsi)	300	200
3	Diameter $\times$ length (mm $\times$ mm)	101.6×152.40	80×80
4	Catalyst coating	Pt:Pd (5:1)	nil
5	Catalyst loading (g/cub. ft)	35	nil
6	Volume (l)	4.9	1.6
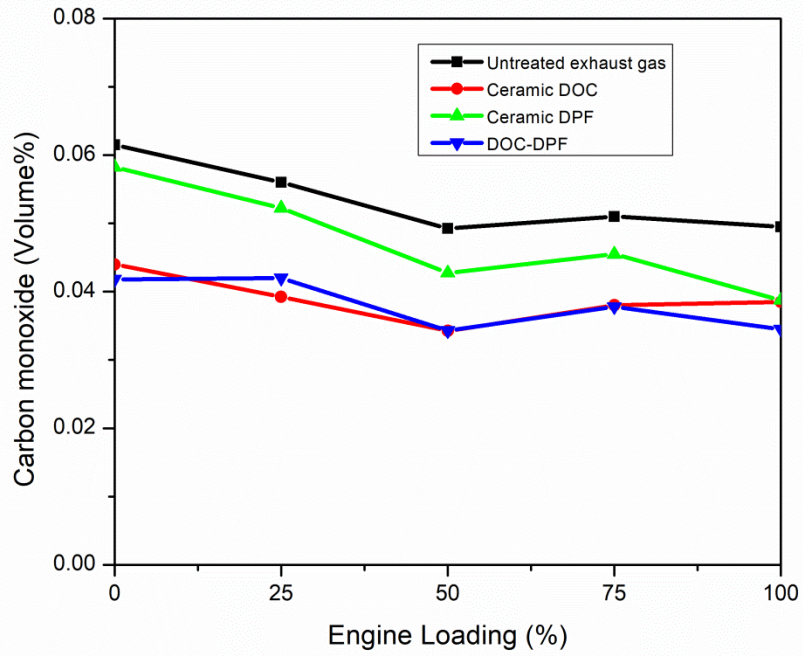
(a)
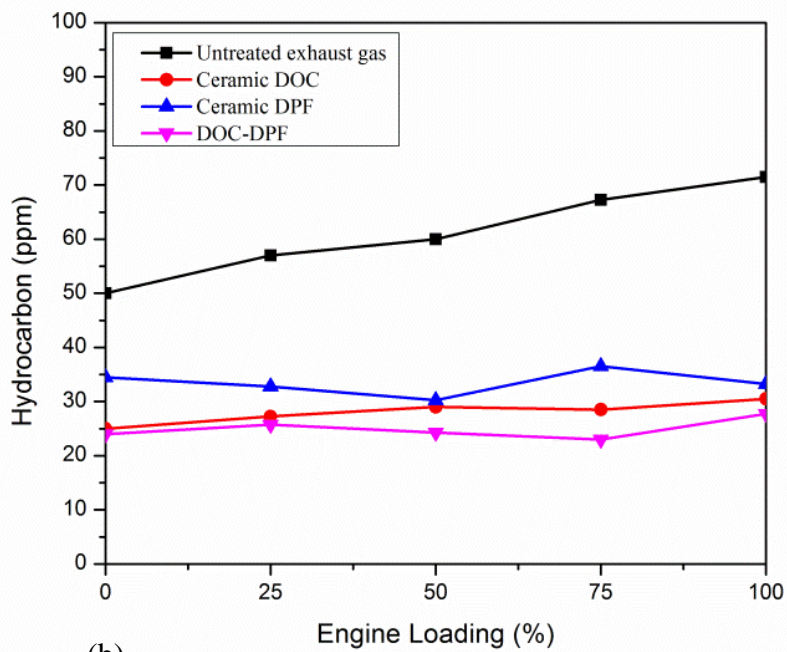
(b)

Figure 5.14. Effect of post-treatment system with DOC & DPF on (a) carbon monoxide (b) hydrocarbon
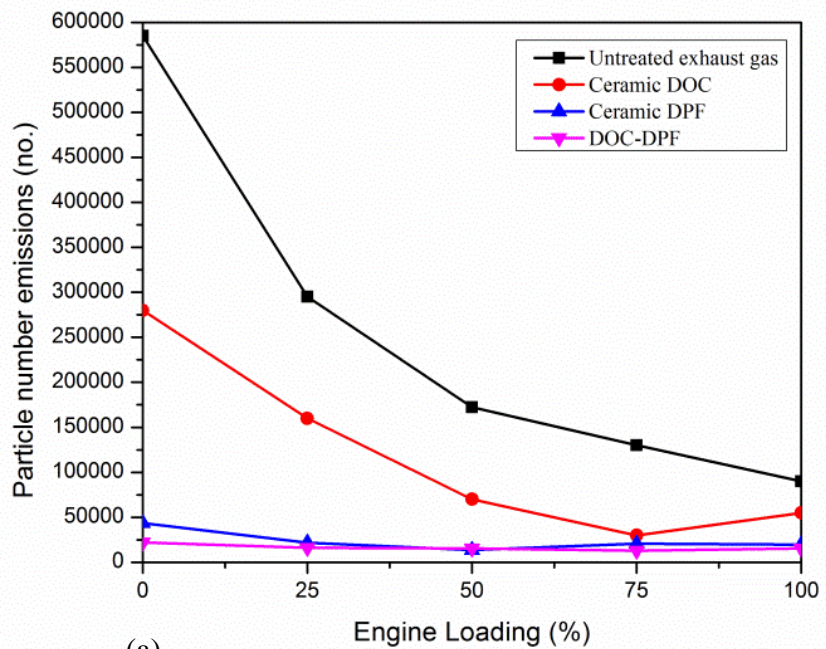
(a)
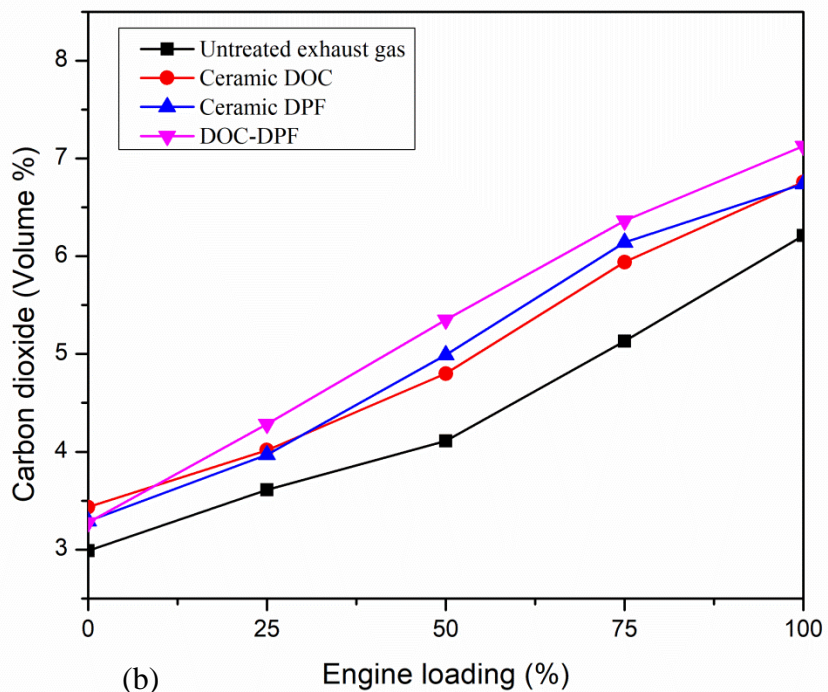
(b)

Figure 5.15. Effect of post-treatment system with DOC & DPF on (a) particle number, and (b) carbon dioxide.

The effects of the post-treatment system (PTS) on gaseous emissions were tested under different loading conditions by following the steady-state cycle. Tests were conducted separately for DOC, DPF and coupled DOC-DPF to determine the effect of each component in the Post-Treatment System (PTS) on engine emissions. The specification of DOC and DPF used in the PTS system are detailed in Table 5.3. DOC system has a monolith substrate with straight channels coated with an alumina washcoat layer in which precious metal catalysts like platinum and palladium are doped. DPF system has a ceramic substrate with alternately plugged filter channels and soot particles are trapped in the porous wall by depth filtration. The effect of DOC, DPF and DOC-DPF system on exhaust gas emissions are shown in Figure 5.14 to 5.16.
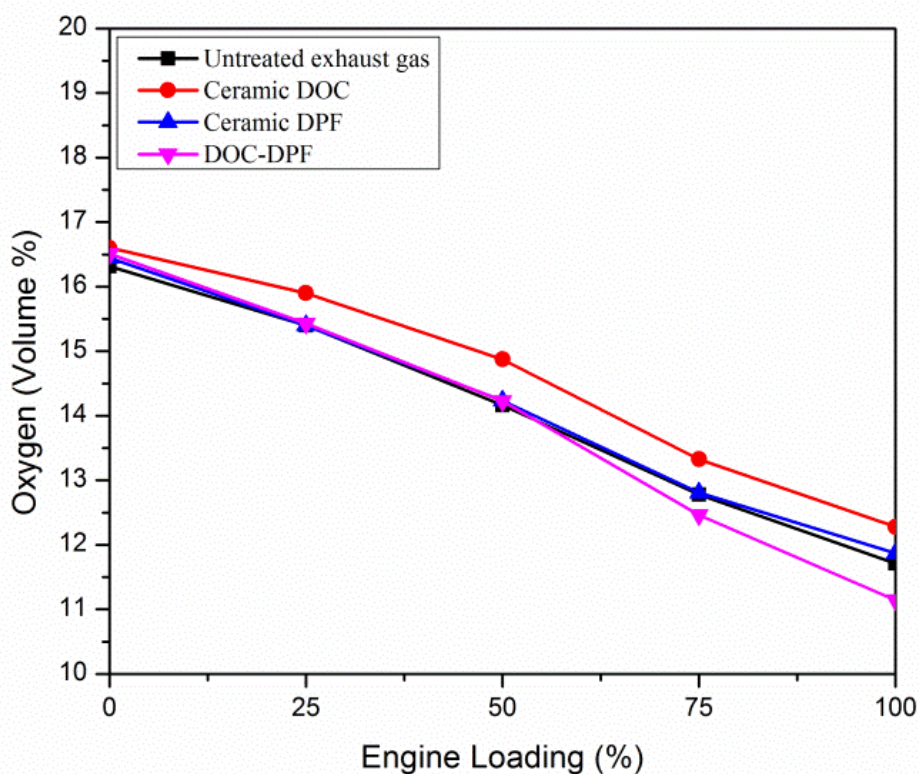
Figure 5.16. Effect of post-treatment system with DOC & DPF on oxygen emissions.

90
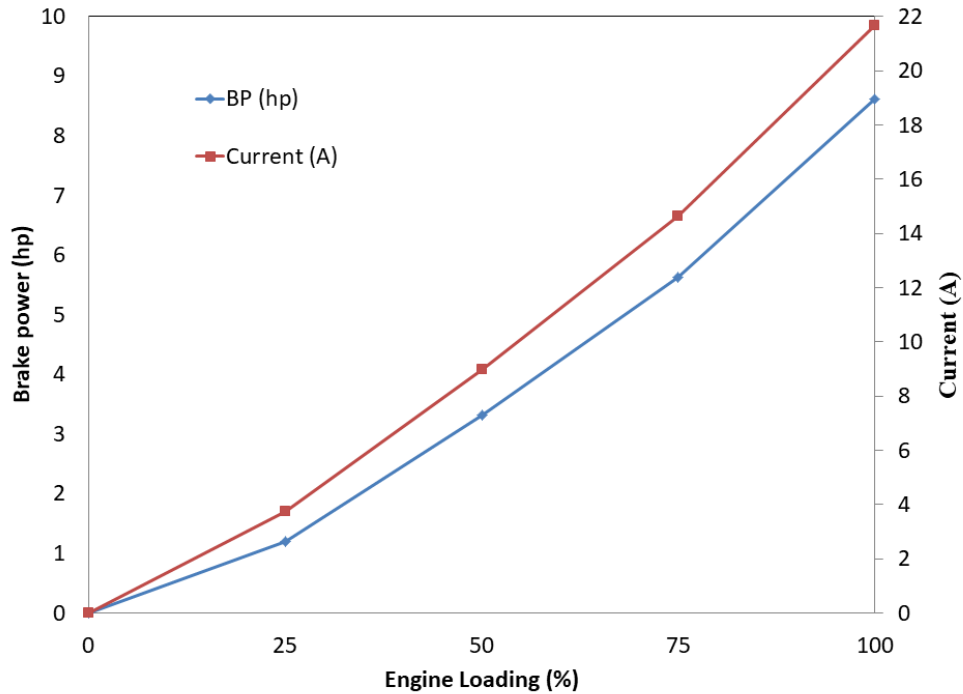
Figure 5.17. Performance characteristics of the engine at different loading condition brake power and current

Carbon monoxide emissions had a decreasing trend with increasing load and the DOC system had an average CO conversion efficiency of 27%, and maximum conversion efficiency of 30% was observed at medium load conditions as shown in Figure 5.14 (a). At higher loads, CO emissions were slightly higher in the case of the DOC-DPF system due to oxidation of the accumulated soot particles trapped in the DPF channels resulting in the formation of emission products. Hydrocarbons in the exhaust gas stream are generated due to various reasons like flame quenching, crevice fuel entrapment, exhaust valve leakage, valve overlap, and lubricant oil desorption. The average conversion efficiency of 53%, 45%, and 59% was observed for hydrocarbon emissions in the case of DOC, DPF and DOC-DPF system as shown in Figure 5.14 (b).
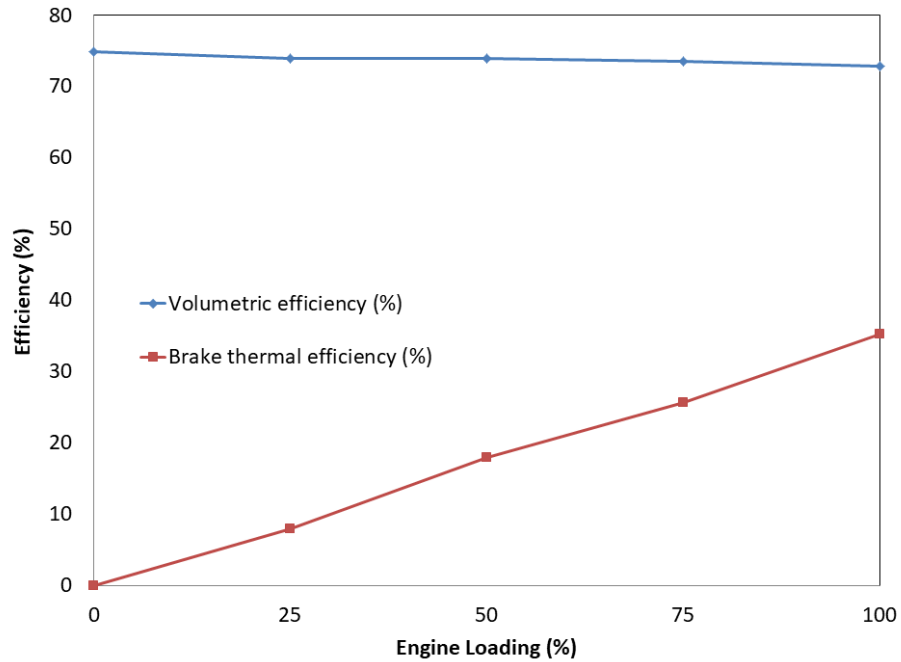
(a)
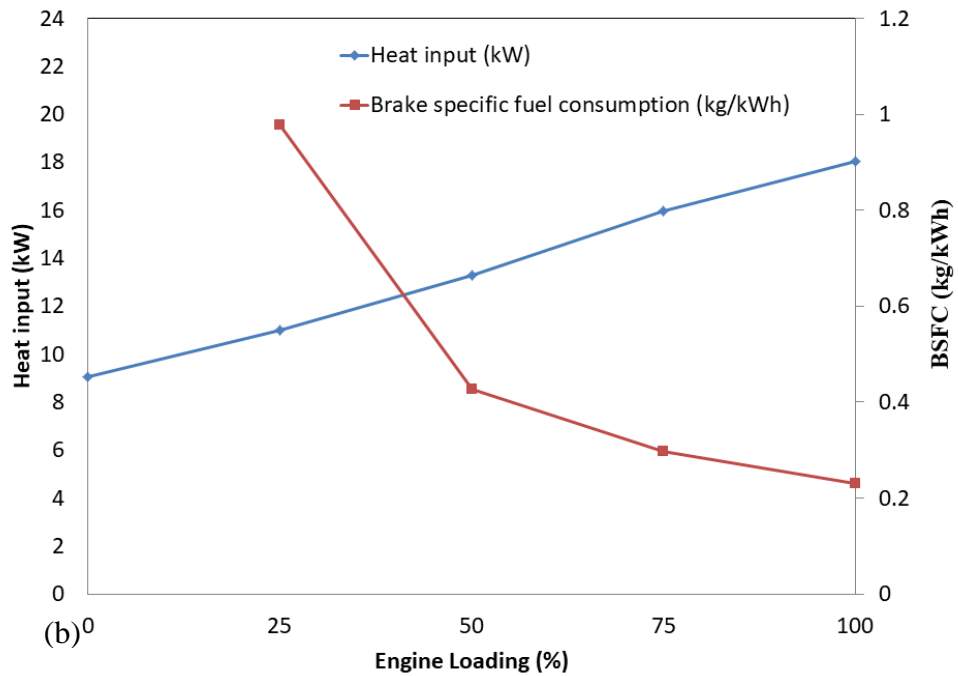
(b)

Figure 5.18. Performance characteristics of the engine at different loading condition
(a) volumetric and brake thermal efficiency and (b) Heat input and brake specific fuel
consumption

At higher loads, the DOC-DPF system had a maximum conversion efficiency of 77% for hydrocarbon emissions as a result of the combined effect from reactions in DOC and DPF wall filtration. Complete combustion of hydrocarbons will result in the formation of carbon dioxide and it is also an associated product in the DOC oxidation reaction. Reduction of hydrocarbon emissions will result in a rise of carbon dioxide emissions and also oxidation of the trapped soot particles will lead to the formation of complete combustion products. The average conversion efficiency of 54%, 88%, and 91% was observed for particle number emissions in case of DOC, DPF and DOC-DPF system as shown in Figure 5.15 (a). Carbon dioxide emissions were increasing with load as shown in Figure 5.15 (b), indicating the reduction of hydrocarbons in the exhaust gas stream.
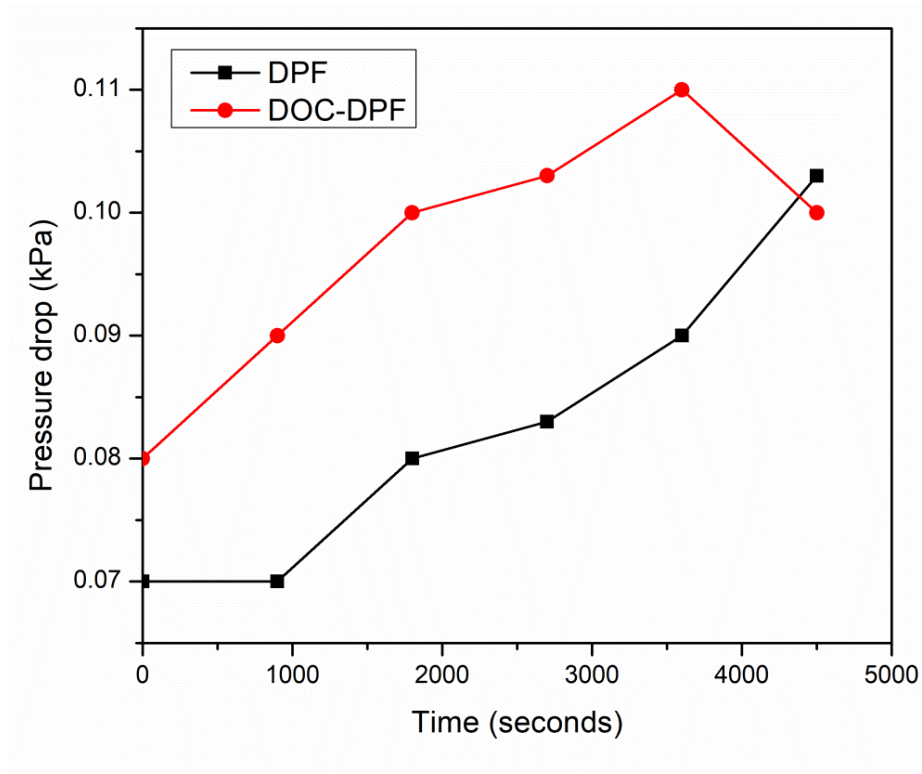
Figure 5.19. Pressure drop across DPF substrate in DPF and DOC-DPF system with respect to time

The concentration of oxygen gas in the exhaust stream was reducing with the load as shown in figure no. 5.16, which is proportional to the rise in fuel consumption resulting in higher oxygen demand for combustion. The performance characteristics of the engine like brake power, torque, volumetric efficiency, heat input and brake thermal efficiency at steady state loading conditions considered in this study are shown in Figure 5.1 and 5.18. The pressure drop across the DPF was tested at steady-state loading conditions for the DPF and DOC integrated DPF systems and the results are as shown in Figure 5.19. There was a steady rise in the pressure drop with the increasing load across the DPF system due to soot accumulation.
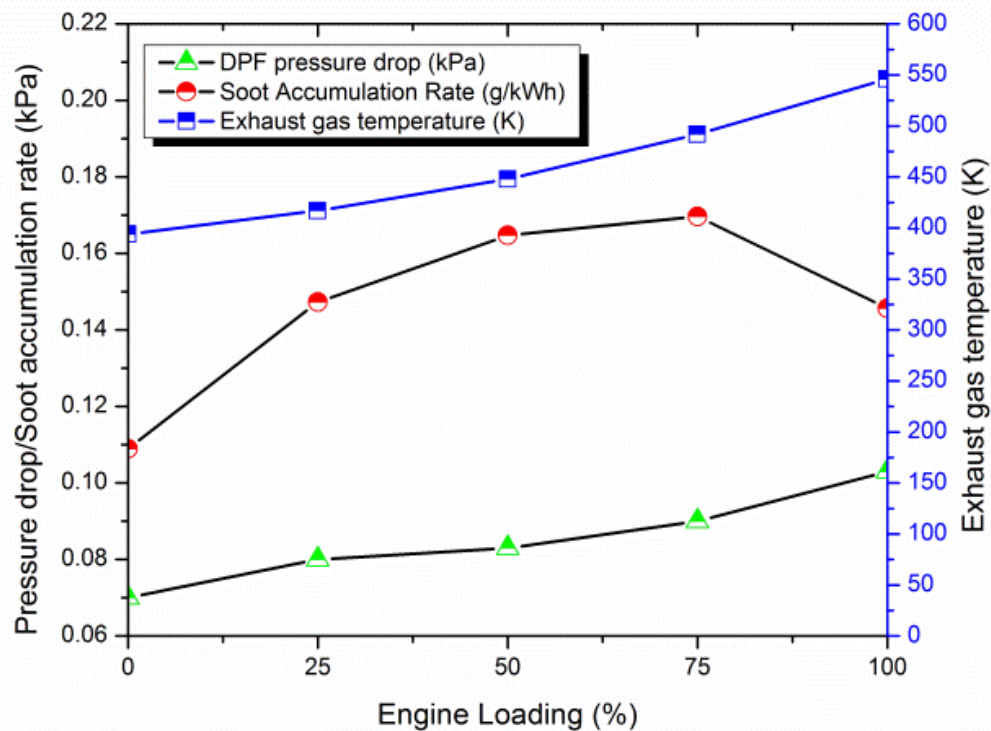
Figure 5.20. DPF soot accumulation rate, pressure drop and exhaust gas temperature at different engine loads

(a)

(b)
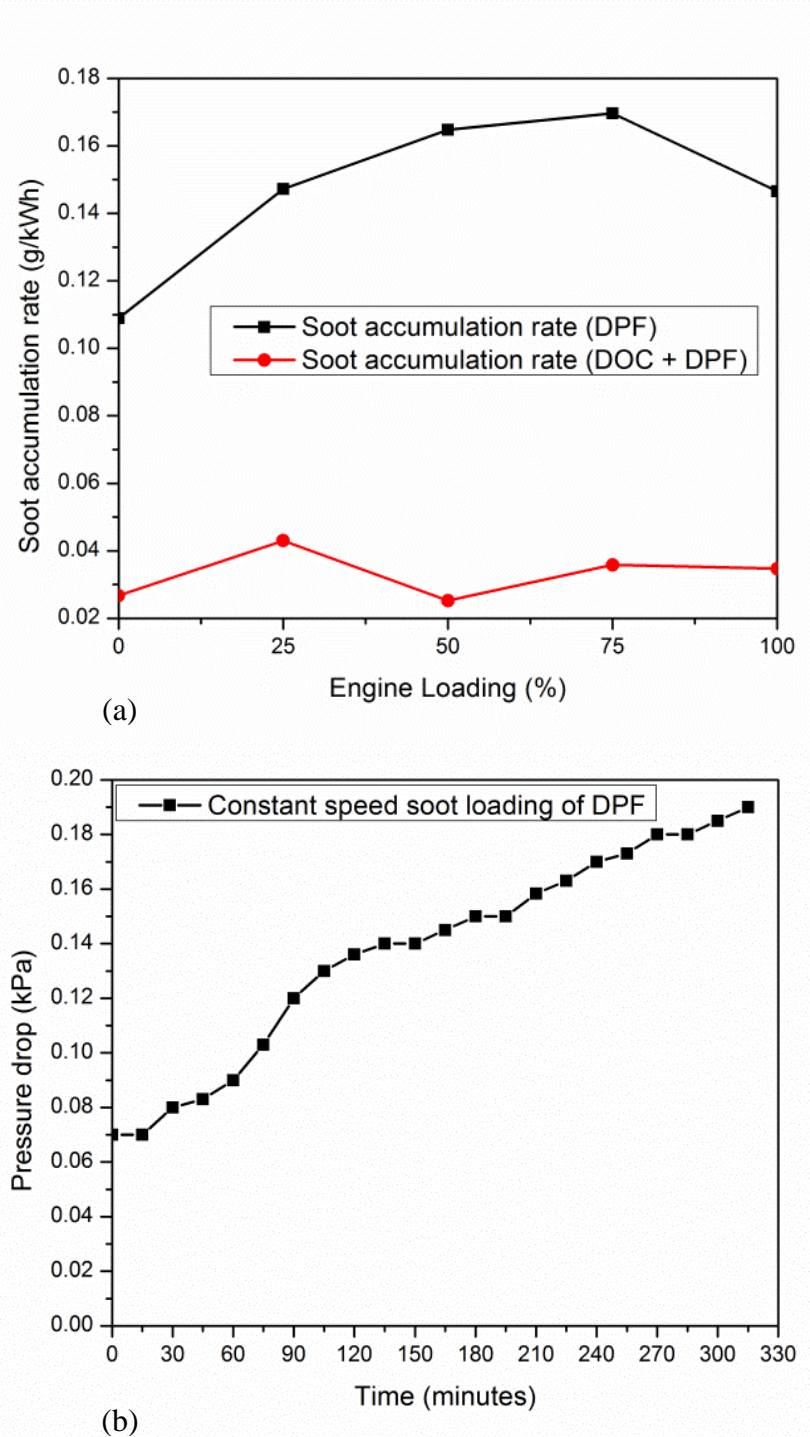
Figure 5.21. (a) Soot accumulation rate in DOC and DOC + DPF system (b) Pressure

drop across DPF at constant speed soot loading

In case of integrated DOC-DPF system, the pressure drop was reducing at higher loads, which shows that DOC assisted passive regeneration was taking place whereas at lower loads, pressure drop was higher than case 1 (DPF alone) due to the pressure loss across the DOC system. Soot accumulation rate in the DPF substrate was evaluated at different loads under steady-state conditions. The rate of soot accumulation was reducing at higher loads as shown in Figure 5.20, since the oxidation of the accumulated soot was taking place at higher exhaust gas temperature. Soot accumulation rate across the DPF during PTS system with DPF and DOC-DPF integrated system was compared as shown in Figure 5.21 (a), where it can be seen that there was an average reduction of 70% in the soot accumulation rate for the case of DOC-DPF integrated system, which indicates that continuous (passive) regeneration of the accumulated soot particles are taking place. Constant speed soot loading test was conducted on the DPF substrate to determine the rise in pressure drop and the results are as shown in Figure 5.21 (b).

5.5 CHARACTERIZATION OF DPF SUBSTRATE

Inverted Metallurgical microscope (Nikon-ECLIPSE MA200) imaging was used for capturing the uniformity of the soot layer formation pattern in the DPF substrate. The variation in functional groups of the DPF substrate after application in the engine test bench was evaluated using Fourier transform Infra-red Spectroscopy (FTIR, Perkin Elmer). FTIR analysis was conducted to determine the molecular composition of the sample by decoding the spectrum of infra-red radiations absorbed by the sample. FTIR sample was prepared using the standard procedure by preparing KBr (Potassium bromide) pellet with the substrate sample [171][172]. The intensity of particle size distribution in the DPF substrate before and after application in the engine test bench was determined using Particle Size Analyzer (Malvern ZEN1690). Particle size analyzer works by the principle of dynamic light scattering and has a

measurement range of 0.3 nm to 5 microns. The sample for PSA analysis was prepared by dispersing the substrate in ethanol solution by using an ultrasonicator. The chemical distribution and microstructure of the DPF substrate was examined using SEM-EDS (Scanning Electron Microscopy – Energy Dispersive X-Ray Spectroscopy) analysis. Formation of the soot layer in alternately plugged channels of the DPF was examined by comparing the microscopic images of the DPF substrate before and after application in diesel engine as shown in Figure 5.22. FTIR (Perkin Elmer, L1 2) analysis was conducted using the standard procedure (KBr pellet with substrate sample) for identifying the functional groups in the DOC and DPF substrate after application in the diesel engine exhaust line.
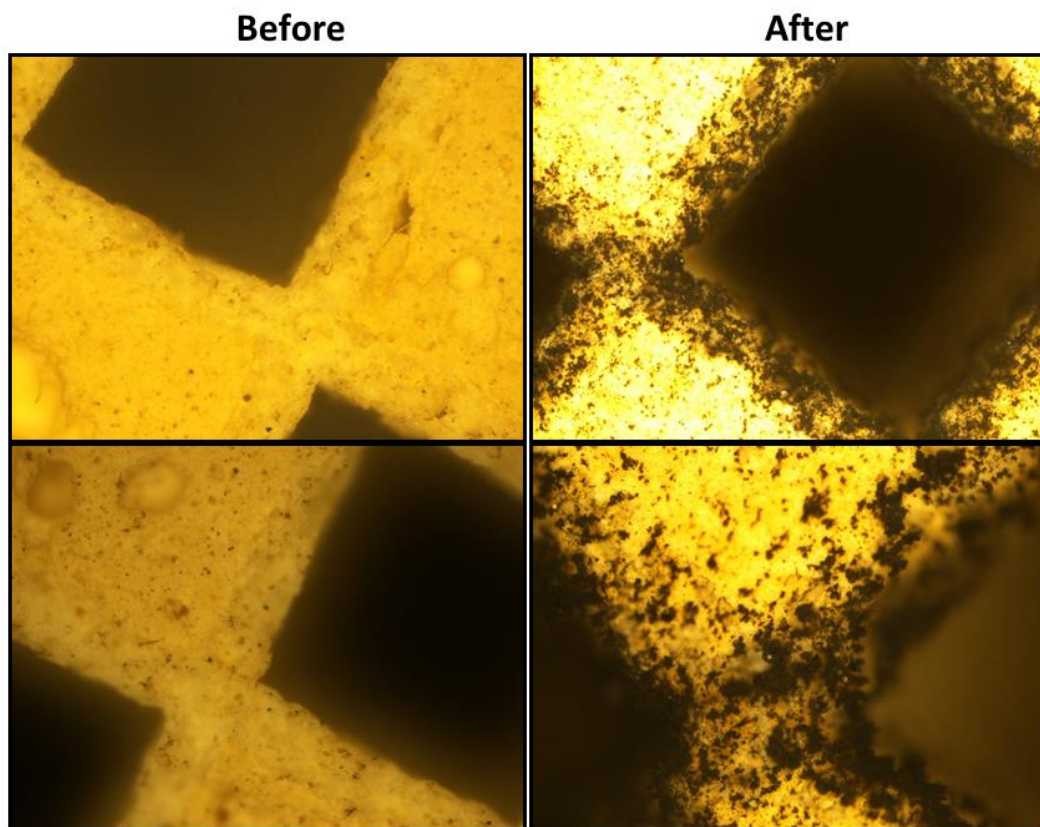
Figure 5.22. Microscopic images of 400 cpsi DPF substrate before and after application in engine exhaust
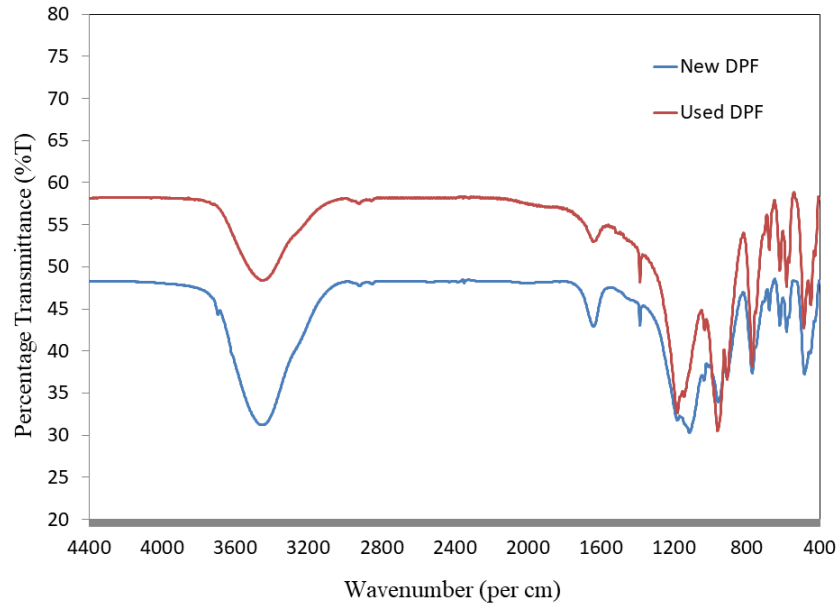
Figure 5.23. FTIR analysis of DPF substrate before and after application in engine exhaust
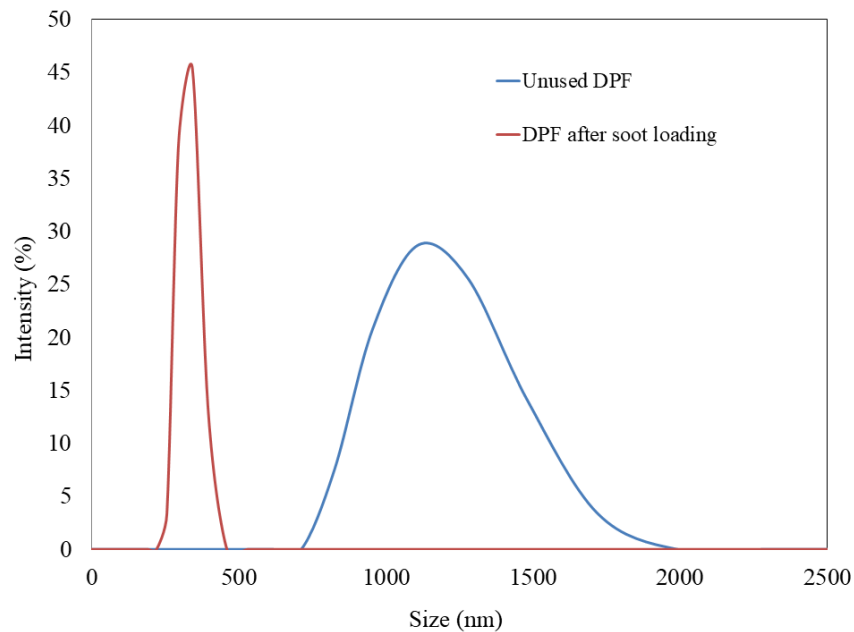
Figure 5.24. Particle size analysis data for average particle size distribution in DPF substrate, before and after application in the engine exhaust stream

Table 5.4. FTIR analysis for DOC and DPF substrate

Sl. No	Vibrational Energy (cm^{-1})	Functional group	Substrate
1	957	Anatase	DOC
2	768	Butanone	DOC
3	1179	Ethylene dichloride	DPF
4	1029	Butyne	DPF
5	447	Tetrachloro ethylene	DPF

As shown in Figure 5.23 and 4.13, variations in vibrational energies were mainly observed in two areas in the case of DOC and three areas in the case of DPF. Using the NIST (National Institute of Standards and Technology) FTIR library [185], functional groups were computed and are enlisted in Table 15. The functional group of ethylene dichloride detected in the FTIR plot of the used DPF substrate is observed to be grouped under the category, "Reasonably anticipated to be human carcinogens", with reference to the 14th report on carcinogens by National Toxicology Program [186]. Tetrachloroethylene detected in the FTIR report of the used DPF substrate is grouped by International Agency for Research on Cancer as, "2A probably carcinogenic to humans".

The intensity of the size distribution for particles in the DPF substrate after application in the emission control system was analyzed using particle size analyzer (Malvern ZEN1690) as shown in Figure 5.24. The results of the study showed that the intensity of particle size distribution was reduced in the case of DPF which shows the presence of trapped soot particles that are of lower size than that of substrate particle size.

Element	Weight %
O K	51.41
Mg K	7.34
Al K	16.47
Si K	24.78
Total	100
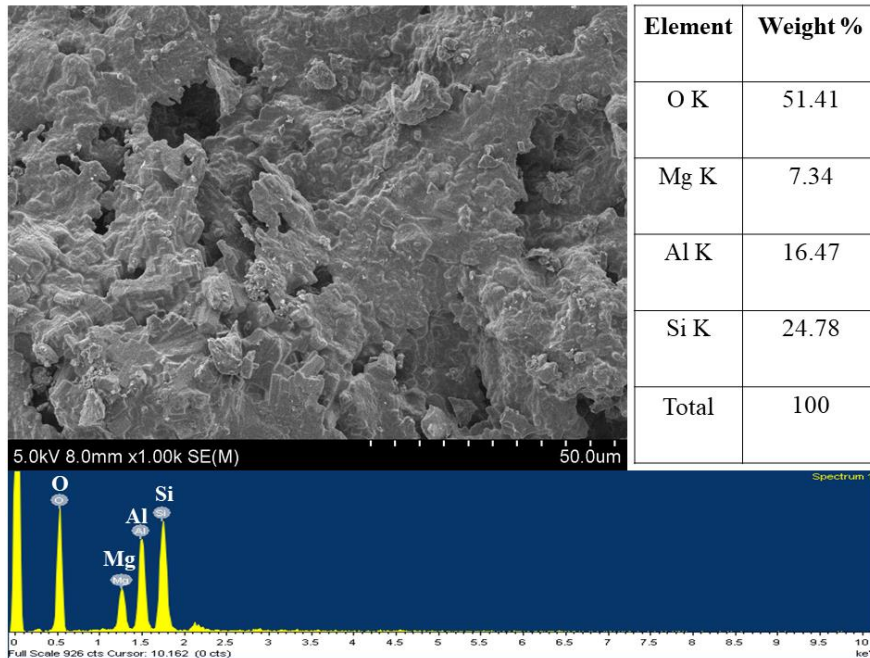
Figure 5.25. SEM images of the DPF cordierite substrate before soot loading with chemical distribution results of SEM-EDS spectra

Element	Weight %
C K	8.53
O K	48.57
Mg K	6.08
Al K	13.78
Si K	23.04
Total	100
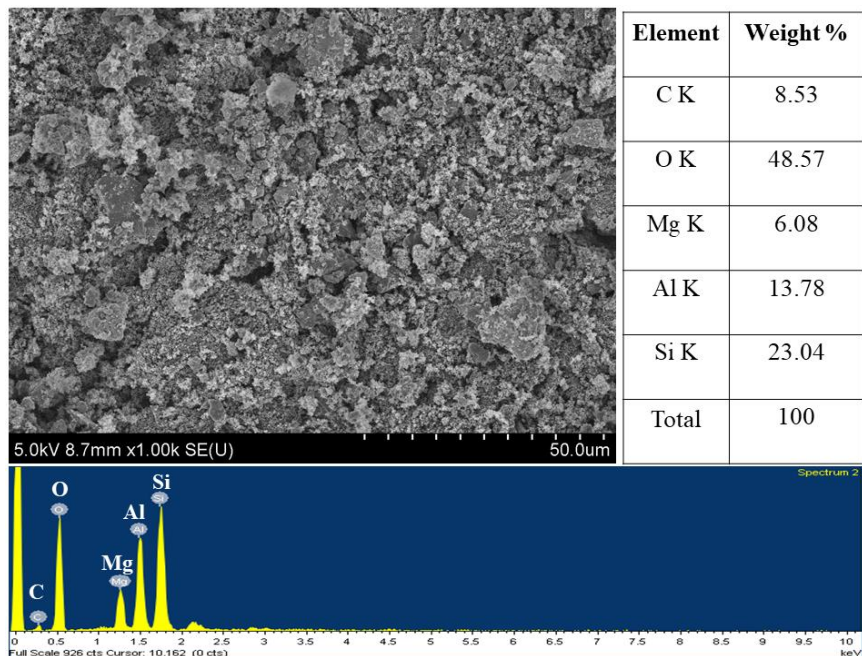
Figure 5.26. SEM images of the DPF cordierite substrate after soot loading with chemical distribution results of SEM-EDS spectra

100

The characterization of the microstructures in the DPF substrate was conducted using SEM-EDS analysis to reveal the physicochemical changes in the substrate after application in the engine exhaust. SEM-EDS results detailed the microstructure of the porous wall in unused DPF substrate along with the elemental maps as shown in Figure 5.25. The morphological characteristics of the accumulated soot particles were observed in the SEM-EDS results for the used DPF substrate as shown in Figure 5.26, where the carbon content of 8.53% was found indicating the presence of soot particles.

DOC substrate with best conversion efficiency with reference to the experiments conducted in chapter 4 was used for conducting experimental studies in this chapter, where the filtration efficiency of the integrated DOC-DPF system was investigated. Soot layer modelling, flow analysis, and soot accumulation rate in the DPF was also covered in this chapter. In continuation to the studies discussed in previous chapters, the modelling, computation study, fabrication and experimentation on microwave assisted composite regeneration system are discussed in chapter 6.

CHAPTER 6. DEVELOPMENT OF MICROWAVE ASSISTED COMPOSITE REGENERATION SYSTEM AND EXPERIMENTAL STUDY

Microwave radiations have gained its popularity in the food processing and chemical industry owing to its fast and volumetric heating properties [187]. The advantage of microwave radiations is that it heats the target material by volumetric heating whereas the conventional technique does it by surface heating [188]. Distribution of temperature with microwave heating can be predicted by the development of a mathematical model using electromagnetic and heat transfer equations. One dimensional analysis on power decay of radiations emitted by magnetron can be determined by analytical equations of Lambert's law [189]. Microwave radiations also don't require any medium for transferring energy from source to target material.

6.1 MICROWAVE HEATING PRINCIPLE

The major components of electromagnetic waves include electric field and magnetic field. Electric and magnetic field changes its position in space when a corresponding electric or magnetic charge in the medium changes its position [190]. The changes in electric and magnetic fields will result in the production of oscillatory waves named electromagnetic waves. Properties of electromagnetic waves are determined by its frequency, field strength, speed of light and wavelength [191]. Electromagnetic radiations were discovered in 1873 by Maxwell and the orientation of elements was established by right-hand thumb rule. The properties of electromagnetic waves can be related by equation no. 23, where 'c' = speed of light (m/s); 'f' = frequency (Hz) and 'λ' = wavelength.

$$c = f\lambda \tag{23}$$

Polarization of molecules in the frequency range between 300 MHz and 300 GHz will result in the heating of dielectric material. The penetration of microwave energy to the target material will result in molecular friction causing dipolar rotation of the molecules producing a volumetric distribution of heat. Major parameters determining the interaction of the electric field and material are dielectric constant and dielectric loss factor as shown in equation no. 24, where 'ε^*' is relative complex permittivity, 'ε'' is dielectric constant, which determines the ability of the material to store electric energy and ε'' is dielectric loss factor which determines the dissipation of electric energy to heat. The materials are classified into low loss and medium loss materials based on its dielectric loss tangent (tan δ) which can be determined by using equation no. 25. The electrical conductivity is given by equation no 26, where 'f' is the frequency (Hz) and 'σ' is the free space permittivity ($8.54 * 10^{-12}$ F/m) [187]. Power per unit volume (W/cubic m) required for conversion of the electric properties of microwave radiation for dissipation of power in a lossy material is given by equation no 27, where E is the electric field strength of the target material and f is the frequency in GHz [192].

$$\varepsilon^* = \varepsilon' - j\varepsilon'' \tag{24}$$

$$\tan\delta = \frac{\varepsilon''}{\varepsilon'} \tag{25}$$

$$\sigma = 2\pi f \varepsilon_o \varepsilon'' \tag{26}$$

$$P_v = 2\pi f \varepsilon_o \varepsilon'' E^2 \tag{27}$$

1-Dimensional microwave power dissipation inside the target material can be calculated using Lambert's law, which is a simplified approach without considering the electric field distribution. It assumes that the radiations incident on the material is normal to the surface and energy dissipated by the radiations are exponentially determined as stated in equation no.28, where 'F_o' is power flux at the surface (W/sq. m), 'd_p' is the penetration depth and 'z' is the spatial distance in the z-direction. The depth of microwave penetration is dependent on the dielectric properties of the material as shown in equation no 29 [191].

$$F = F_o \exp(\frac{-z}{d_p}) \tag{28}$$

$$d_p = \frac{C_o}{2\pi f}[2\varepsilon'((1+(\frac{\varepsilon''}{\varepsilon'})^2)^{0.5}-1)]^{-0.5} \tag{29}$$

The microwave heating of material by considering variations in electric and magnetic fields are governed by Maxwell equations. The relation between electric field intensity and magnetic induction is given by Faraday's law as shown in equation no 30, where E is electric field intensity, 'B' is magnetic induction, 'H' is magnetic field intensity, 'ω' is the angular frequency, 'μ_m' is permeability and 'ε' is the permittivity. The second governing equation is to determine the magnetic field intensity which is the sum of current flux and rate of change of electric displacement as shown in equation no 31, where J is current flux, The other two governing equations for finding the electric displacement (D) and magnetic induction (B) is as shown in equation no.32 [193].

$$\nabla E = -\frac{\partial B}{\partial t} = -\frac{\partial}{\partial t}(\mu_m \omega H(t)) \tag{30}$$

$$\nabla H = J + \frac{\partial D}{\partial t} = \sigma \omega E(t) + \frac{\partial}{\partial t}(\varepsilon \omega E(t)) \qquad (31)$$

$$\nabla.D = \nabla.\varepsilon E \text{ and } \nabla.B = 0 \qquad (32)$$

6.2 MODELLING AND ANALYSIS OF MICROWAVE ASSISTED REGENERATION SYSTEM (COMSOL MULTIPHYSICS)

6.2.1 Magnetron Port at Middle and Top of Oven Cavity

The heat transfer pattern during regeneration of diesel particulate filtration system was studied using CFD software COMSOL Multiphysics [193]. The filter substrate of the diesel particulate filtration system was made of cordierite based ceramic material and its associated properties have been recorded in Table 6.1.

The filter substrate was contained in a metallic box made of GI sheet which acts as the oven cavity and whose dimensions are 26.7 cm × 27 cm × 18.8 cm. Microwave radiations were introduced into the oven cavity by placing a magnetron port in one of the faces of the box. The frequency of the excitation wave was 2.45 GHz and the port input power was 1 kW. The prime objective of this simulation study was to determine the pattern of electric field distribution and temperature distribution in the oven cavity with a cordierite filter substrate at its center. Magnetron port was assumed to be a rectangular waveguide operating at the TE10 mode. The initial temperature of the filter was assumed to be 50 °C and the simulations were carried out for 120 seconds post-excitation. For studying the microwave excitation, the frequency domain modules of electromagnetic waves were selected with steady-state conditions. Module for heat transfer in solids was selected in Time-Dependent mode to study the temperature rise in the DPF.
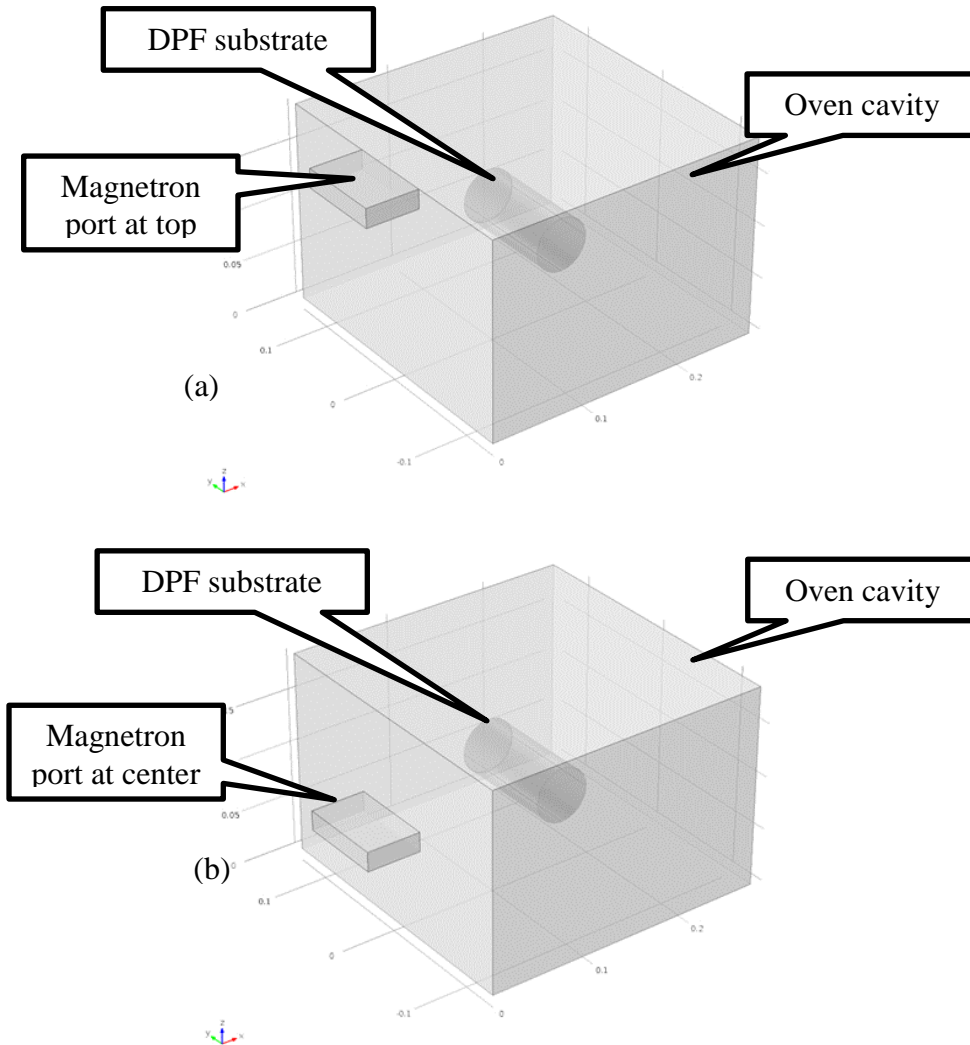
Figure 6.1. (a) Model of the microwave-based emission control system with magnetron port at the top. (b) Model of the microwave-based emission control system with magnetron port at the center

Two models were considered in this study for determining the temperature distribution and electric field distribution inside the oven cavity of the microwave-based regeneration system. One with the magnetron port located at the top of the oven cavity and the other with the port located at the center of the wall as shown in Figure 6.1 (a) & (b), respectively. The study

solves the electromagnetic field in the box and the corresponding temperature by coupling Maxwell's equations and the general energy transport equation for temperature. The mesh for solving the numerical equations has been generated automatically using one-fifth of the wavelength for the electromagnetic wave as the maximum mesh element control parameter. The contours of electric field distribution after the steady-state simulation of microwave excitation from the magnetron for both cases with the port located at top and center are as shown in Figure 6.2 (a) and (b).

It can be inferred that the distribution of the electric field is more uniform in the case where the port was located at the center. The uniformity of the electric field makes the second case, the one with waveguide port at the center as a more effective alternative for microwave-based regeneration system. The temperature distribution for both the cases mentioned above can be observed in Figure 6.3 (a) and (b). It can be seen that the temperature distribution pattern (owing to the difference in electric field distribution) for both the cases are different, but there are only negligible changes in the magnitude of temperature for both cases. This can be attributed to the fact that cordierite has low sensitivity towards microwave excitation. Also, the temperature drop in 120 seconds is relatively low due to the high heat capacity of cordierite. Hence, with these observations in mind, it can be concluded that the ceramic cordierite based filter substrate is the most suitable material for the development of an emission control system with microwave-based regeneration since it is transparent to microwave radiations. Development of a system that will burn only the accumulated soot particles without causing any damage to the filter substrate will be an effective alternative for a fuel-based regeneration system. Theoretical study on the effectiveness of the microwave-based regeneration system was conducted in this work by modelling and conducting simulations by creating a virtual environment in CFD software COMSOL Multiphysics.
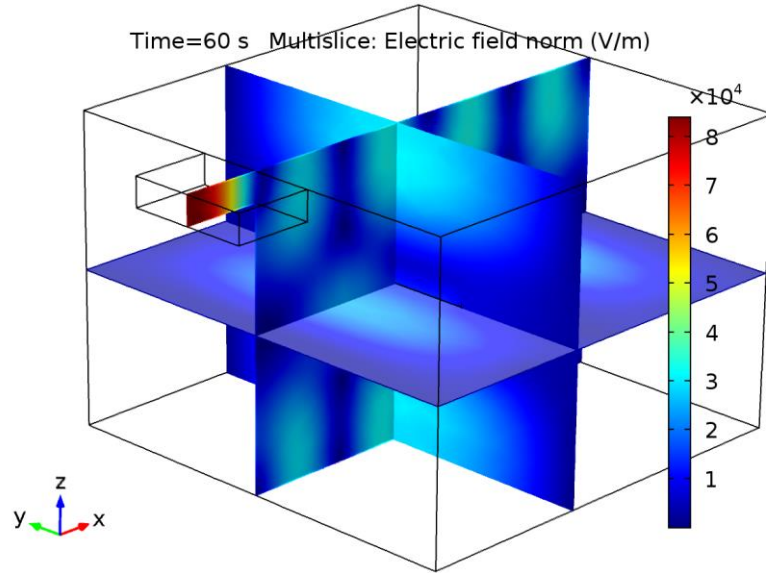
(a)
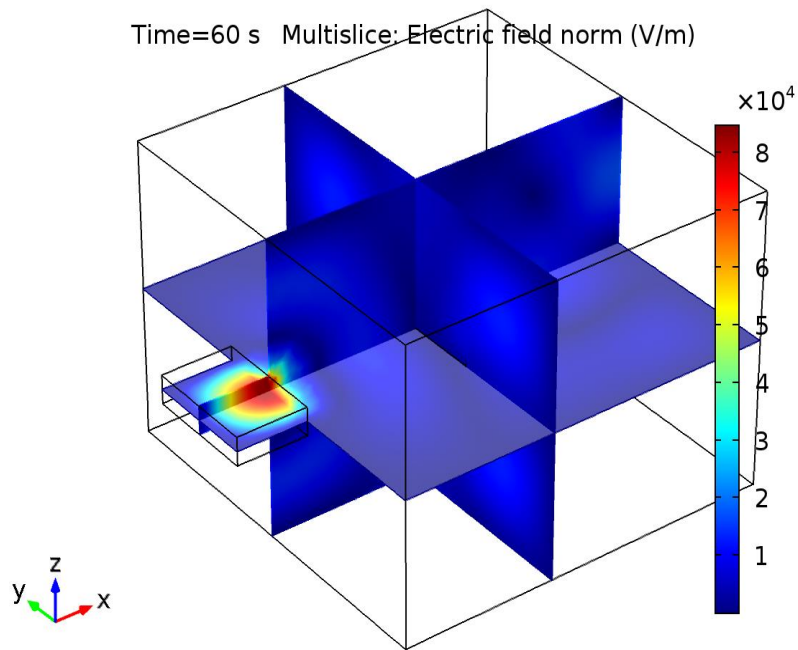
(b)

Figure 6.2. (a) Contour of electric field distribution in different planes for microwave-based emission control system with magnetron port at the top, (b) Contour of electric field distribution in different planes for microwave-based emission control system with magnetron port at the center
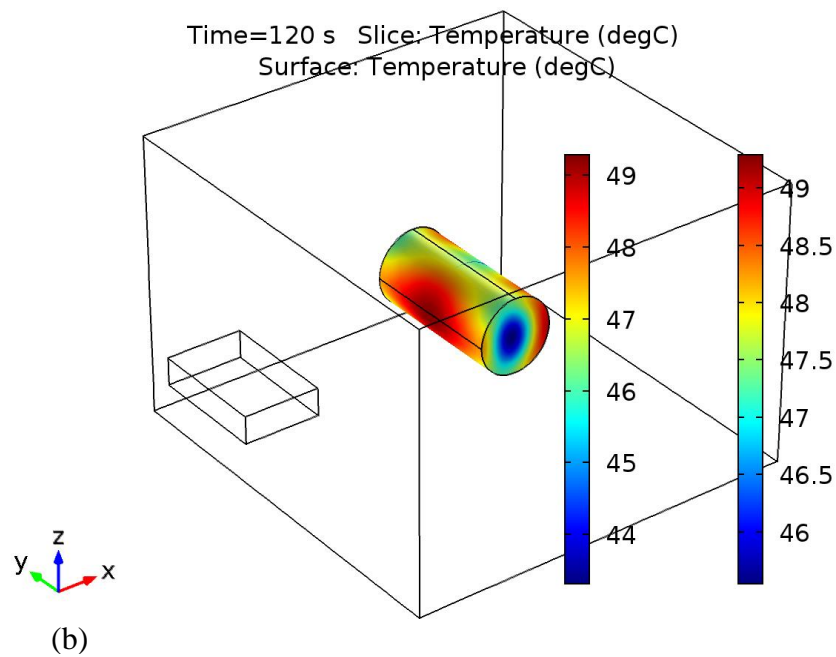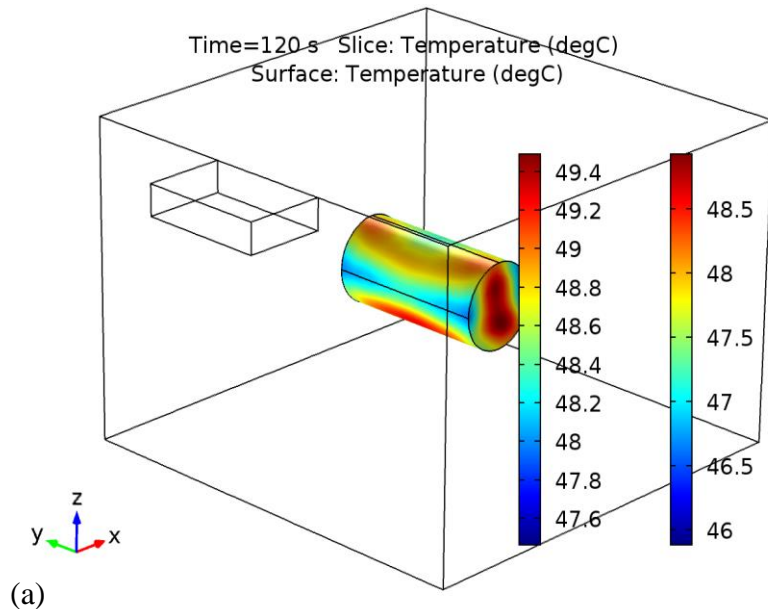
Figure 6.3. (a) Contour of temperature distribution in filter substrate of the microwave-based emission control system with magnetron port at top (b) Contour of temperature distribution in filter substrate of the microwave-based emission control system with magnetron port at the center

A comparative study on the electric field distribution in the system with magnetron port at top and center was conducted to determine the effective position for uniform distribution of the electric field inside the oven cavity. The contours of electric field distribution showed that the electric field distribution is uniform in the case of the model with a magnetron port at the center. The results of the simulation showed that the ceramic cordierite based filter substrate is transparent to the microwave radiations since there was no appreciable rise in the temperature of the filter substrate. Hence the theoretical validation of the proposed microwave-based regeneration system was done.

6.2.2 Heat Distribution in DPF Substrate

COMSOL Multiphysics software is used for modelling of heat transfer during microwave-based regeneration of diesel particulate filter. The filter substrate is modeled by providing the properties of soot and cordierite to alternate layers as shown in Table 6.1. The model of the regeneration system with an oven cavity was developed with a magnetron port in the middle of the cavity allowing radiation to enter in the radial direction of exhaust gas flow as shown in Figure 6.4. The port of the magnetron is assumed to be rectangular waveguide operating in at TE10 mode and the frequency of excitation is taken to be 2.45 GHz with a port input power of 1 kW. Steady-state conditions were selected for the electromagnetic waves and the time-dependent mode was selected for heat transfer in solids for monitoring the temperature rise in DPF substrate.

Temperature and electric field distribution in the DPF substrate with alternate layers of soot and cordierite for different regeneration times were studied with the help of CFD software COMSOL MULTIPHYSICS. Simulations were conducted for different regeneration times ranging from 30 to 180 seconds (30 seconds interval), to determine the temperature rise in the DPF substrate. The contours of temperature distribution in the microwave

110

regeneration system for 180 seconds of regeneration are shown in Figure 6.5. Temperature rise in the DPF substrate for 180 seconds at intervals of 30 seconds is as shown in Figure 6.6 (a). A maximum temperature of 800 K was attained after 180 seconds of regeneration and the average distribution of temperature was close to 700 K. Isothermal contours of the DPF substrate generated after 180 seconds of microwave regeneration in DPF are as shown in Figure 6.6 (b).
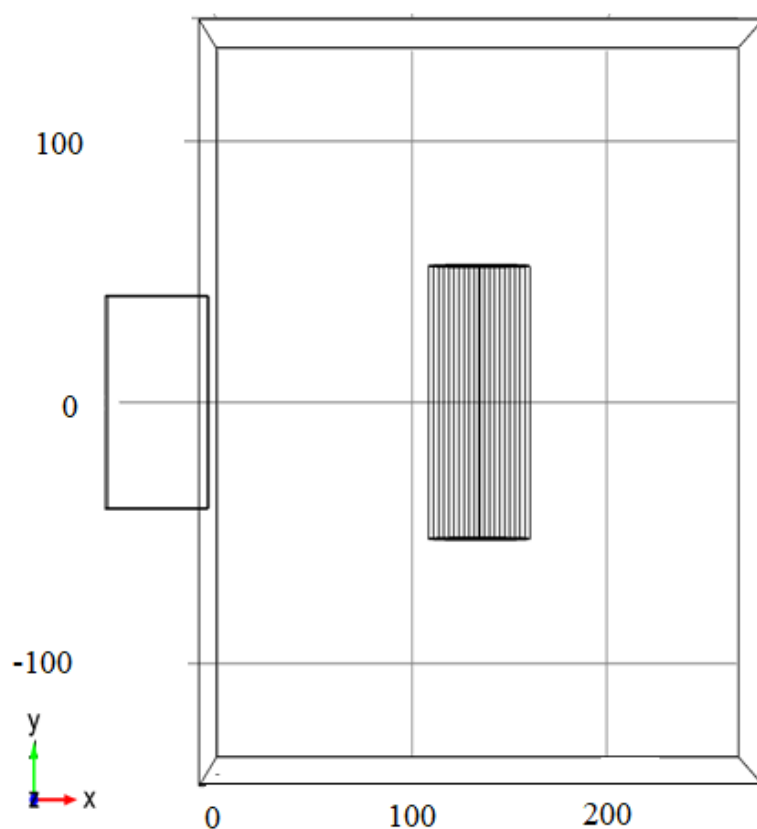
Figure 6.4. Top view of the microwave-based emission control system with magnetron port at the center

Table 6.1. Properties of Cordierite and soot considered for regeneration modelling

Properties	Cordierite	Soot
Relative Permeability	1	1
Relative Permittivity	2.9 + 0.14j	10.7-3.6*j
Electrical Conductivity, S/m	0	0.025
Thermal Conductivity, W/m-K	3.0	0.041
Density, kg/ m^3	2600	1800
Heat Capacity, J/kg-K	1465.38	840

The oxidation of soot takes place at temperatures above 873K, which can be attained by the combined effect of heat energy from microwave radiations and exhaust gas. Model of microwave-assisted active regeneration system was proposed in this study and CFD analysis of the proposed model was conducted using COMSOL MULTIPHYSICS 5.4 software. Simulation results showed that microwave radiations can raise the temperature of the accumulated soot particles close to its soot oxidation temperature and assistance of the heat energy supplemented by the exhaust will ensure complete regeneration of the accumulated soot particles. Based on the obtained results it can be concluded that the microwave regeneration system is a promising technique for the regeneration of accumulated soot particles in the

DPF filter walls and for minimizing the toxicity levels of engine exhaust emissions. The initial temperature of the system was assumed to be at room temperature for the simulation purpose whereas in actual case the exhaust gas temperature will also add to the initial temperature of the substrate.
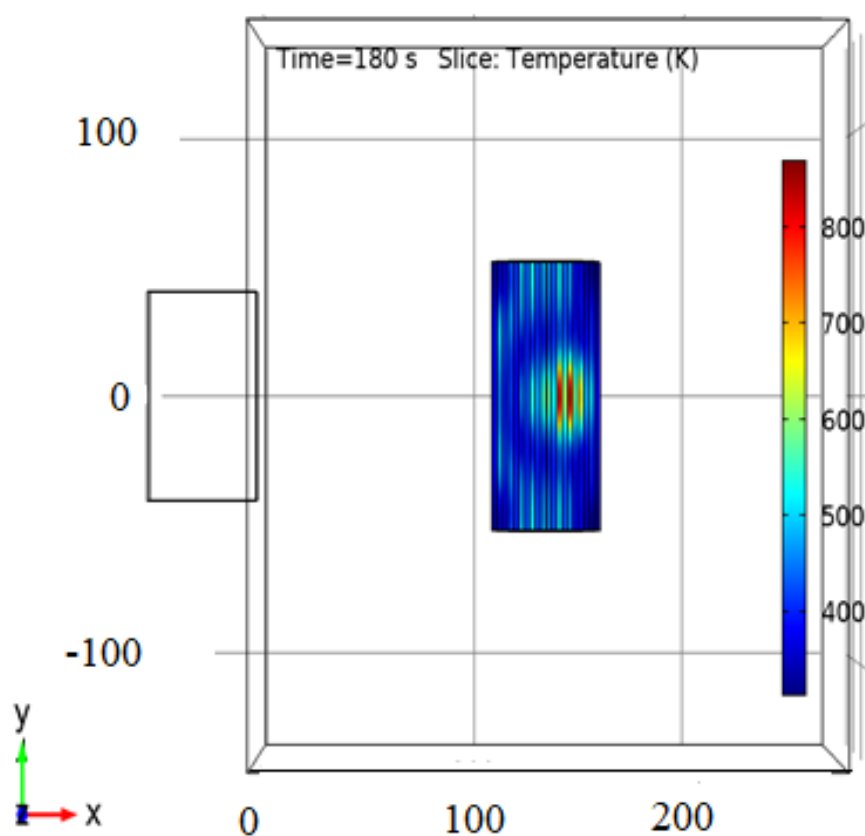
Figure 6.5. Contours of temperature distribution in microwave regeneration system for 180 seconds of regeneration
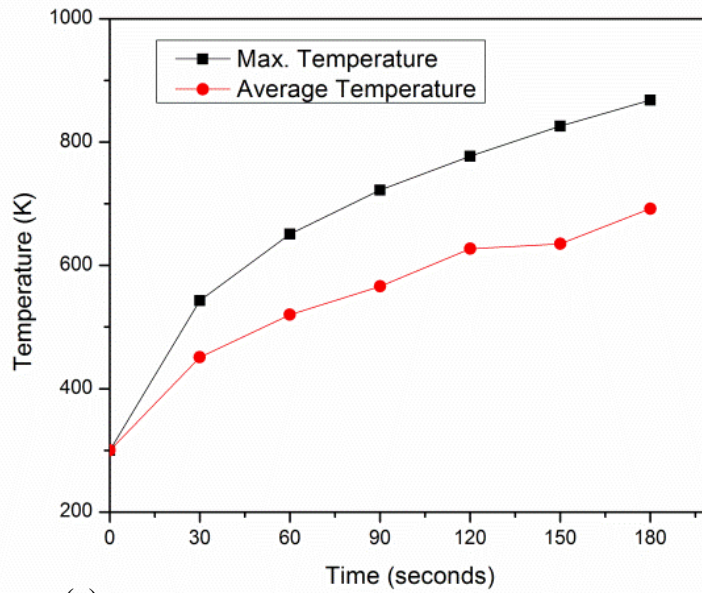
(a)
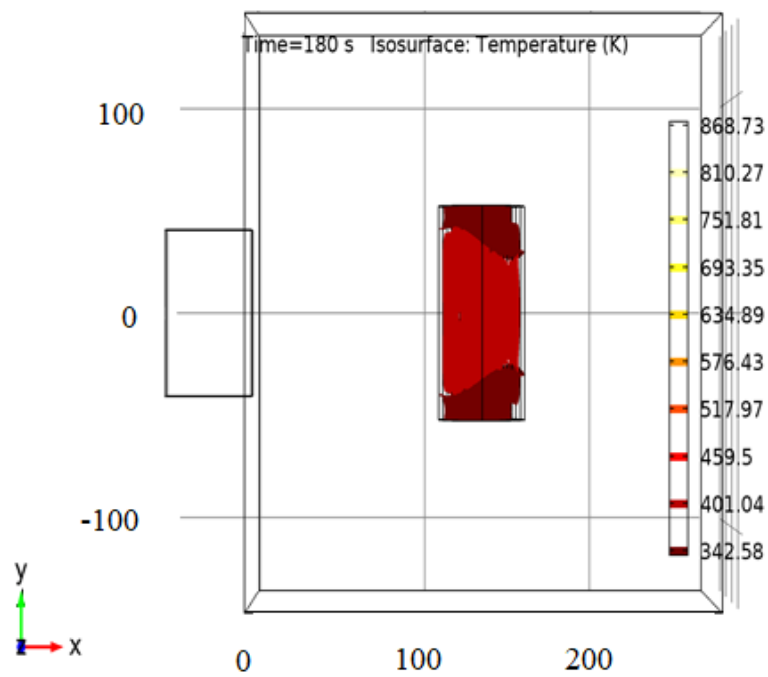
(b)

Figure 6.6. (a). Temperature rise in DPF substrate after 180 seconds of regeneration
(b) Isothermal thermal contour of DPF substrate after 180 seconds of regeneration

6.3 MODEL OPTIMIZATION TO IMPROVE HEAT DISTRIBUTION IN DPF

The microwave regeneration system was remodeled and simulations were repeated to improve the performance of the system by reducing the size of the oven cavity (14 cm × 14 cm × 22.5 cm) and power rating of magnetron port. Heat transfer and temperature distribution during microwave-based regeneration were modeled using COMSOL Multiphysics software. The properties of the soot and cordierite were defined to alternate layers in the DPF substrate as shown in Table 6.1. Magnetron inlet port to the oven cavity was assumed to be rectangular waveguide with an excitation frequency of 2.45 GHz. Inlet port to the oven cavity was placed at the center and microwave radiations were allowed to enter the oven cavity in the radial direction as shown in Figure 6.7 (a). Physics controlled fine mesh (max. element size: 37.4 μm and min. element size: 1.12 μm) was generated in the substrate for computational study as shown in Figure 6.7 (b). The temperature rise of the substrate was evaluated for a different output power of magnetron port ranging from 100 to 700 Watts for time duration of 175 seconds. Governing equations for microwave heating of the material due to variation in the electric and magnetic fields are Maxwell equations as shown in equation no. 33 to 34.

$$\nabla E = -\frac{\partial B}{\partial t} = -\frac{\partial}{\partial t}(\mu_m \omega H(t)) \tag{33}$$

$$\nabla H = J + \frac{\partial D}{\partial t} = \sigma \omega E(t) + \frac{\partial}{\partial t}(\varepsilon \omega E(t)) \tag{34}$$

Temperature rise in the DPF substrate with alternate layers of soot and cordierite was evaluated by conducting simulations in CFD software COMSOL MULTIPHYSICS. Heat transfer in the DPF substrate was

115

monitored by defining time-dependent mode and electromagnetic radiations were produced under steady-state conditions.

(a)

(b)
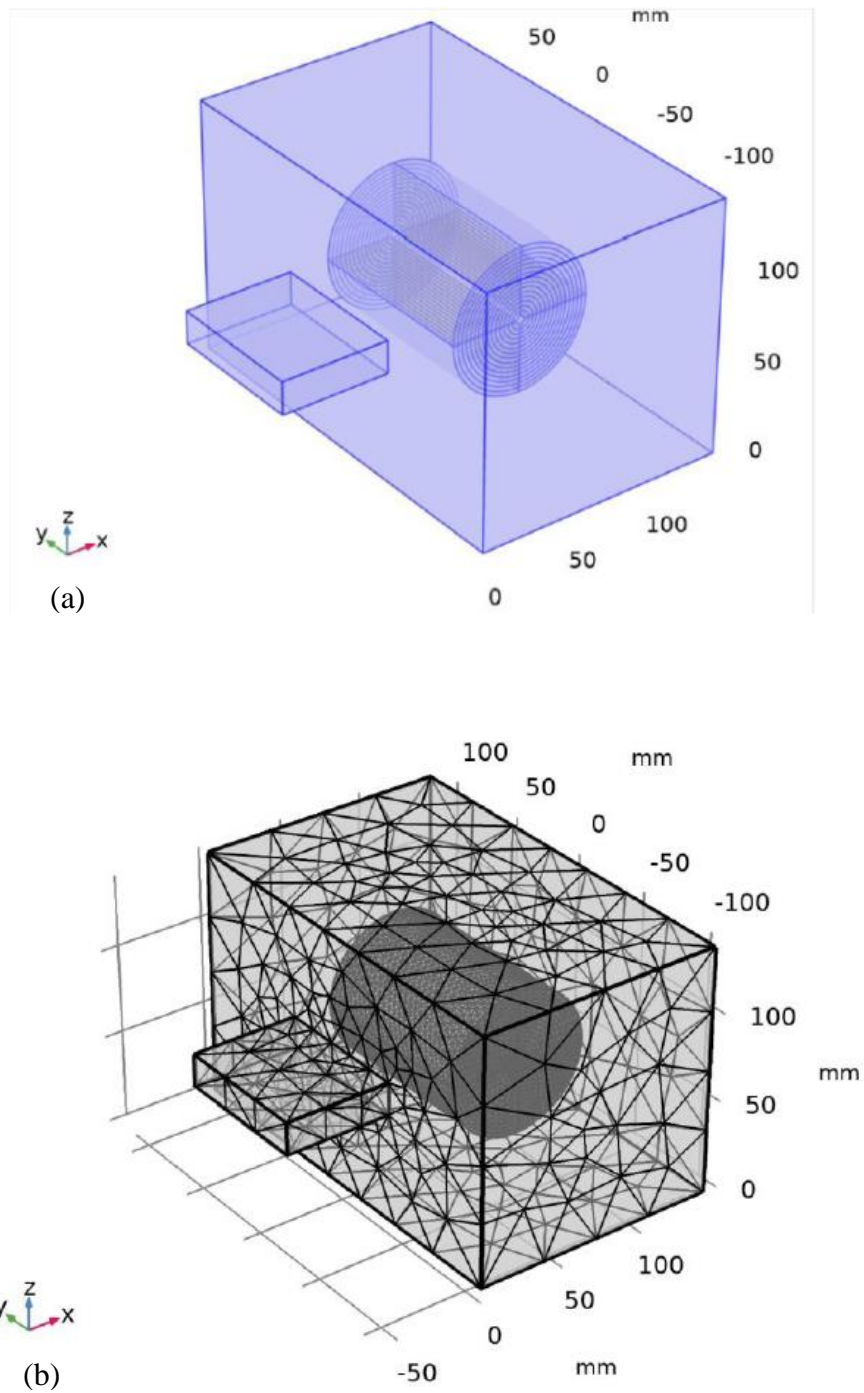
Figure 6.7. (a). Microwave based regeneration system CAD model (b). Meshed model of the microwave-based regeneration system
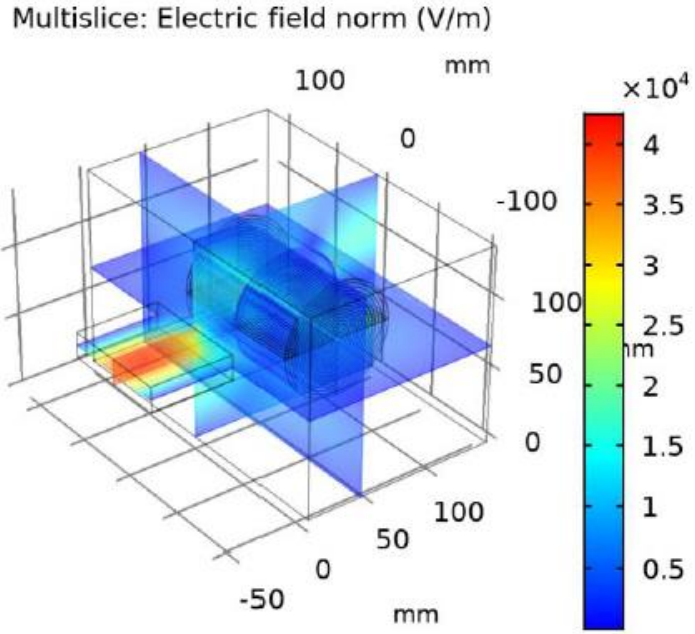
Figure 6.8. Contours of electric field distribution in the microwave regeneration
system after 175 seconds of regeneration at a power rating of 700 W
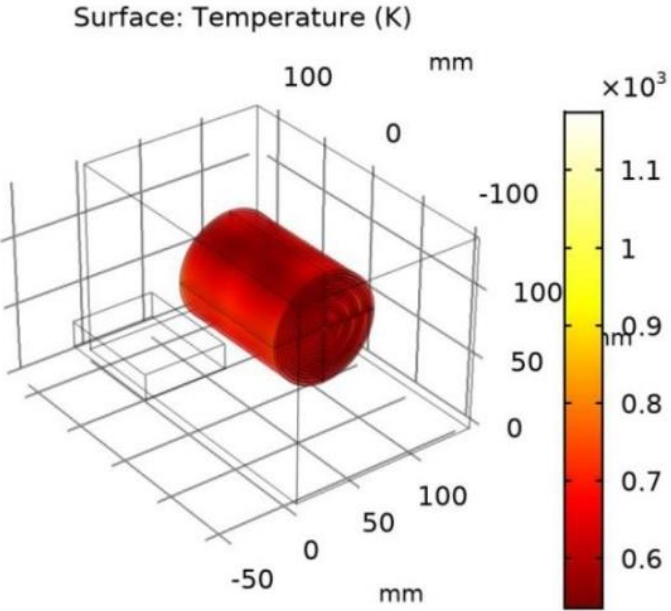
Figure 6.9. Contours of temperature distribution in the microwave regeneration
system after 175 seconds of regeneration at a power rating of 700 W
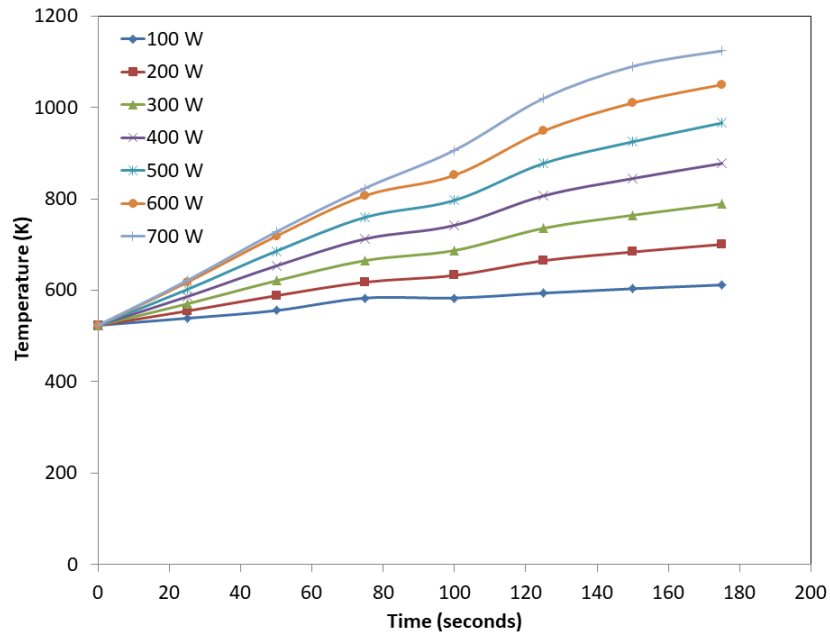
Figure 6.10. Temperature rise in DPF substrate after 180 seconds of regeneration
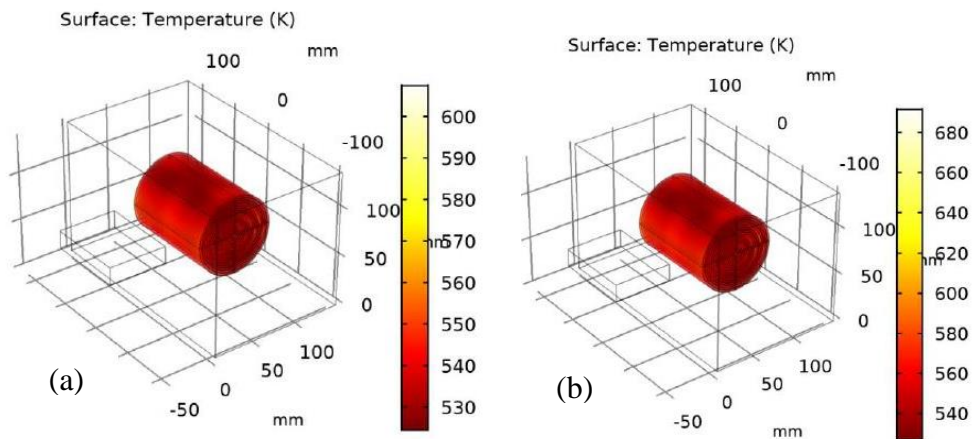
Figure 6.11. Contours of temperature distribution in microwave regeneration system after 150 seconds of regeneration at power rating of (a) 100 W and (b) 200 W
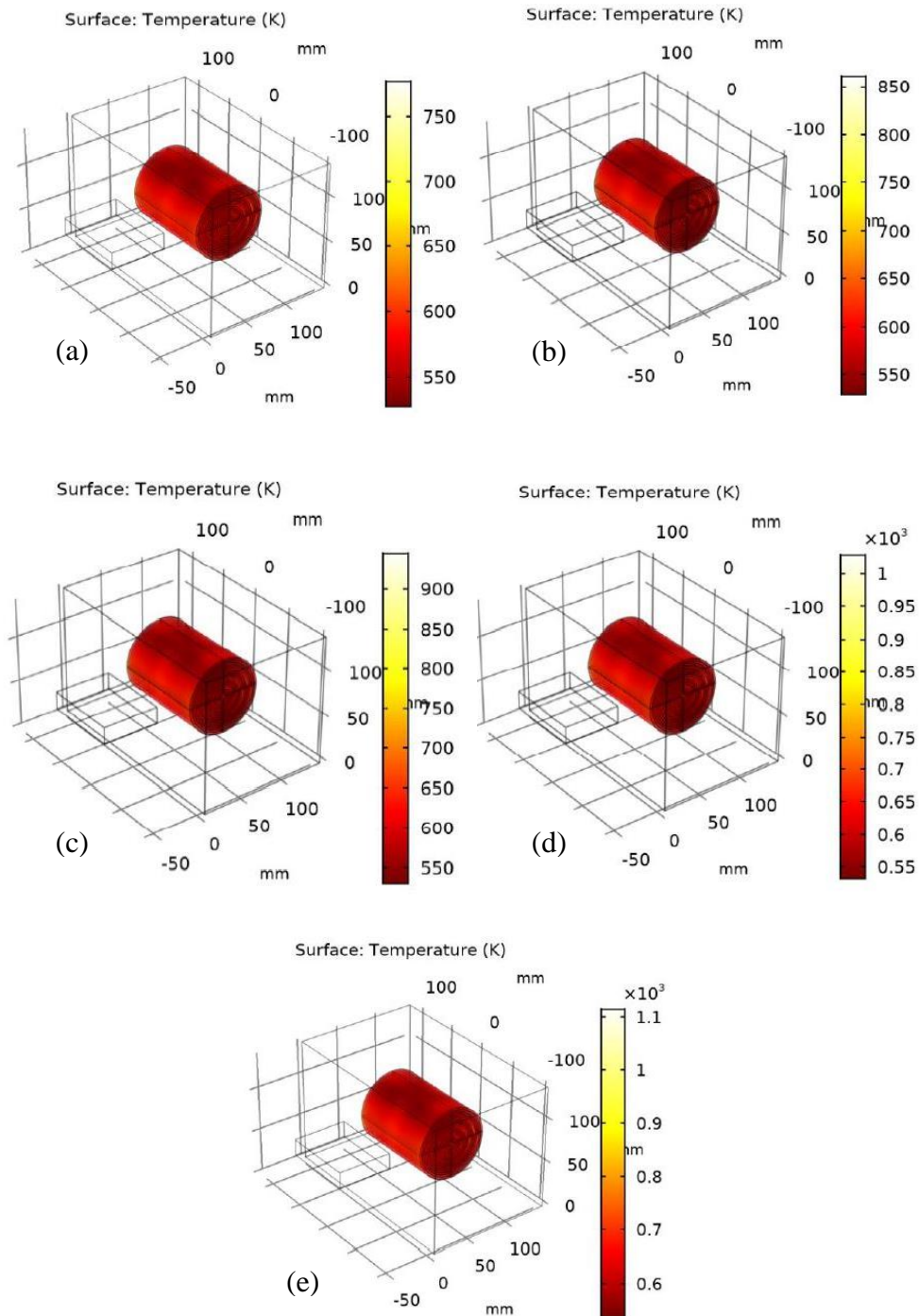
Figure 6.12. Contours of temperature distribution in microwave regeneration system after 150 seconds of regeneration at power rating of (a) 300 W (b) 400W (c) 500W (d) 600 W and (e) 700W

119

Simulations were carried out for a time period of 200 seconds (25 seconds interval) at different magnetron port power ranging from 100 W to 700 W. The system was assumed to be at room temperature (298 K) at the initial state for the simulation purpose and maximum temperature of 1100 K was reached in the substrate after regeneration time of 175 seconds at power rating of 700 W. The contour maps of electric field and temperature distribution in the microwave system for regeneration time of 175 seconds are shown in Figure 6.8 and 6.9. The maximum temperature rise in the DPF substrate for different regeneration time at port power ranging from 100 to 700 W is as shown in Figure 6.10. The soot oxidation temperature is 873 K and the maximum temperature achieved in the simulation results is much higher than 873 K, hence the power rating of the magnetron input power can be reduced for the experimental analysis. The soot oxidation temperature was achieved lowest in the case of 400 W input power after 150 seconds of regeneration. The contour of temperature distribution in the DPF substrate after 150 seconds of regeneration for the power rating varying from 100 to 700 Watts is as shown in Figure 6.11 and 6.12. Iso-surface temperature contours for microwave regeneration are detailed in Annexure IV.

6.4 FABRICATION OF MICROWAVE ASSISTED REGENERATION SYSTEM

Stringent emission regulations have made it a mandated requirement to retrofit particulate filter based emission control systems to reduce the particulate matter emissions from compression ignition engines. The particulate filter has a ceramic monolith substrate with alternately plugged straight channels. The exhaust gas enters the substrate through the unplugged filter channels in the inlet side and will be forced to flow through the porous filter wall where the soot particles will be trapped by depth filtration. As the soot particles start accumulating along the porous wall, the pressure drop across the filter

substrate starts increasing. The thickness of the soot deposition layer increases with time and after a certain limit, the accumulated soot layer acts as a medium for trapping soot particles, which is referred to as cake filtration.
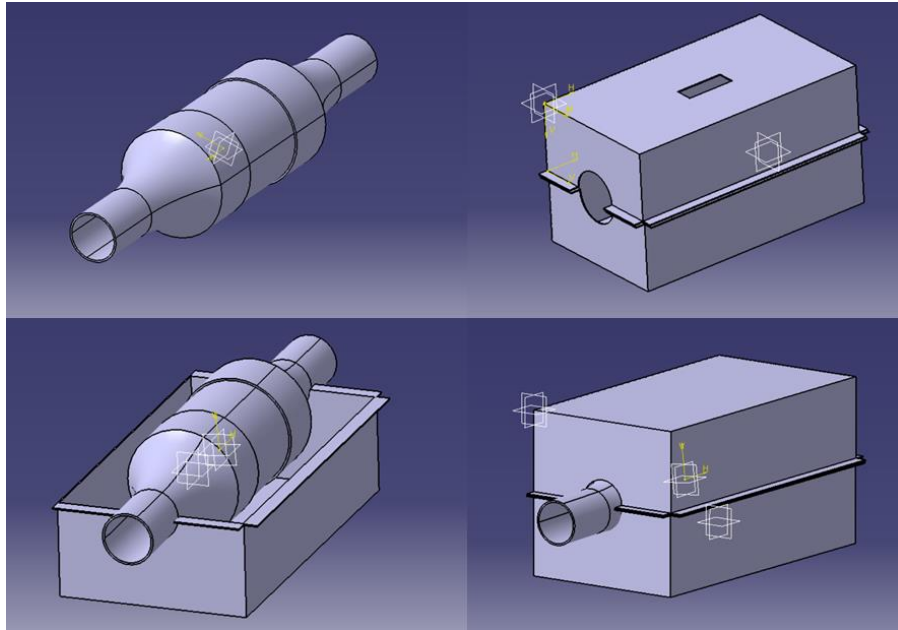
Figure 6.13. CAD model of the CRS system

When the filtration process undergoes a transition from depth filtration to cake filtration, there will be a higher pressure drop across the substrate resulting in backflow affecting engine performance. Accumulated soot particles have to be regenerated at regular intervals to avoid the rise in backpressure. The existing fuel-based regeneration technique involves the injection of fuel into the filter substrate where spontaneous combustion takes place due to the heat provided by exhaust gas. Fuel based regeneration is leading to uncontrolled combustion inside the filter substrate which is affecting the service life of the filter substrate by causing catastrophic failure. Alternate microwave-based regeneration is developed in this work, which can selectively burn the accumulated soot particles without affecting the filter substrate.

The developed device is a composite regeneration system (CRS) that uses electromagnetic radiations in the microwave region for selective burning of the accumulated soot particles in the filter channels. The model of the microwave-assisted regeneration system developed in this work is shown in Figure 6.13. The oven cavity is made of galvanized iron sheet and the inside surface of the oven cavity is coated with mica sheets and nitrile rubber layers to insulate the microwave radiations as shown in Figure 6.14. The wiring diagram for the CRS system is as shown in Figure 6.15. Metal lofts are coated with polyamide heat resistant tape and nitrile rubber layer to yield the microwave radiations so that chances for sparks can be avoided as shown in Figure 6.16. Oven cavity and DPF system are developed in such a way that only the filter substrate is exposed to microwave burning and all other parts are insulated with shielding materials to avoid sparks and uncontrolled burning.
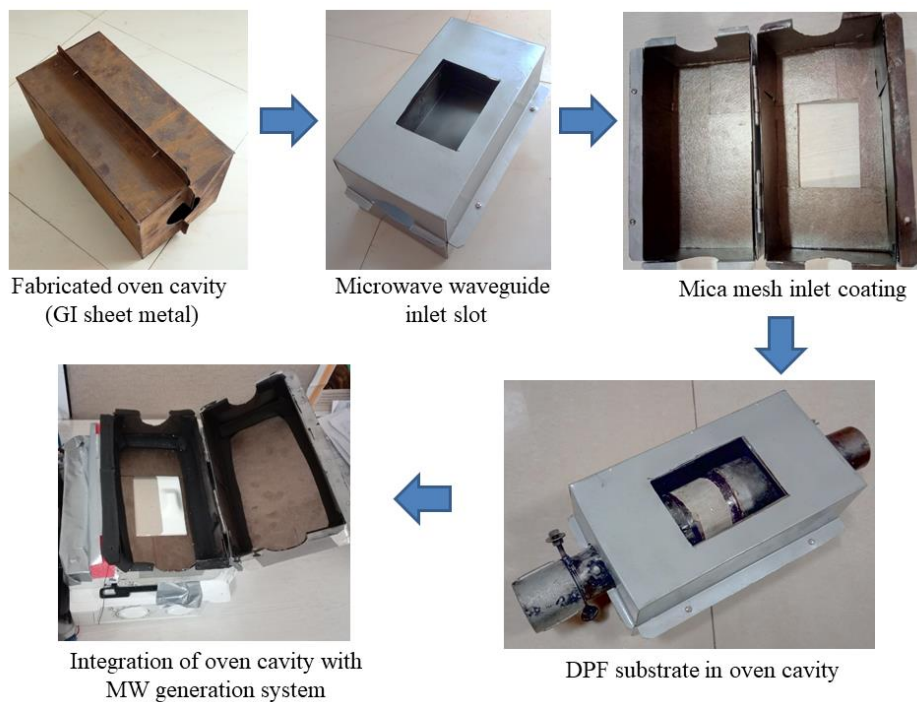
Figure 6.14. Fabrication of oven cavity in the Composite Regeneration (CR) system
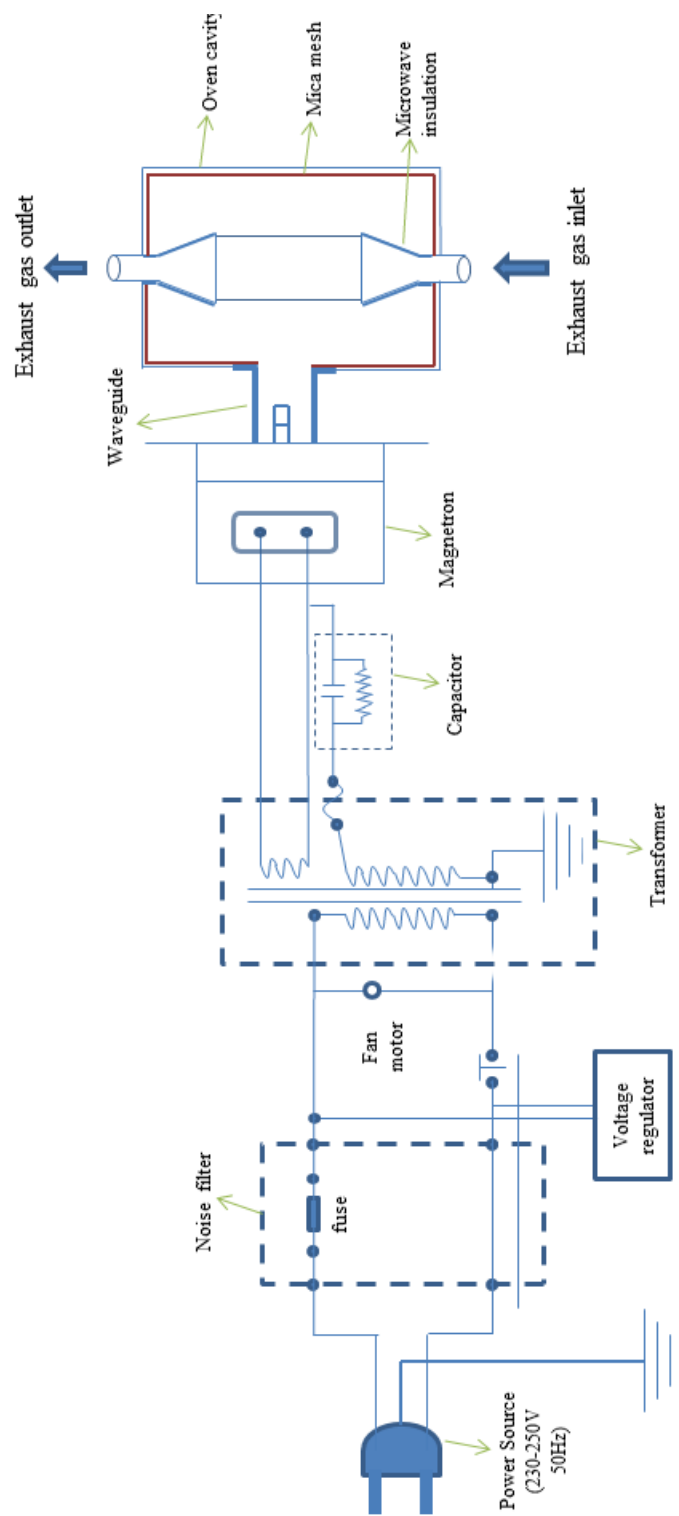
Figure 6.15. Electrical wiring diagram of the system
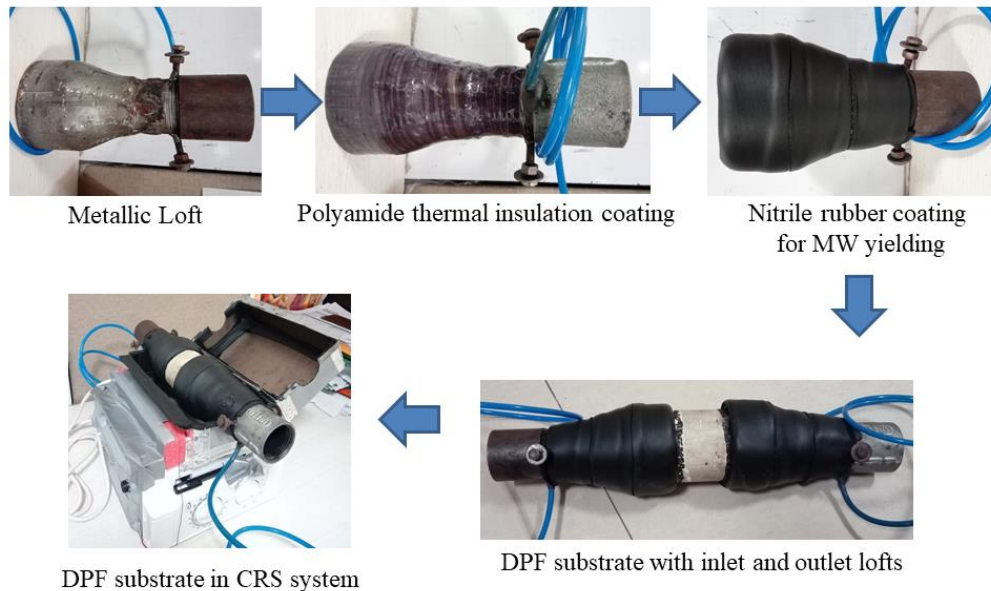
Figure 6.16. Microwave yielding material coating in the metal cavity

Microwave radiations can penetrate the filter substrate and can selectively burn the soot particles owing to its dielectric properties. Cordierite ceramic filter substrate has good permeability which allows microwave radiations to pass through without any heating effects whereas the soot particles get heated up by dielectric heating. Components of the device include the oven cavity (stainless steel coated in internal surface with mica sheet), magnetron, high voltage transformer, high voltage capacitor, cooling fan, voltage regulator, timer and waveguide as detailed in Figure 6.17 and 6.18. Power source microwave radiations are produced in this system with the help of a magnetron. Magnetron requires higher voltage for the generation of microwave radiations; hence transformer is used to amplify the electric signal to a higher voltage which is maintained consistently using a high voltage capacitor. Microwave radiations generated by the magnetron are directed to the oven cavity through a rectangular waveguide. DPF (Diesel Particulate Filtration) system comprising of the metal lofts and ceramic filter substrate are enclosed inside the oven cavity.

Side view

- Oven cavity
- Front panel (Voltage regulator and timer)
- Magnetron
- Fan
- High Voltage Capacitor
- High Voltage Transformer
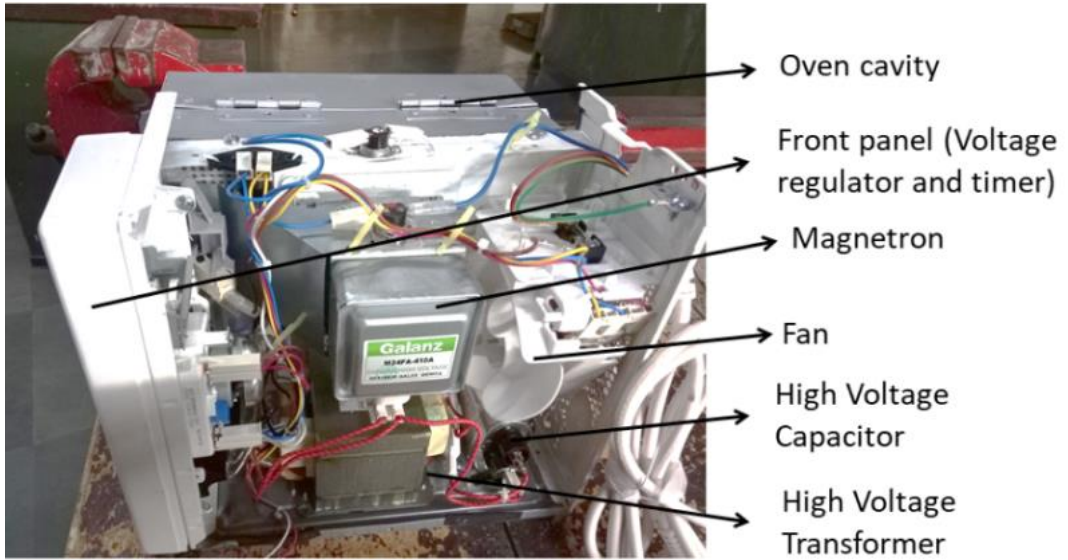
Top view   **Front view**

Oven cavity   Magnetron   Voltage regulator   Timer

Figure 6.17. Side view, top view and front view of fabricated CRS system
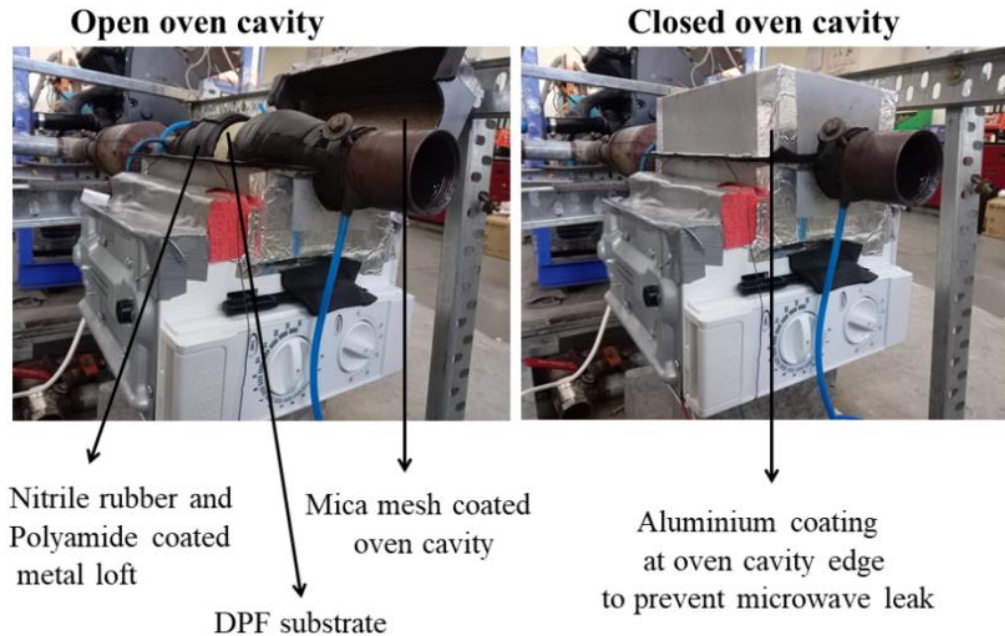
Figure 6.18. CRS system installed in the engine exhaust

The proposed system has to be retrofitted in the exhaust line of the diesel engine and regeneration of the DPF system has to be done when the pressure drop across the system is more than 0.5 kPa [73]. The pressure drop during transition from depth filtration to cake filtration is .45 kPa and 0.7 kPa is considered as the maximum pressure drop limit after which reverse flow would begin and will affect the engine performance. Presently the developed system has been tested in stationary diesel engine and AC power source was used for its working. The integration of the system with the electronic control unit of vehicle and DC power source includes the future scope of this work.

6.5 EXPERIMENTAL STUDY ON EFFECTIVENESS OF COMPOSITE REGENERATION SYSTEM

The schematic diagram of the engine setup with a post-treatment system comprising of DOC and microwave-assisted composite regeneration system are as shown in Figure 6.19. Effectiveness of the composite regeneration

system was evaluated by retrofitting the fabricated composite regeneration system in the exhaust line of the multi-cylinder compression ignition engine test bench as shown in Figure 6.20. The DPF filter substrate which was loaded with soot was placed in the oven cavity of the developed Composite Regeneration System (CRS) by considering the structural parameters [194][195].
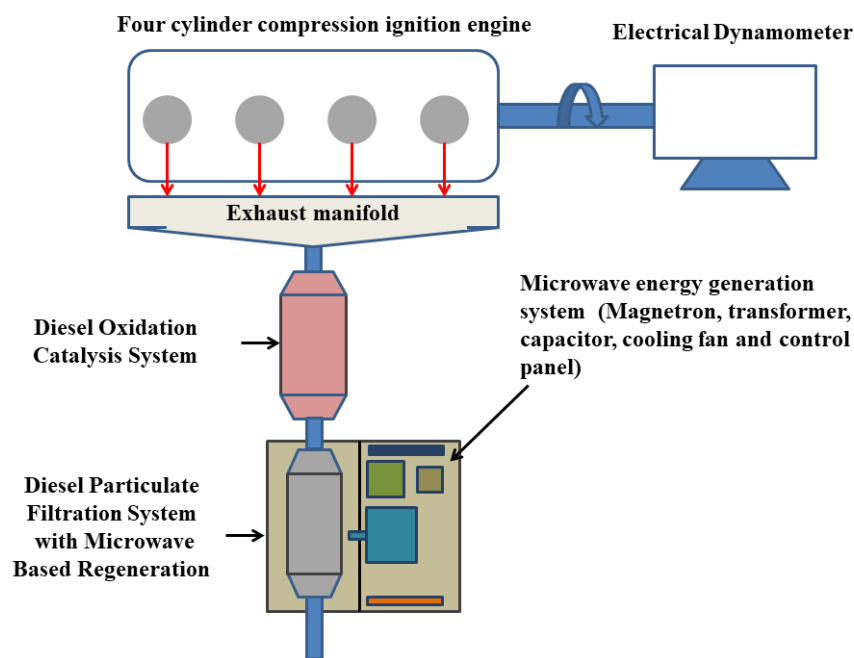
Figure 6.19. Schematic diagram of engine setup with DOC and microwave regeneration based DPF system

The regeneration rate of the microwave system was evaluated on a mass basis by conducting the regeneration for 30 seconds at the specified power output. Four stages of the power output were considered for the experimental study, namely 17%, 40%, 48% and 66% of the microwave power output. Magnetron used in the developed system has a microwave power output of 700 Watts at an operation frequency of 2450 MHz. The DPF system substrate was removed from the system and weighed after each regeneration cycle to determine the regeneration rate in grams per minute and

the results of the experimental investigation are as shown in Figure 6.21. The magnetron in the composite regeneration system which is the source for microwave radiations works in the pi mode for sustaining the oscillations.
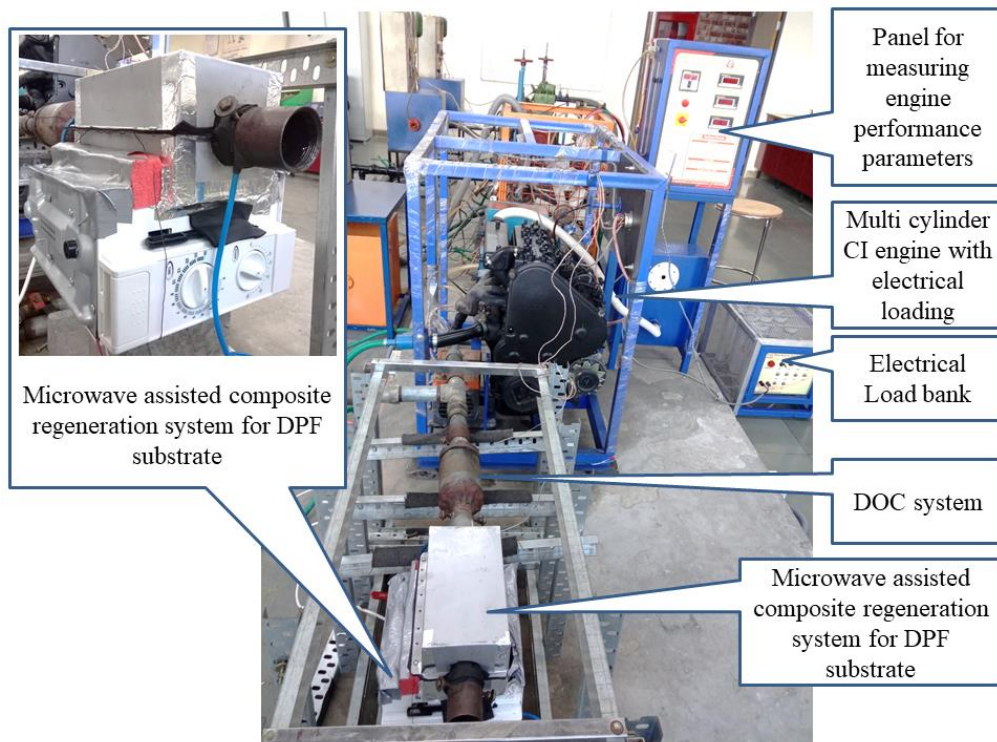
Figure 6.20. Experimental setup of multi-cylinder diesel engine retrofitted with CRS system

Magnetron works on negative resistance (non-linear) where energy is absorbed in one cycle and released in the next one. Time constant experiments were conducted for different power levels of the microwave system and the results showed that the regeneration rate increased to the maximum peak value of 0.21 g/min at 50% power level and at higher power levels regeneration rates were lower. At higher power, the uniformity of heating in the substrate was getting disturbed resulting in higher heating at specific areas affecting the overall regeneration rate. Average soot accumulation rate in the case of post-treatment system with integrated DOC and DPF system was 0.033 g/kWh and

considering the maximum regeneration rate of 0.21 g/min, the results show that one minute of regeneration at 50% microwave output power will regenerate the soot accumulated in the DPF during 6 hours of engine operation. The maximum allowable pressure drop across the DPF substrate is 0.7 kPa and in the present experimental study pressure drop across the substrate after soot loading for 6 hours (320 min) was 0.19 kPa. Hypothetically the system can run for 18 hours for reaching the maximum soot loading capacity with allowable backpressure.
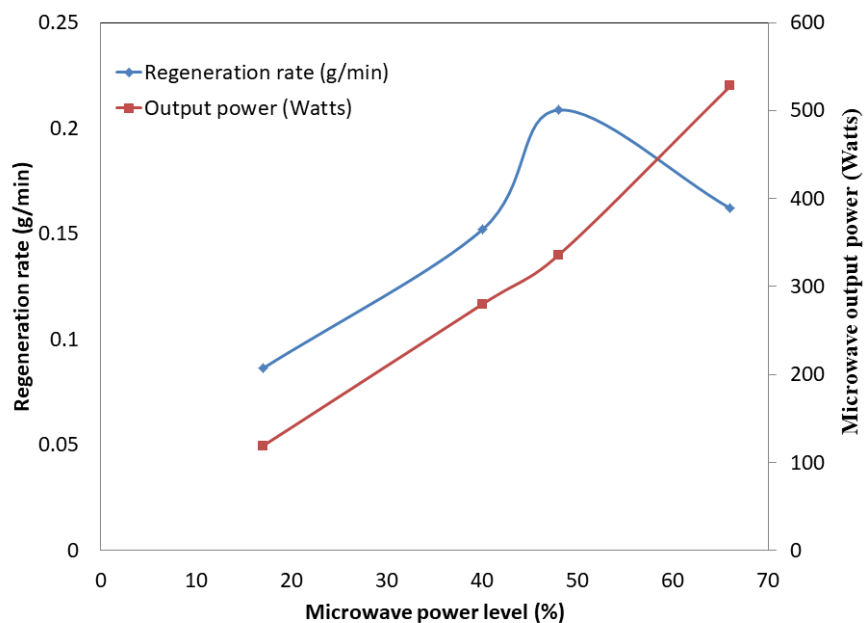
Figure 6.21. Regeneration rate of DPF substrate at different power levels

A comparative analysis of the energy consumption pattern in the DPF regeneration systems developed in the previous research works has been detailed in table no. 6.2, where it can be found that the microwave system developed in the present work has the lowest energy consumption as compared to fuel post-injection, electric heater, and non-thermal plasma discharge systems. The design of the oven cavity plays a major role in the

improvement of energy efficiency and hence the oven cavity has to be designed specifically to the size of the DPF substrate.

Table 6.2. Comparative analysis of energy consumption in alternate DPF regeneration techniques

Sl. No	Regeneration Strategy	Energy Consumption	DPF size
1	Microwave Regeneration – Magnetron based (Present work)	0.35 kW	$\Phi 80 \times 80$ mm
2	Non-Thermal plasma induced by dielectric barrier discharge [181]	17.5 kVA / 14 kW	$\Phi 144 \times 152$ mm
3	Electric heater [196][197]	15 kW	$\Phi 170 \times 203$ mm
4	Fuel post injection [197]	13.87 µL/injection or 506.3 kJ	$\Phi 190 \times 240$ mm
5	Microwave Regeneration – Magnetron based [136]	0.9 kW	$\Phi 190 \times 260$ mm
6	Early and late post fuel injection [198] [199]	8mg/stroke/cylinder or 360 kJ/stroke/cylinder	Not specified

6.6 CHARACTERIZATION OF DPF SUBSTRATE AFTER MICROWAVE ASSISTED REGENERATION

Functional group analysis and particle size analysis of the substrate was conducted using Fourier transform Infra-red Spectroscopy (FTIR) and Particle Size Analyzer (Malvern ZEN1690) to determine the effect of microwave regeneration on substrate properties. FTIR sample was prepared using the standard procedure by preparing KBr (Potassium bromide) pellet with a substrate sample [171][172]. The functional group peaks for the DPF substrate

at three different stages (a) new DPF, (b) DPF after soot loading and (c) DPF after regeneration are as shown in Figure 6.22, where it can be seen that the functional group peaks of the DPF substrate after regeneration is almost in the similar pattern of the new DPF substrate indicating the occurrence of effective regeneration.
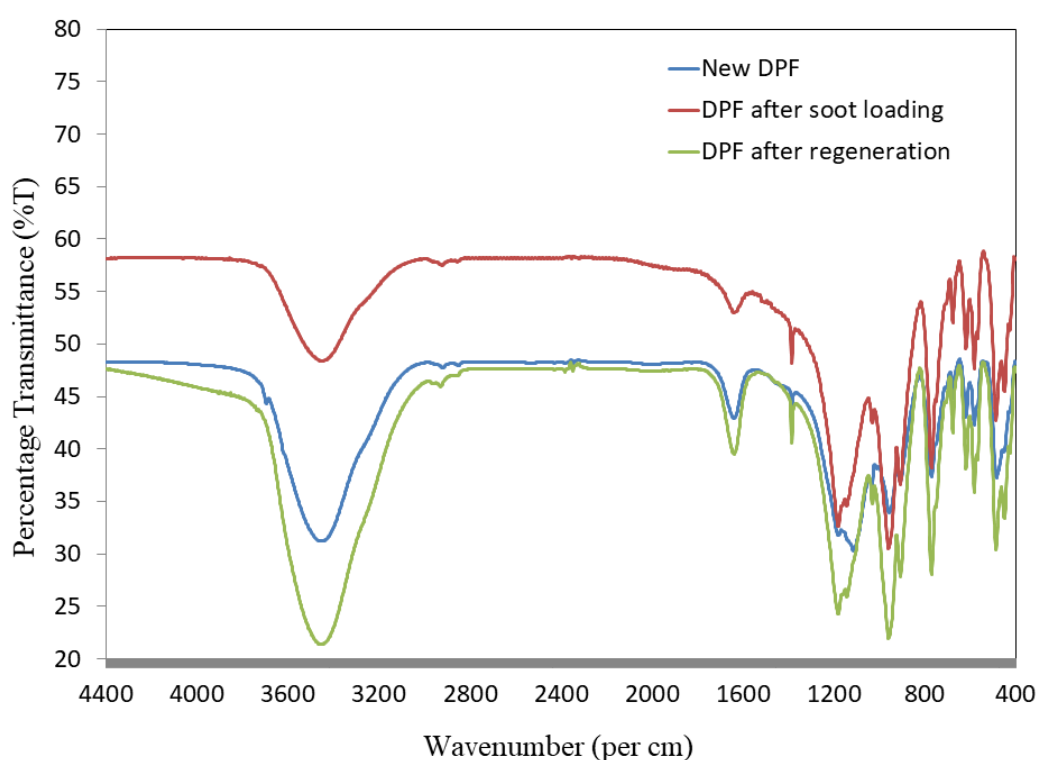
Figure 6.22. FTIR analysis of DPF substrate, vibrational energy revealed the functional group of the substrate before and after application in diesel engine exhaust stream

The effect of soot accumulation and regeneration on the intensity of particle size distribution in th DPF substrate was analysed by Particle Size Analyzer (Malvern ZEN1690). The particle size distribution is related to pore size of the substrate wall and hence it indirectly highlights the effectiveness of the regeneration in reducing pressure drop across substrate.
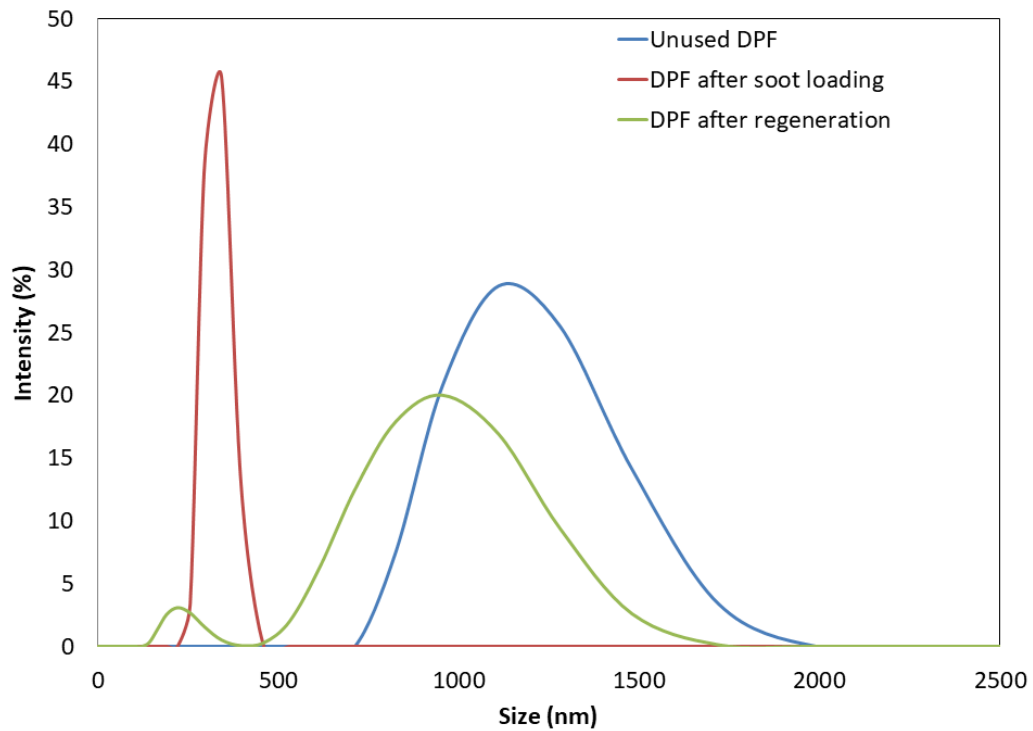
Figure 6.23. Particle size analyzer date for average particle size distribution in DPF substrate

The results of particle size analysis showed that the intensity of particle size distribution in the DPF substrate was reduced to an average size of 328 nm (after soot loading) from 1172 nm (unused DPF substrate) as shown in Figure 6.23, indicating the deposition of smaller size soot particles in the porous wall. The PSA results of the DPF substrate after regeneration showed that the intensity of particle size distribution was increased to 938.5 nm indicating the removal of smaller size soot particles from the porous walls.

CHAPTER 7. CONCLUSIONS

Stringent emission norms made it a mandatory requirement to retrofit emission control systems in the exhaust line of the vehicle since it is the most effective solution. In this work, modelling, computational analysis, development, and experimental study was conducted on emission control technique comprising of diesel oxidation catalysis and diesel particulate filtration system.

Development of a post-treatment emission control system with composite regeneration setup (i) Modelling and fabrication. Wherein three dimensional models of the DOC and DPF system were developed in design software (CATIA) and geometrical analysis of the models was conducted in CFD software (ANSYS) to validate the geometric design of the models before fabrication. The length of the loft and the loft angle is an important parameter which decides the flow through the substrate. The loft has to be designed in such a way that the pressure drop occurring in the flow due to its effect must be as low as possible. For determining the loft length with lowest pressure drop, CFD simulations were carried out for different models with varying loft angle and the results of simulation showed that the pressure drop is lowest in the case of the model with a loft length of 55 mm and loft angle of 61 degrees. The inlet and outlet lofts for the filtration system were fabricated with reference to the dimensions as per simulation results by sheet metal work.

Single-channel flow analysis was carried out for the DPF substrate to determine the effect of porous medium on the pressure drop across alternately plugged channels. Simulations were carried out for different mass flow rates of exhaust gas both in the case of DPF channel with porous medium and without the porous medium. The results of the simulation showed that the presence of the porous medium caused a pressure drop of around 60%. Also,

the results showed that the mass flow rate has direct proportionality with the inlet and outlet pressure.

Theoretical study on the effectiveness of the microwave-based regeneration system was carried out in this work by modelling and conducting simulations by creating a virtual environment in CFD software COMSOL Multiphysics. A comparative study on the electric field distribution in the system with magnetron port at top and center was conducted to determine the effective position for uniform distribution of the electric field inside the oven cavity. The contours of electric field distribution showed that the distribution of the electric field is uniform in the case of the model with a magnetron port at the center. The results of the simulation showed that the ceramic cordierite-based filter substrate is transparent to the microwave radiations since there was no appreciable rise in the temperature of the filter substrate.

Soot layer built up in the filter channels was evaluated using CFD software (COMSOL MULTIPHYSICS) by considering the rise in soot layer thickness with respect to time as the major parameter. The simulation results showed that the soot layer thickness was raised to 0.2025 mm after 1500 seconds and the velocity contours also indicated a positive flow across the substrate. Heat distribution and temperature rise in the DPF substrate (alternate layers of cordierite and soot) during microwave-assisted composite regeneration was modelled in COMSOL MULTIPHYSICS by considering time-dependent mode and steady-state electromagnetic radiations for magnetron port power of 1 kW. The dimension of the modelled oven cavity was 26.7 cm $\times$ 27 cm $\times$ 18.8 cm and the results of simulation showed that the maximum temperature of 800 K was attained after 180 seconds of regeneration with an average temperature distribution of 700 K. The size of the oven cavity was remodelled to improve the energy efficiency and heat distribution in the DPF substrate. The dimensions of the revised model for the

oven cavity were 14 cm × 14 cm × 22.5 cm and the simulations were carried out for different magnetron input power ranging from 100 to 700 Watts. The simulation results showed that the soot oxidation temperature of 873 K was achieved at a magnetron port power of 400 W (at regeneration time of 150 seconds) which inferred that the power rating of the magnetron can be optimized further for the experimental analysis. The soot oxidation temperature is 873 K and the maximum temperature achieved in the simulation results was much higher than 873 K, indicating that the modeled microwave-assisted regeneration system can effectively oxidize the accumulated soot particles. Microwave-assisted composite regeneration system was fabricated by integrating the oven cavity with magnetron arrangement

Experimental analysis of the developed emission control system; (i) Comparison of the conversion efficiency (metallic and ceramic DOC with different catalyst loading); (ii) Analysis of soot accumulation rate and filtration efficiency of DPF at different loads; (iii) Analyze the effectiveness of microwave-assisted composite regeneration system. Experimental studies were conducted on the fabricated DOC system to determine the conversion efficiency, and the performance of four commercially available DOC substrates was compared to determine the best retrofit combination in the proposed system (on four-cylinder, four-stroke engine at 1400 ± 50 rpm speed and power of 10 hp max.). Ceramic DOC substrate (400 cpsi) with a catalyst loading of platinum and palladium in the ratio 5:1 (35 g/cub. ft) exhibited the best conversion efficiency of 54% for hydrocarbons, 27% for carbon monoxide and 55% for particle number emissions.

Filtration efficiency of PTS system with DPF substrate alone was also experimentally determined and was observed to be 45% for hydrocarbons, 11% for carbon monoxide and 88% for particle number emissions. The DOC system was integrated with the DPF substrate and the conversion efficiency of

the combination was experimentally determined. Integrated DOC-DPF system had an average conversion efficiency of 59% for hydrocarbons, 28.7% for carbon monoxide and 91% for particle number emissions (at 1400 ± 50 rpm speed and power of 10 hp max.).

Soot accumulation rate in the DPF substrate was evaluated for different engine loads and it had an average soot accumulation rate of 0.147 g/kWh and integrated DOC-DPF substrate had an average soot accumulation rate of 0.033 g/kWh due to DOC-assisted continuous regeneration. The regeneration rate of the DPF substrate was evaluated by placing the loaded DPF substrate in the developed CR (Composite Regeneration) system and time constant power variable tests were conducted. The experimental results showed that the CR system had a maximum regeneration rate of 0.21 g/min at 50% power level.

Characterization of the filter substrate to determine the effects of filtration on substrate properties. The effect of filtration on the morphology, microstructure, chemical composition and particle size of DOC and DPF substrate were examined using characterization studies like Scanning Electron Microscopy – Energy Dispersive X-Ray Spectroscopy (SEM-EDS), Fourier Transform Infra-Red spectroscopy (FTIR), Particle Size Analysis (PSA) and microscopic imaging. The soot deposition in the DOC and DPF substrate were visually examined by microscopic imaging.

The functional group analysis of the DOC and DPF substrate were conducted using FTIR analysis. Anatase functional group detected in the DOC substrate indicated the formation of platinum oxides due to the poisoning of catalysts. Tetrachloroethylene detected in the FTIR report of the used DPF substrate is grouped by International Agency for Research on Cancer as, "2A probably carcinogenic to humans". The functional group peaks of the DPF

substrate after regeneration were observed to be in a similar pattern of the unused DPF substrate, indicating the occurrence of effective regeneration.

The results of the PSA (Particle Size Analysis) showed that the intensity of particle size distribution is increasing in the case of DOC from 389 nm to 417 nm, indicating the occurrence of catalyst poisoning by the formation of oxides. In the case of DPF, PSA results showed that the intensity of particle size distribution in the DPF substrate was reduced to an average size of 328 nm (after soot loading) from 1172 nm (unused DPF substrate), indicating the deposition of smaller size soot particles in the porous wall. The PSA results of the DPF substrate after regeneration showed that the intensity of particle size distribution was increased to 938.5 nm indicating the removal of smaller size soot particles from the porous walls. SEM-EDS results detailed the microstructure of the porous wall in unused DPF substrate and the morphological characteristics of the accumulated soot particles in the used DPF substrate, where the carbon content of 8.53% was found indicating the presence of soot particles. Energy consumed by the developed composite regeneration system was compared with other alternate regeneration techniques and the results showed that the system developed in this work has the lowest energy consumption owing to the geometric design of the oven cavity and also mica mesh coating reducing heat losses.

.

CHAPTER 8. FUTURE SCOPE OF WORK

Some of the limitations of the present research work that could be considered in the future scope of the study are indicated below.

- The engine test bench used for this work has a maximum loading capacity of 10hp (at 1400 rpm and 20 A) with exhaust temperature at the range of 550 K. The developed system can be tested in engine setup with higher loading capacity in the future works, which will improve the exhaust gas temperature, conversion efficiency of the DOC system and passive regeneration in DPF.

- The particle number emissions from the engine were measured using the DSM 501A sensor module which has a particle measurement accuracy of 1 µm. Engine exhaust particle sizer (EEPS) can be considered in the future scope of this work since the spectrometer has the measurement accuracy for particles in the size distribution of 5.6 - 560 nm.

- The DOC substrate can be coated with insulation layers in future studies to reduce the heat losses, which will enhance the conversion efficiency of the system by improving catalyst activity.

- The selective catalytic reduction system has to be integrated downstream of the DPF system in the future works to control the NOx emissions since the same is not considered in the present work.

- The performance and emission characteristics of the engine could be improved in the future works by supplementation of HHO (hydroxy) gas from the brown gas generator along the inlet air stream.

8.1 SOLID-REDUCTANT BASED SELECTIVE CATALYTIC REDUCTION

The development of an effective after-treatment system for reducing the toxicity level of exhaust emissions from internal combustion engines has become a mandatory requirement for the implementation of the latest emission regulations like EURO VI and Bharat Stage VI [200][201]. For example, in India, Bharat Stage IV emission norms have been enforced since April 2017 and it has been proposed to enforce Bharat Stage VI emission norms across the entire country by April 2020. The leap from BS IV to BS VI is very critical since the limit for particulate matter emission and nitrate (NO_x) emission from vehicles has to be brought down by an average of 73% and 76% for vehicles in all categories in the latest emission norm [6][152]. Performance and durability of the existing emission control systems has to be improved to meet these stringent emission norms [116][202].
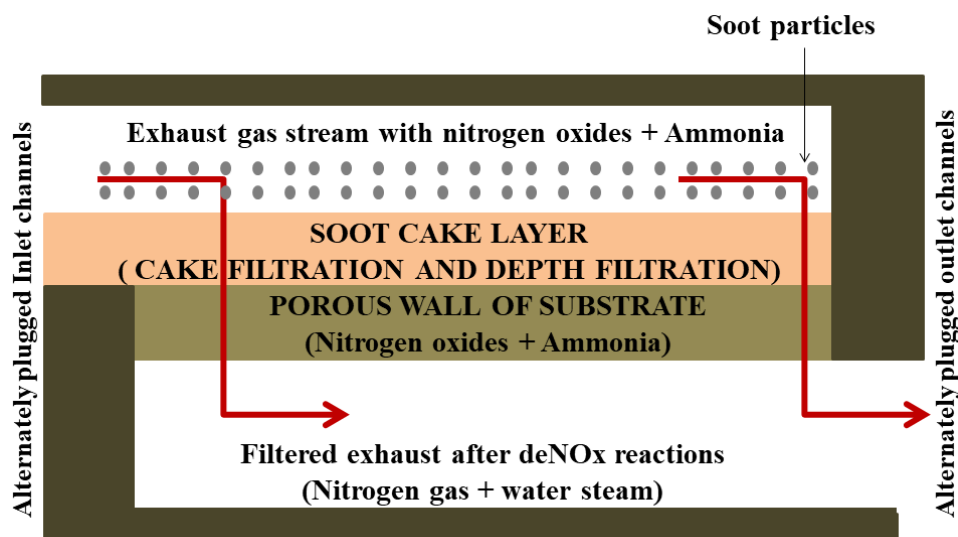
Figure 8.1. Schematic diagram on the working of the SCR system in a pair of alternately plugged channels

Selective Catalytic reduction based emission control system has proved to exhibit better NOx reduction efficiency compared to alternative

139

techniques and Diesel Particulate Filtration System with alternately plugged filter channels can trap the particulate matter emissions by significant amounts to meet these emission regulations [67][203][204]. In this work, gaseous and particulate matter emissions from the engines were reduced by the application of a composite regeneration system with DOC and DPF system, whereas the nitrate emissions from the engine exhaust were not considered [205][206]. The future scope of this work includes the integration of the Selective catalytic reduction (SCR) system with the developed CR system. Integrated SCR and DPF system with catalyst coating in the particulate filter channels and provision for injection of aqueous urea before the inlet channels are commercially used for deNOx and particulate trapping applications [207][208]. Schematic diagram on the working of the SCR system is shown in Figure 8.1, where it can be seen that the exhaust gas stream with ammonia generated by hydrolysis of urea is introduced to the inlet channels of the substrate.

8.1.1 Ammonia Generation from Solid Reductants

Commercially available SCR systems work by injection of urea (aqueous solution) to the exhaust gas stream for the generation of ammonia by hydrolysis reactions [209][210]. Some of the properties of urea like corrosive nature, lower freezing point and tendency to decompose at temperatures above 50-60 °C have raised the need for the development of an alternative technique for the generation of ammonia in SCR system [211][212]. Also, the generation of ammonia from urea would vary depending on the engine operating modes and exhaust conditions; hence it is very complicated to design a system for generating uniform concentration of ammonia [213][214]. Also, the temperature window for operation of the SCR system has been narrowed by the urea-based ammonia generation since the hydrolysis reactions are difficult to occur at temperatures below 200 °C [215]. The exhaust gas temperature

during the urban range is found to be below 200 °C, hence injection of aqueous urea during these operating conditions will result in the production of undesired byproducts [216][217].

All these limitations for the operation of the SCR system could be overcome if a system for injection of ammonia gas can be developed since it will broaden the operating temperature window and also the production of undesirable products can be avoided [110][218]. Major properties that decide the application of solid reactants for the generation of ammonia gas include its volumetric efficiency, mass efficiency, and ammonia release temperatures [219][220]. Some of the solid reactants which can generate ammonia gas include solid urea, ammonium salts, and metal amine chlorides [221]. Ammonium salts like ammonium carbamate and ammonium carbonate can be decomposed to release ammonia gas in two steps concerning the thermogravimetric analysis performed, where it was observed that ammonium carbamate decomposes readily at low temperature. Two-stage decomposition reaction of ammonium carbamate is as shown in equation no. 35 and 36.

$$NH_4COONH_2 \leftrightarrow NH_3 + HCOONH_2 \tag{35}$$

$$HCOONH_2 \leftrightarrow NH_3 + CO_2 \tag{36}$$

$$Ca(NH_3)_8Cl_2 \leftrightarrow Ca(NH_3)_2Cl_2 + 6NH_3 \tag{37}$$

$$Ca(NH_3)_2Cl_2 \leftrightarrow CaNH_3Cl_2 + NH_3 \tag{38}$$

$$CaNH_3Cl_2 \leftrightarrow CaCl_2 + NH_3 \tag{39}$$
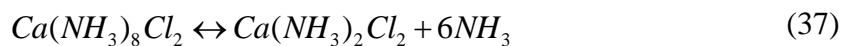
Metal ammines have complex coordination structures in which ammonia forms ligand bond with the central metal cation and ammonia generation from these depends on the coordination sites of ammonia molecules. Metal ammines like magnesium ammine chloride, strontium ammine chloride, and calcium ammine chloride release ammonium molecules in a multi-step process upon heating, where molecules attached to the equatorial sites are released first followed by the molecules attached to the apical sites [222]. The three-step process involved in the release of ammonium molecules from calcium ammine chloride is as shown in equation no. 37 to 39, where a total number of 8 ammonium molecules are released during the overall reaction. Replacement of the aqueous urea solution commercially known as AdBlue Diesel Exhaust Fluid (DEF) with the solid reductants would be the most possible alternative for improving the deNOx efficiency at broader temperature range.
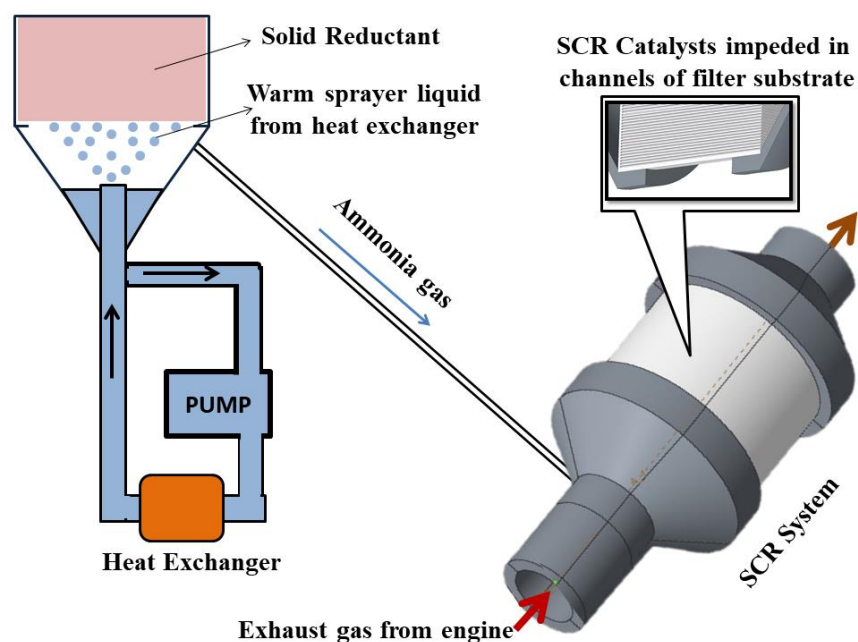
Figure 8.2. Schematic diagram on the working of the solid reductant based SCR system

Solid reductant based SCR system would require a closed container setup like a reactor where warm liquid at a temperature around 60 °C has to be sprayed on the solid reductant for the decomposition of the reductant to produce ammonia gas. The sprayer liquid has to be pumped back to the reservoir and recirculated hence working as a closed system [114]. The ammonia gas released from the reactor is directed to the exhaust flow line via gas flowmeter where the flow rate of the gas injected can be varied accordingly. The schematic concept diagram of the solid reductant based SCR system is as shown in Figure 8.2. Solid reductant based SCR system using ammonium carbamate for ammonia generation was developed by bai et al, where the results showed that ammonium carbamate released a sufficient amount of ammonia gas producing an overall conversion efficiency of 80 to 90% in the SCR system. Ammonium carbamate decomposes to ammonia at a temperature of 60 °C, which is achieved by the spraying of heat transfer fluid onto the solid reductant [67]. The pressure inside the reactor system will rise as the generation of ammonia gas continues and it is introduced to the exhaust flow stream via the dosage control valve. The dosage of the ammonia gas will vary depending on the operating mode of the engine. The threat of urea slip and undesired deposits during cold start and low load conditions can be eliminated by the introduction of a solid reductant based SCR system [223]. Ammonia density of the solid reductants is also higher hence the reactor will be compatible with the exhaust line and also ensures a longer range of service life [224].

Selective catalytic reduction based emission control system is a mandatory external attachment for meeting emission regulations like US 2010 and EURO VI. Urea based SCR system with catalyst coating of copper or iron zeolite is commercially available SCR technique, but the occurrence of undesired reactions leading to release for more toxic byproducts has led to the development of alternate deNOx techniques. The solid reductant based SCR

143

system is observed to be an effective alternative for ammonia generation as compared to urea-based SCR systems. Ammonium salts like ammonium carbamate and ammonium carbonate can generate ammonia for about 80 to 90% NOx conversion for small, light and medium-duty diesel engine applications. Undesired reactions occurring in urea-based SCR systems during cold start and cold transient cycles can be rectified by introducing SSCR systems which will also reduce the deposit risks. The performance of the SCR system can be enhanced by using solid reductants for ammonia generation owing to its higher ammonia generation density hence the refill interval can be extended.

8.2 HHO GAS SUPPLEMENTATION USING BROWN GAS GENERATOR

Brown gas is produced by electrolysis of water where direct current is passed through the electrolyte resulting in decomposition of water to produce hydrogen, oxygen and their ions [225]. The mixture of hydrogen and oxygen gases produced by electrolysis setup is observed to have good thermodynamic properties. The production of HHO (hydroxy) gas by electrolysis of water was first discovered by Yull Brown in 1977 for welding purpose, hence it is also known by the name Brown's gas [226]. HHO gas has properties similar to that of hydrogen and has ionization energy of around 13.6 eV. HHO gas is composed of hydrogen and oxygen in the form of atomic clusters (H, O), dimers (H-O), molecules (H_2 and O_2) and water vapor. Hence it can be considered to be a potential alternative energy source [227]. Brown gas generated by electrolysis of water is observed to be an effective alternate energy source for internal combustion engines owing to its ability to combust at its auto-ignition temperature and the energy required for it is around 20 µJ at 570 °C [228][229]. At standard temperature and pressure, oxyhydrogen can

burn when it is between about 4% oxygen and 95% hydrogen by volume [230].

8.2.1 Working Principle of Brown Gas Generator

The byproducts released after the electrolysis of water include a mixture of hydrogen gas, oxygen gas and their ions [231]. The rate of gas generated by the system depends on the applied potential difference across the anode and cathode. Reactions taking place in the cathode and anode of the system are as shown in equation no. 40 and 41. Water is decomposed to hydrogen and hydroxyl ion at the cathode which is known as Hydrogen Evolution reaction (HER) and hydroxyl ion is oxidized to produce oxygen gas and water at the anode, which is known as Oxygen Evolution Reaction (OER) [232].
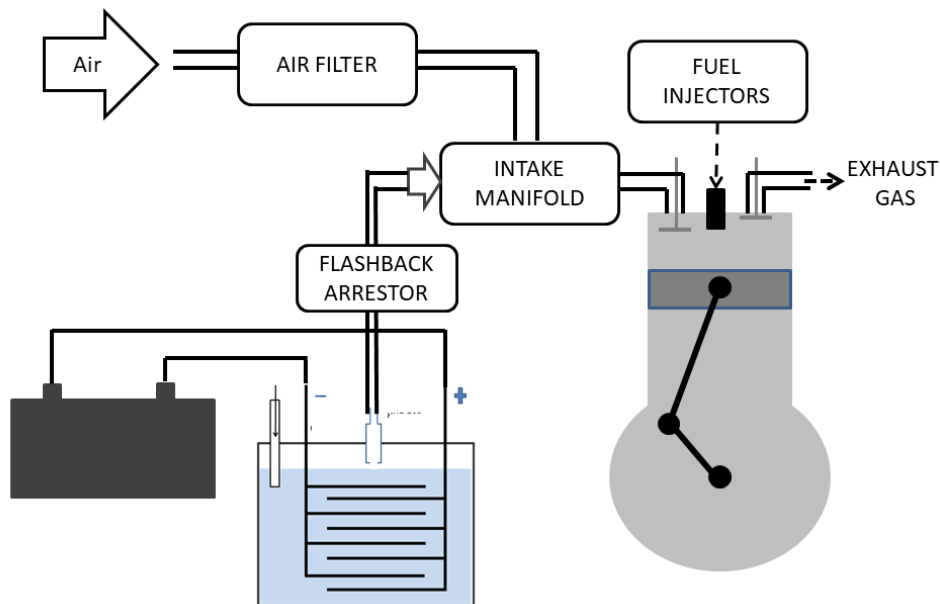
Figure 0.3. Proposed system for HHO gas supplementation in engines

$$H_2O + 2e^- \rightarrow H_2 + 2OH^- \tag{40}$$

$$H_2O + 2e^- \rightarrow H_2 + 2OH^- \tag{41}$$

The overall reaction taking place in the system is the decomposition of water to hydrogen and oxygen gas as shown in equation no. 40 [233]. The potential difference applied across the electrodes must be greater than the reversible cell voltage, which is the minimum voltage to overcome the difference in potential across anode and cathode. At room temperature, it is difficult to achieve the reversible cell voltage to initiate the electrochemical reaction without the application of external voltage sources [234]. The current density of the system depends on various factors like surface property of electrode, electrode potential and ion distribution in different layers of the electrolyte solution. The double-layer is formed in the electrolyte near the electrodes by variation in ion distribution at the inner and outer Helmholtz layer, which results in potential difference across electrode and electrolyte [235]. The future scope of this work also includes the supplementation of HHO gas to the intake manifold of the CI engines to improve the performance and emission characteristics of the engine and the schematic diagram of the proposed system is as shown in Figure 8.3. The combined effect of pre-treatment (HHO gas supplementation) and post-treatment (DOC + DPF + SSCR) will help to reduce the emission levels and will also have a significant impact on engine performance.

REFERENCES

[1]   S. Levitus *et al.*, "World ocean heat content and thermosteric sea level change (0--2000 m), 1955--2010," *Geophysical Research Letters*, vol. 39, no. 10, 2012.

[2]   B. Meyssignac and A. Cazenave, "Sea level: A review of present-day and recent-past changes and variability," *Journal of Geodynamics*, vol. 58, pp. 96–109, Jul. 2012.

[3]   M. Christenson, H. Manz, and D. Gyalistras, "Climate warming impact on degree-days and building energy demand in Switzerland," *Energy Conversion and Management*, vol. 47, no. 6, pp. 671–686, Apr. 2006.

[4]   M. Yu, D. Luss, and V. Balakotaiah, "Analysis of flow distribution and heat transfer in a diesel particulate filter," *Chemical Engineering Journal*, vol. 226, pp. 68–78, Jun. 2013.

[5]   A. A. Lindley and A. McCulloch, "Regulating to reduce emissions of fluorinated greenhouse gases," *Journal of Fluorine Chemistry*, vol. 126, no. 11–12, pp. 1457–1462, Dec. 2005.

[6]   D. Bose, C. Kurien, A. Sharma, S. Sharma, and A. Sharma, "Low Cost Cathode Performance of Microbial Fuel Cell for Treating Food Wastewater.," *Nature Environment & Pollution Technology*, vol. 17, no. 3, 2018.

[7]   M. Shelef, "Selective catalytic reduction of NOx with N-free reductants," *Chemical Reviews*, vol. 95, no. 1, pp. 209–225, 1995.

[8]   \.Ibrahim Aslan Re\csito\uglu, K. Altini\csik, and A. Keskin, "The pollutant   emissions   from   diesel-engine   vehicles   and   exhaust

aftertreatment systems," *Clean Technologies and Environmental Policy*, vol. 17, no. 1, pp. 15–27, 2015.

[9] A. J. Cohen *et al.*, "Estimates and 25-year trends of the global burden of disease attributable to ambient air pollution: an analysis of data from the Global Burden of Diseases Study 2015," *The Lancet*, vol. 389, no. 10082, pp. 1907–1918, 2017.

[10] W. Huang *et al.*, "Air pollution and autonomic and vascular dysfunction in patients with cardiovascular disease: interactions of systemic inflammation, overweight, and gender," *American journal of epidemiology*, vol. 176, no. 2, pp. 117–126, 2012.

[11] M. Ambrogio, G. Saracco, V. Specchia, C. van Gulijk, M. Makkee, and J. A. Moulijn, "On the generation of aerosol for diesel particulate filtration studies," *Separation and Purification Technology*, vol. 27, no. 3, pp. 195–209, Jun. 2002.

[12] R. Finesso, D. Misul, and E. Spessa, "Development and validation of a semi-empirical model for the estimation of particulate matter in diesel engines," *Energy Conversion and Management*, vol. 84, pp. 374–389, Aug. 2014.

[13] D. E. Newby *et al.*, "Expert position paper on air pollution and cardiovascular disease," *European heart journal*, vol. 36, no. 2, pp. 83–93, 2014.

[14] M. F. Piepoli *et al.*, "2016 European Guidelines on cardiovascular disease prevention in clinical practice: The Sixth Joint Task Force of the European Society of Cardiology and Other Societies on Cardiovascular Disease Prevention in Clinical Practice (constituted by representati," *European heart journal*, vol. 37, no. 29, pp. 2315–2381,

2016.

[15] S. Vidale and C. Campana, "Ambient air pollution and cardiovascular diseases: From bench to bedside," *European Journal of Preventive Cardiology*, vol. 25, no. 8, pp. 818–825, 2018.

[16] E. Akintoye *et al.*, "Association between fine particulate matter exposure and subclinical atherosclerosis: A meta-analysis," *European journal of preventive cardiology*, vol. 23, no. 6, pp. 602–612, 2016.

[17] Q. Sun *et al.*, "Long-term air pollution exposure and acceleration of atherosclerosis and vascular inflammation in an animal model," *Jama*, vol. 294, no. 23, pp. 3003–3010, 2005.

[18] C. Carlsten, J. D. Kaufman, A. Peretz, C. A. Trenga, L. Sheppard, and J. H. Sullivan, "Coagulation markers in healthy human subjects exposed to diesel exhaust," *Thrombosis research*, vol. 120, no. 6, pp. 849–855, 2007.

[19] R. D. Brook *et al.*, "Reduced metabolic insulin sensitivity following sub-acute exposures to low levels of ambient fine particulate matter air pollution," *Science of the Total Environment*, vol. 448, pp. 66–71, 2013.

[20] E. Thiering *et al.*, "Long-term exposure to traffic-related air pollution and insulin resistance in children: results from the GINIplus and LISAplus birth cohorts," *Diabetologia*, vol. 56, no. 8, pp. 1696–1704, 2013.

[21] S. Rajagopalan and R. D. Brook, "Air pollution and type 2 diabetes: mechanistic insights," *Diabetes*, vol. 61, no. 12, pp. 3037–3045, 2012.

[22] R. Durand, G. Pellerin, J. Thibodeau, E. Fraboulet, A. Marette, and L. Bazinet, "Screening for metabolic syndrome application of a herring

by-product hydrolysate after its separation by electrodialysis with ultrafiltration membrane and identification of novel anti-inflammatory peptides," *Separation and Purification Technology*, vol. 235, p. 116205, Mar. 2020.

[23] R. D. Brook and S. Rajagopalan, "Particulate matter, air pollution, and blood pressure," *Journal of the American Society of Hypertension*, vol. 3, no. 5, pp. 332–350, 2009.

[24] K. J. Chuang *et al.*, "Particulate air pollution as a risk factor for ST-segment depression in patients with coronary artery disease," *Circulation*, vol. 118, no. 13, p. 1314, 2008.

[25] I. A. Resitoglu, K. Altinisik, A. Keskin, and K. Ocakoglu, "The effects of Fe2O3 based DOC and SCR catalyst on the exhaust emissions of diesel engines," *Fuel*, vol. 262, p. 116501, Feb. 2020.

[26] Z. Meng *et al.*, "Particle emission characteristics of DPF regeneration from DPF regeneration bench and diesel engine bench measurements," *Fuel*, vol. 262, p. 116589, Feb. 2020.

[27] M. Elkelawy *et al.*, "Study of diesel-biodiesel blends combustion and emission characteristics in a CI engine by adding nanoparticles of Mn (II) supramolecular complex," *Atmospheric Pollution Research*, vol. 11, no. 1, pp. 117–128, Jan. 2020.

[28] B. A. Oni and D. Oluwatosin, "Emission characteristics and performance of neem seed (Azadirachta indica) and Camelina (Camelina sativa) based biodiesel in diesel engine," *Renewable Energy*, vol. 149, pp. 725–734, Apr. 2020.

[29] H.-J. Liu, R.-H. Chen, and W.-C. Wang, "The non-regulated emissions from a turbo-charged diesel engine under steady-state operation with

hydro-processed renewable diesel (HRD)," *Fuel*, vol. 263, p. 116762, Mar. 2020.

[30] S. Mishra, A. Chauhan, and K. B. Mishra, "Role of binary and ternary blends of WCO biodiesel on emission reduction in diesel engine," *Fuel*, vol. 262, p. 116604, Feb. 2020.

[31] F. S. Mirhashemi and H. Sadrnia, "NOX emissions of compression ignition engines fueled with various biodiesel blends: A review," *Journal of the Energy Institute*, vol. 93, no. 1, pp. 129–151, Feb. 2020.

[32] S. Das, D. Kashyap, P. Kalita, V. Kulkarni, and Y. Itaya, "Clean gaseous fuel application in diesel engine: A sustainable option for rural electrification in India," *Renewable and Sustainable Energy Reviews*, vol. 117, p. 109485, Jan. 2020.

[33] C. Deheri, S. K. Acharya, D. N. Thatoi, and A. P. Mohanty, "A review on performance of biogas and hydrogen on diesel engine in dual fuel mode," *Fuel*, vol. 260, p. 116337, Jan. 2020.

[34] W. W.-F. Leung and Y. T. Chau, "Experiments on filtering nano-aerosols from vehicular and atmospheric pollutants under dominant diffusion using nanofiber filter," *Separation and Purification Technology*, vol. 213, pp. 186–198, Apr. 2019.

[35] P. A. Kumar, M. D. Tanwar, S. Bensaid, N. Russo, and D. Fino, "Soot combustion improvement in diesel particulate filters catalyzed with ceria nanofibers," *Chemical Engineering Journal*, vol. 207–208, pp. 258–266, Oct. 2012.

[36] S. K. Kurre, S. Pandey, and M. Saxena, "Effect of compression ratio on diesel engine performance and emission with diesel-ethanol blends," *International Journal of Scientific & Engineering Research*, vol. 4, no.

151

10, pp. 775–779, 2013.

[37] M. Abdalla, M. Nasser, A. Kayvani Fard, H. Qiblawey, A. Benamor, and S. Judd, "Impact of combined oil-in-water emulsions and particulate suspensions on ceramic membrane fouling and permeability recovery," *Separation and Purification Technology*, vol. 212, pp. 215–222, Apr. 2019.

[38] M. Schejbal, M. Marek, M. Kubíček, and P. Kočí, "Modelling of diesel filters for particulates removal," *Chemical Engineering Journal*, vol. 154, no. 1–3, pp. 219–230, Nov. 2009.

[39] M. Pan *et al.*, "Experimental study of the spray, combustion, and emission performance of a diesel engine with high n-pentanol blending ratios," *Energy Conversion and Management*, vol. 194, pp. 1–10, Aug. 2019.

[40] A. I. EL-Seesy, H. Kosaka, H. Hassan, and S. Sato, "Combustion and emission characteristics of a common rail diesel engine and RCEM fueled by n-heptanol-diesel blends and carbon nanomaterial additives," *Energy Conversion and Management*, vol. 196, pp. 370–394, Sep. 2019.

[41] Y. Li, L. Cao, D. Hu, and C. Yang, "Uncommon wetting on a special coating and its relevance to coalescence separation of emulsified water from diesel fuel," *Separation and Purification Technology*, vol. 176, pp. 313–322, Apr. 2017.

[42] O. Ogunkunle and N. A. Ahmed, "A review of global current scenario of biodiesel adoption and combustion in vehicular diesel engines," *Energy Reports*, vol. 5, pp. 1560–1579, Nov. 2019.

[43] J. Thangaraja and C. Kannan, "Effect of exhaust gas recirculation on

advanced diesel combustion and alternate fuels - A review," *Applied Energy*, vol. 180, pp. 169–184, Oct. 2016.

[44]   D. Zhu and X. Zheng, "Fuel consumption and emission characteristics in asymmetric twin-scroll turbocharged diesel engine with two exhaust gas recirculation circuits," *Applied Energy*, vol. 238, pp. 985–995, Mar. 2019.

[45]   A. Calam, "Effects of the fusel oil usage in HCCI engine on combustion, performance and emission," *Fuel*, vol. 262, p. 116503, Feb. 2020.

[46]   M. Puškár and M. Kopas, "System based on thermal control of the HCCI technology developed for reduction of the vehicle NOX emissions in order to fulfil the future standard Euro 7," *Science of The Total Environment*, vol. 643, pp. 674–680, Dec. 2018.

[47]   P. Zhang, J. He, H. Chen, X. Zhao, and L. Geng, "Improved combustion and emission characteristics of ethylene glycol/diesel dual-fuel engine by port injection timing and direct injection timing," *Fuel Processing Technology*, vol. 199, p. 106289, Mar. 2020.

[48]   Z. Lee and S. Park, "Particulate and gaseous emissions from a direct-injection spark ignition engine fueled with bioethanol and gasoline blends at ultra-high injection pressure," *Renewable Energy*, vol. 149, pp. 80–90, Apr. 2020.

[49]   Z. Meng *et al.*, "Experimental study on regeneration performance and particle emission characteristics of DPF with different inlet transition sections lengths," *Fuel*, vol. 262, p. 116487, Feb. 2020.

[50]   Y. Shi, Y. Cai, R. Fan, Y. Cui, Y. Chen, and L. Ji, "Characterization of soot inside a diesel particulate filter during a nonthermal plasma

promoted regeneration step," *Applied Thermal Engineering*, vol. 150, pp. 612–619, Mar. 2019.

[51]   Y.-C. Lin, Y.-C. Li, K. T. T. Amesho, F.-C. Chou, and P.-C. Cheng, "Characterization and quantification of PM2.5 emissions and PAHs concentration in PM2.5 from the exhausts of diesel vehicles with various accumulated mileages," *Science of The Total Environment*, vol. 660, pp. 188–198, Apr. 2019.

[52]   E. G. Giakoumis, C. D. Rakopoulos, A. M. Dimaratos, and D. C. Rakopoulos, "Exhaust emissions of diesel engines operating under transient conditions with biodiesel fuel blends," *Progress in Energy and Combustion Science*, vol. 38, no. 5, pp. 691–715, Oct. 2012.

[53]   L. D. Claxton, "The history, genotoxicity, and carcinogenicity of carbon-based fuels and their emissions. Part 3: Diesel and gasoline," *Mutation Research/Reviews in Mutation Research*, vol. 763, pp. 30–85, Jan. 2015.

[54]   K. Hauff, U. Tuttlies, G. Eigenberger, and U. Nieken, "Platinum oxide formation and reduction during NO oxidation on a diesel oxidation catalyst – Experimental results," *Applied Catalysis B: Environmental*, vol. 123–124, pp. 107–116, Jul. 2012.

[55]   K. Yang, J. T. Fox, and R. Hunsicker, "Characterizing Diesel Particulate Filter Failure During Commercial Fleet Use due to Pinholes, Melting, Cracking, and Fouling," *Emission Control Science and Technology*, vol. 2, no. 3, pp. 145–155, 2016.

[56]   A. Liati, D. Schreiber, P. Dimopoulos Eggenschwiler, and Y. Arroyo Rojas Dasilva, "Metal Particle Emissions in the Exhaust Stream of Diesel Engines: An Electron Microscope Study," *Environmental*

Science & Technology, vol. 47, no. 24, pp. 14495–14501, 2013.

[57]   R. O. McClellan, T. W. Hesterberg, and J. C. Wall, "Evaluation of carcinogenic hazard of diesel engine exhaust needs to consider revolutionary changes in diesel technology," *Regulatory Toxicology and Pharmacology*, vol. 63, no. 2, pp. 225–258, 2012.

[58]   R. Sindhu, G. A. P. Rao, and K. M. Murthy, "Effective reduction of NOx emissions from diesel engine using split injections," *Alexandria Engineering Journal*, 2017.

[59]   C. Guan, X. Li, B. Liao, and Z. Huang, "Effects of fuel injection strategies on emissions characteristics of a diesel engine equipped with a particle oxidation catalyst (POC)," *Journal of Environmental Chemical Engineering*, vol. 4, no. 4, pp. 4822–4829, 2016.

[60]   S. K. Kurre, R. Garg, and S. Pandey, "A review of biofuel generated contamination, engine oil degradation and engine wear," *Biofuels*, vol. 8, no. 2, pp. 273–280, 2017.

[61]   J. Fang *et al.*, "The effect of operating parameters on regeneration characteristics and particulate emission characteristics of diesel particulate filters," *Applied Thermal Engineering*, vol. 148, pp. 860–867, Feb. 2019.

[62]   J. Fu, J. Li, Y. Tang, F. Yan, Y. He, and Y. Li, "Recirculation zone characteristics research on a sudden expansion swirl burner for DPF regeneration," *Environmental Progress & Sustainable Energy*, vol. 37, no. 6, pp. 2000–2009, 2018.

[63]   X. Pu *et al.*, "Diesel particulate filter (DPF) regeneration using non-thermal plasma induced by dielectric barrier discharge," *Journal of the Energy Institute*, vol. 91, no. 5, pp. 655–667, Oct. 2018.

[64] P. Jiao, Z. Li, B. Shen, W. Zhang, X. Kong, and R. Jiang, "Research of DPF regeneration with NOx-PM coupled chemical reaction," *Applied Thermal Engineering*, vol. 110, pp. 737–745, Jan. 2017.

[65] Q. Dawei, L. Jun, and L. Yu, "Research on particulate filter simulation and regeneration control strategy," *Mechanical Systems and Signal Processing*, vol. 87, pp. 214–226, 2017.

[66] M. Feulner, F. Seufert, A. Müller, G. Hagen, and R. Moos, "Influencing Parameters on the Microwave-Based Soot Load Determination of Diesel Particulate Filters," *Topics in Catalysis*, vol. 60, no. 3–5, pp. 374–380, 2017.

[67] S. Bai, G. Chen, Q. Sun, G. Wang, and G. Li, "Influence of active control strategies on exhaust thermal management for diesel particular filter active regeneration," *Applied Thermal Engineering*, vol. 119, pp. 297–303, 2017.

[68] V. Palma, E. Meloni, M. Caldera, D. Lipari, V. Pignatelli, and V. Gerardi, "Catalytic wall flow filters for soot abatement from biomass boilers," *Chemical Engineering Transactions*, vol. 50, pp. 253–258, 2016.

[69] V. Palma and E. Meloni, "Microwave susceptible catalytic diesel particulate filter," *Chemical Engineering Transactions*, vol. 52, pp. 445–450, 2016.

[70] K. Yamazaki, Y. Sakakibara, S. Daido, and S. Okawara, "Particulate Matter Oxidation over Ash-Deposited Catalyzed Diesel Particulate Filters," *Topics in Catalysis*, vol. 59, no. 10–12, pp. 1076–1082, 2016.

[71] G. Z. Jiaqiang E , Longfu Xie, Qingsong Zuo, "Effect analysis on regeneration speed of continuous regeneration-diesel particulate filter

based on NO2-assisted regeneration," *Atmospheric Pollution Research*, vol. 7, no. 1, pp. 9–17, 2016.

[72] V. Bermúdez, J. R. Serrano, P. Piqueras, and O. García-Afonso, "Pre-DPF water injection technique for pressure drop control in loaded wall-flow diesel particulate filters," *Applied Energy*, vol. 140, pp. 234–245, 2015.

[73] V. Palma, P. Ciambelli, E. Meloni, and A. Sin, "Catalytic DPF microwave assisted active regeneration," *Fuel*, vol. 140, pp. 50–61, 2015.

[74] V. Di Sarli and A. Di Benedetto, "Modeling and simulation of soot combustion dynamics in a catalytic diesel particulate filter," *Chemical Engineering Science*, vol. 137, pp. 69–78, 2015.

[75] R. Ramdas, E. Nowicka, R. Jenkins, D. Sellick, C. Davies, and S. Golunski, "Using real particulate matter to evaluate combustion catalysts for direct regeneration of diesel soot filters," *Applied Catalysis B: Environmental*, vol. 176–177, no. 2, pp. 436–443, 2015.

[76] F. Fornarelli, S. Camporeale, R. Dadduzio, B. Fortunato, and M. Torresi, "Numerical simulation of the flow field and chemical reactions within a NSC diesel catalyst," *Energy Procedia*, vol. 82, no. x, pp. 381–388, 2015.

[77] Q. Zuo, J. E, J. Gong, D. M. Zhang, T. Chen, and G. Jia, "Performance evaluation on field synergy and composite regeneration by coupling cerium-based additive and microwave for a diesel particulate filter," *Journal of Central South University*, vol. 21, no. 12, pp. 4599–4606, 2014.

[78] K. Graupner *et al.*, "Pulsed discharge regeneration of diesel particulate

filters," *Plasma Chemistry and Plasma Processing*, vol. 33, no. 2, pp. 467–477, 2013.

[79] V. Palma, P. Ciambelli, and E. Meloni, "Catalyst Load Optimization for Microwave Susceptible Catalysed DPF," vol. 32, no. Figure 1, pp. 799–804, 2013.

[80] G. Corro, U. Pal, E. Ayala, and E. Vidal, "Diesel soot oxidation over silver-loaded SiO2 catalysts," *Catalysis Today*, vol. 212, pp. 63–69, 2013.

[81] Y. K. L. and Y. J. K. H.J Kim, B. Han, W.S Hong, W.H. Shin, G.B. Cho, "Developmentof elctrostatic Diesel Particulate Filtration systems combined with a metallic flow through filter and electrostatic methods," *International Journal of Automotive Technology*, vol. 11, no. 4, pp. 447–453, 2010.

[82] Z. H. Zhang, S. M. Chua, and R. Balasubramanian, "Comparative evaluation of the effect of butanol-diesel and pentanol-diesel blends on carbonaceous particulate composition and particle number emissions from a diesel engine," *Fuel*, vol. 176, pp. 40–47, 2016.

[83] J. . Z. D. Wang, Z.C Liu, J.Tian, J.W Liu, "Investigation of particle emission characteristics from a Diesel engine with a Diesel Particulate Filter for alternative fuels," *International Journal of Automotive Technology*, vol. 13, no. 7, pp. 1023–1032, 2012.

[84] H. Caliskan and K. Mori, "Environmental, enviroeconomic and enhanced thermodynamic analyses of a diesel engine with diesel oxidation catalyst (DOC) and diesel particulate filter (DPF) after treatment systems," *Energy*, vol. 128, no. Supplement C, pp. 128–144, 2017.

[85] S. I. Seher, M. N. Ess, H. Bladt, R. Niessner, G. Eigenberger, and U. Nieken, "A comparison of diesel soot oxidation rates measured with two different isothermal set-ups," *Journal of Aerosol Science*, vol. 91, no. x, pp. 94–100, 2016.

[86] J. R. Serrano, H. Climent, P. Piqueras, and E. Angiolini, "Filtration modelling in wall-flow particulate filters of low soot penetration thickness," *Energy*, vol. 112, pp. 883–898, 2016.

[87] C. Kurien and A. K. Srivastava, "Advancement in the Design of Automotive Catalytic Filter for Meeting Environmental Emission Norms Key Words :," *Nature Environment and Pollution technology*, vol. 17, no. 2, pp. 433–438, 2018.

[88] M. Lapuerta, J. Rodríguez-Fernández, and F. Oliva, "Effect of soot accumulation in a diesel particle filter on the combustion process and gaseous emissions," *Energy*, vol. 47, no. 1, pp. 543–552, 2012.

[89] S. Mohankumar and P. Senthilkumar, "Particulate matter formation and its control methodologies for diesel engine: A comprehensive review," *Renewable and Sustainable Energy Reviews*, vol. 80, pp. 1227–1238, 2017.

[90] O. I. Smith, "Fundamentals of soot formation in flames with application to diesel engine particulate emissions," *Prog. Energy Combust. Sci*, vol. 7, no. 4, pp. 275–291, 1981.

[91] B. S. Haynes, "Wag ner, HG, Soot For ma tion," *Prog ress in En ergy and Com bus tion Sci ence*, vol. 7, no. 4, 1981.

[92] C. W. Bruce, T. F. Stromberg, K. P. Gurton, and J. B. Mozer, "Trans-spectral absorption and scattering of electromagnetic radiation by diesel soot," *Applied optics*, vol. 30, no. 12, pp. 1537–1546, 1991.

[93] D. R. Tree and D. E. Foster, "Optical measurements of soot particle size, number density, and temperature in a direct injection diesel engine as a function of speed and load," *SAE transactions*, pp. 318–330, 1994.

[94] M. Koegl, B. Hofbeck, S. Will, and L. Zigan, "Investigation of soot formation and oxidation of ethanol and butanol fuel blends in a DISI engine at different exhaust gas recirculation rates," *Applied Energy*, vol. 209, pp. 426–434, 2018.

[95] P. Tan, Y. Li, and H. Shen, "Exhaust particle properties from a light duty diesel engine using different ash content lubricating oil," *Journal of the Energy Institute*, vol. 91, no. 1, pp. 55–64, Feb. 2018.

[96] R. K. Gehmlich, C. J. Mueller, D. J. Ruth, C. W. Nilsen, S. A. Skeen, and J. Manin, "Using ducted fuel injection to attenuate or prevent soot formation in mixing-controlled combustion strategies for engine applications," *Applied Energy*, vol. 226, pp. 1169–1186, 2018.

[97] B. Wang, S. Mosbach, S. Schmutzhard, S. Shuai, Y. Huang, and M. Kraft, "Modelling soot formation from wall films in a gasoline direct injection engine using a detailed population balance model," *Applied Energy*, vol. 163, pp. 154–166, 2016.

[98] A. Trubetskaya *et al.*, "Characterization and reactivity of soot from fast pyrolysis of lignocellulosic compounds and monolignols," *Applied Energy*, vol. 212, pp. 1489–1500, 2018.

[99] D. B. Olson, J. C. Pickens, and R. J. Gill, "The effects of molecular structure on soot formation II. Diffusion flames," *Combustion and Flame*, vol. 62, no. 1, pp. 43–60, 1985.

[100] K. Tsurutani, Y. Takei, Y. Fujimoto, J. Matsudaira, and M. Kumamoto, "The effects of fuel properties and oxygenates on diesel exhaust

emissions," 1995.

[101] J. Warnatz, U. Maas, and R. W. Dibble, "Physical and chemical fundamentals, modeling and simulation, experiments, pollutant formation," *Springer, Berlin Frenklach M, Wang H (1990) Detailed kinetic modelling of soot particle nucleation and growth. Proc Comb Inst*, vol. 23, pp. 1559–1566, 2006.

[102] D. W. Dockery, J. Schwartz, and J. D. Spengler, "Air pollution and daily mortality: associations with particulates and acid aerosols," *Environmental research*, vol. 59, no. 2, pp. 362–373, 1992.

[103] E. J. Calabrese, G. S. Moore, R. A. Guisti, C. A. Rowan, and E. N. Schulz, "A review of human health effects associated with exposure to diesel fuel exhaust," *Environment International*, vol. 5, no. 4–6, pp. 473–477, 1981.

[104] J. M. de Brito *et al.*, "Acute exposure to diesel and sewage biodiesel exhaust causes pulmonary and systemic inflammation in mice," *Science of The Total Environment*, vol. 628–629, pp. 1223–1233, 2018.

[105] S. A. McDowell *et al.*, "Differential gene expression in the initiation and progression of nickel-induced acute lung injury," *American journal of respiratory cell and molecular biology*, vol. 23, no. 4, pp. 466–474, 2000.

[106] P. T. J. Scheepers, J. L. G. Theuws, and R. P. Bos, "Mutagenicity of urine from rats after 1-nitropyrene and 2-nitrofluorene administration using new sensitive Salmonella typhimurium strains YG1012 and YG1024," *Mutation Research/Genetic Toxicology*, vol. 260, no. 4, pp. 393–399, 1991.

[107] R. L. Williams and S. J. Swarin, "Benzo (a) pyrene emissions from

gasoline and diesel automobiles," *SAE Transactions*, pp. 1561–1566, 1979.

[108] H. Reis *et al.*, "Diesel exhaust exposure, its multi-system effects, and the effect of new technology diesel exhaust," *Environment International*, vol. 114, pp. 252–265, 2018.

[109] A. Z. Taibani and V. Kalamkar, "Experimental and computational analysis of behavior of three-way catalytic converter under axial and radial flow conditions .," *International Journal of Fluid Machinery and Systems*, vol. 5, no. 3, pp. 134–142, 2012.

[110] H. Huang, B. Jiang, L. Gu, Z. Qi, and H. Lu, "Promoting effect of vanadium on catalytic activity of Pt/Ce-Zr-O diesel oxidation catalysts," *Journal of Environmental Sciences (China)*, vol. 33, no. 2005, pp. 135–142, 2015.

[111] M. M. Azis, X. Auvray, L. Olsson, and D. Creaser, "Evaluation of H2 effect on NO oxidation over a diesel oxidation catalyst," *Applied Catalysis B: Environmental*, vol. 179, no. 2, pp. 542–550, 2015.

[112] J. M. Herreros, S. S. Gill, I. Lefort, A. Tsolakis, P. Millington, and E. Moss, "Enhancing the low temperature oxidation performance over a Pt and a Pt-Pd diesel oxidation catalyst," *Applied Catalysis B: Environmental*, vol. 147, pp. 835–841, 2014.

[113] A. Arvajová, P. Kočí, V. Schmeißer, and M. Weibel, "The impact of CO and C3H6 pulses on PtOx reduction and NO oxidation in a diesel oxidation catalyst," *Applied Catalysis B: Environmental*, vol. 181, pp. 644–650, 2016.

[114] F. J. P. Schott, S. Steigert, S. Zuercher, M. Endisch, and S. Kureti, "Reactor design for the evaluation of diesel oxidation catalysts

supported by sintered metal filters," *Chemical Engineering and Processing: Process Intensification*, vol. 62, pp. 54–58, 2012.

[115] and C. G.-B. Yoon, Cheon-Seog, "Study of Design & CFD Analysis for Partial DPF Utilizing Metal Foam," *Transactions of the Korean society of Automotive Engineers*, vol. 17, no. 1, pp. 24–34, 2009.

[116] C. P. Om Ariara Guhan, G. Arthanareeswaren, and K. N. Varadarajan, "CFD Study on Pressure Drop and Uniformity Index of Three Cylinder LCV Exhaust System," *Procedia Engineering*, vol. 127, pp. 1211–1218, 2015.

[117] R. E. Hayes, A. Fadic, J. Mmbaga, and A. Najafi, "CFD modelling of the automotive catalytic converter," *Catalysis Today*, vol. 188, no. 1, pp. 94–105, 2012.

[118] X. Feng *et al.*, "Experimental study on the nitrogen dioxide and particulate matter emissions from diesel engine retrofitted with particulate oxidation catalyst," *Science of the Total Environment*, vol. 472, pp. 56–62, 2014.

[119] A. Dittler, "The Application of Diesel Particle Filters???From Past to Present and Beyond," *Topics in Catalysis*, vol. 60, no. 3–5, pp. 342–347, 2017.

[120] H. . Hardenberg, "Urban Bus Application of a Ceramic Fiber Coil Particulate Trap," *SAE Technical Paper*, no. 870011, p. 12, 1987.

[121] D. H. and E. H. Hardenberg H, "Particulate Trap Regeneration Induced by Means of Oxidizing Agents injected Into the Exhaust Gas," *SAE Technical Paper*, no. 870016, p. 16, 1987.

[122] S. Bensaid, D. L. Marchisio, and D. Fino, "Numerical simulation of

163

soot filtration and combustion within diesel particulate filters," *Chemical Engineering Science*, vol. 65, no. 1, pp. 357–363, 2010.

[123] T. Tang, J. Zhang, D. Cao, S. Shuai, and Y. Zhao, "Experimental study on filtration and continuous regeneration of a particulate filter system for heavy-duty diesel engines," *Journal of Environmental Sciences (China)*, vol. 26, no. 12, pp. 2434–2439, 2014.

[124] P. Salvat, O. Marez and G. and Belot, "Passenger Car Serial Application of a Particulate Filter System on a Common Rail Direct Injection Diesel Engine," *SAE Technical Paper*, no. 2000-01–0473, p. 15, 2000.

[125] V. R. Pérez and A. Bueno-López, "Catalytic regeneration of Diesel Particulate Filters: Comparison of Pt and CePr active phases," *Chemical Engineering Journal*, vol. 279, pp. 79–85, 2015.

[126] G. Corro, S. Cebada, U. Pal, J. L. G. Fierro, and J. Alvarado, "Hydrogen-reduced Cu/ZnO composite as efficient reusable catalyst for diesel particulate matter oxidation," *Applied Catalysis B: Environmental*, vol. 165, pp. 555–565, 2015.

[127] V. Palma, P. Ciambelli, E. Meloni, and A. Sin, "Study of the catalyst load for a microwave susceptible catalytic DPF," *Catalysis Today*, vol. 216, pp. 185–193, 2013.

[128] C. He, J. Li, Z. Ma, J. Tan, and L. Zhao, "High NO_2/NO_x emissions downstream of the catalytic diesel particulate filter: An influencing factor study," *Journal of Environmental Sciences (China)*, vol. 35, no. 2, pp. 55–61, 2015.

[129] E. Jiaqiang, W. Zuo, J. Gao, Q. Peng, Z. Zhang, and P. M. Hieu, "Effect analysis on pressure drop of the continuous regeneration-diesel

particulate filter based on NO2 assisted regeneration," *Applied Thermal Engineering*, vol. 100, pp. 356–366, 2016.

[130] W. E. C. Systems, "Integrated emissions control solutions meet global requirements while optimizing efficiency, reliability, and performance," 2017. [Online]. Available: http://www.woodward.com/emissioncontrols.aspx.

[131] J. Lup??e, M. Campolo, and A. Soldati, "Modelling soot deposition and monolith regeneration for optimal design of automotive DPFs," *Chemical Engineering Science*, vol. 151, pp. 36–50, 2016.

[132] H. Ranji-Burachaloo, S. Masoomi-Godarzi, A. A. Khodadadi, and Y. Mortazavi, "Synergetic effects of plasma and metal oxide catalysts on diesel soot oxidation," *Applied Catalysis B: Environmental*, vol. 182, pp. 74–84, 2016.

[133] F. E. Tuler, R. Portela, P. Ávila, J. P. Bortolozzi, E. E. Miró, and V. G. Milt, "Development of sepiolite/SiC porous catalytic filters for diesel soot abatement," *Microporous and Mesoporous Materials*, vol. 230, no. x, pp. 11–19, 2016.

[134] V. Palma and E. Meloni, "Microwave assisted regeneration of a catalytic diesel soot trap," *Fuel*, vol. 181, pp. 421–429, 2016.

[135] H. S. Hauck, "Design considerations for microwave oven cavities," *Industry and General Applications, IEEE Transactions on*, vol. I, no. 1, pp. 74–80, 1970.

[136] B. Zhang *et al.*, "Multidisciplinary design optimization of the diesel particulate filter in the composite regeneration process," *Applied Energy*, vol. 181, pp. 14–28, 2016.

[137] V. Chintala, P. Godkhe, S. Phadtare, M. Tadpatrikar, J. K. Pandey, and S. Kumar, "A comparative assessment of single cylinder diesel engine characteristics with plasto-oils derived from municipal mixed plastic waste," *Energy Conversion and Management*, vol. 166, pp. 579–589, Jun. 2018.

[138] Q. Liu *et al.*, "Comparative study on thermodynamics, combustion and emissions of turbocharged gasoline direct injection (GDI) engine under NEDC and steady-state conditions," *Energy Conversion and Management*, vol. 169, pp. 111–123, Aug. 2018.

[139] H. Park, E. Shim, and C. Bae, "Improvement of combustion and emissions with exhaust gas recirculation in a natural gas-diesel dual-fuel premixed charge compression ignition engine at low load operations," *Fuel*, vol. 235, pp. 763–774, Jan. 2019.

[140] A. Yousefi, H. Guo, M. Birouk, and B. Liko, "On greenhouse gas emissions and thermal efficiency of natural gas/diesel dual-fuel engine at low load conditions: Coupled effect of injector rail pressure and split injection," *Applied Energy*, vol. 242, pp. 216–231, May 2019.

[141] A. Yousefi, H. Guo, and M. Birouk, "Effect of diesel injection timing on the combustion of natural gas/diesel dual-fuel engine at low-high load and low-high speed conditions," *Fuel*, vol. 235, pp. 838–846, Jan. 2019.

[142] P. Boutikos, A. Žák, and P. Kočí, "CO and hydrocarbon light-off inhibition by pre-adsorbed NOx on Pt/CeO2/Al2O3 and Pd/CeO2/Al2O3 diesel oxidation catalysts," *Chemical Engineering Science*, vol. 209, p. 115201, Dec. 2019.

[143] S. Ye, Y. H. Yap, S. T. Kolaczkowski, K. Robinson, and D. Lukyanov,

"Catalyst 'light-off' experiments on a diesel oxidation catalyst connected to a diesel engine—Methodology and techniques," *Chemical Engineering Research and Design*, vol. 90, no. 6, pp. 834–845, Jun. 2012.

[144] C. KURIEN and A. Kumar, "Investigation on gas conversion efficiency and filtration behavior of Diesel Oxidation Catalysis System," *Australian Journal of Mechanical Engineering*, 2019.

[145] M. Vijay Kumar, A. Veeresh babu, P. Ravi Kumar, and T. Manoj Kumar Dundi, "Influence of different nozzle hole orifice diameter on performance, combustion and emissions in a diesel engine," *Australian Journal of Mechanical Engineering*, pp. 1–6, 2018.

[146] Caneon Kurien, Ajay Kumar Srivastava, and Joris Naudin, "Modelling of regeneration and filtration mechanism in diesel particulate filter for development of composite regeneration emission control system," *Archive of Mechanical Engineering*, vol. 65, no. 2, pp. 277–290, 2018.

[147] K. Caneon and A. K. Srivastav, "Geometrical Modelling and Analysis of Automotive Oxidation Catalysis System for Compliance with Environmental Emission Norms," *Nature Environment & Pollution Technology*, vol. 17, no. 4, pp. 1207–1212, 2018.

[148] P.-Y. Peng, M. P. Harold, and D. Luss, "Sustained concentration and temperature oscillations in a diesel oxidation catalyst," *Chemical Engineering Journal*, vol. 336, pp. 531–543, 2018.

[149] D. Fino, S. Bensaid, M. Piumetti, and N. Russo, "A review on the catalytic combustion of soot in Diesel particulate filters for automotive applications: From powder catalysts to structured reactors," *Applied Catalysis A: General*, vol. 509, pp. 75–96, 2016.

[150] G. Ionescu, D. Zardi, W. Tirler, E. C. Rada, and M. Ragazzi, "A critical analysis of emissions and atmospheric dispersion of pollutants from plants for the treatment of residual municipal solid waste," *UPB Scientific Bulletin, Series D: Mechanical Engineering*, vol. 74, no. 4, pp. 227–240, 2012.

[151] P. C. Shukla, T. Gupta, N. K. Labhasetwar, R. Khobaragade, N. K. Gupta, and A. K. Agarwal, "Effectiveness of non-noble metal based diesel oxidation catalysts on particle number emissions from diesel and biodiesel exhaust," *Science of The Total Environment*, vol. 574, pp. 1512–1520, 2017.

[152] C. Kurien and A. K. Srivastava, "Advancement in the design of automotive catalytic filter for meeting environmental emission norms," *Nature Environment and Pollution Technology*, vol. 17, no. 2, pp. 433–438, 2018.

[153] C. Kurien and A. K. Srivastava, "Active Regeneration of Diesel Particulate Filter Using Microwave Energy for Exhaust Emission Control," in *Intelligent Communication, Control and Devices*, 2018, pp. 1233–1241.

[154] G. S. Warkhade and A. V. Babu, "Combustion characteristics of linseed (Linum usitatissimum) methyl ester fuelled biodiesel blends in variable compression ratio diesel engine," *Australian Journal of Mechanical Engineering*, pp. 1–14, 2018.

[155] M. Skoglundh, L. O. Löwendahl, and J.-E. Otterated, "Combinations of platinum and palladium on alumina supports as oxidation catalysts," *Applied Catalysis*, vol. 77, no. 1, pp. 9–20, 1991.

[156] C. P. Hubbard, K. Otto, H. S. Gandhi, and K. Y. S. Ng, "Propane

Oxidation over Platinum Supported on Zirconia," *Journal of Catalysis*, vol. 139, no. 1, pp. 268–276, 1993.

[157] R. M. Heck and R. J. Farrauto, "Automobile exhaust catalysts," *Applied Catalysis A: General*, vol. 221, no. 1, pp. 443–457, 2001.

[158] Y. Yazawa, H. Yoshida, S. Komai, and T. Hattori, "The additive effect on propane combustion over platinum catalyst: control of the oxidation-resistance of platinum by the electronegativity of additives," *Applied Catalysis A: General*, vol. 233, no. 1, pp. 113–124, 2002.

[159] M. V Twigg, "Development of platinum catalysts and their use in the control of vehicle exhaust emissions," *Applied Earth Science*, vol. 114, no. 3, pp. 158–172, 2005.

[160] S. K. Sharma, P. Goyal, and R. K. Tyagi, "Conversion efficiency of catalytic converter," *International Journal of Ambient Energy*, vol. 37, no. 5, pp. 507–512, 2016.

[161] A. K. Neyestanaki, F. Klingstedt, T. Salmi, and D. Y. Murzin, "Deactivation of postcombustion catalysts, a review," *Fuel*, vol. 83, no. 4, pp. 395–408, 2004.

[162] T. Qiu, X. Li, H. Liang, X. Liu, and Y. Lei, "A method for estimating the temperature downstream of the SCR (selective catalytic reduction) catalyst in diesel engines," *Energy*, vol. 68, pp. 311–317, 2014.

[163] J. Ning and F. Yan, "Composite Control of DOC-out Temperature for DPF regeneration," *IFAC-PapersOnLine*, vol. 49, no. 11, pp. 20–27, 2016.

[164] S. C. Su, J. N. Carstens, and A. T. Bell, "A Study of the Dynamics of Pd Oxidation and PdO Reduction by H2and CH4," *Journal of*

Catalysis, vol. 176, no. 1, pp. 125–135, 1998.

[165] T. Watanabe *et al.*, "New DOC for light duty diesel DPF system," *SAE Technical Paper*, 2007.

[166] M. Wilklow-Marnell and W. D. Jones, "Catalytic oxidation of carbon monoxide by α-alumina supported 3nm cerium dioxide nanoparticles," *Molecular Catalysis*, vol. 439, pp. 9–14, 2017.

[167] I. Keren and M. Sheintuch, "Modeling and analysis of spatiotemporal oscillatory patterns during CO oxidation in the catalytic converter," *Chemical engineering science*, vol. 55, no. 8, pp. 1461–1475, 2000.

[168] C. Kurien, A. K. Srivastava, and J. Naudin, "Modelling of regeneration and filtration mechanism in diesel particulate filter for development of composite regeneration emission control system," *Archive of Mechanical ENgineering*, vol. 65, no. 2, pp. 277–290, 2018.

[169] A. A. Barresi and G. Baldi, "Deep catalytic oxidation of aromatic hydrocarbon mixtures: reciprocal inhibition effects and kinetics," *Industrial & engineering chemistry research*, vol. 33, no. 12, pp. 2964–2974, 1994.

[170] S. S. Mulla *et al.*, "Reaction of NO and O2 to NO2 on Pt: Kinetics and catalyst deactivation," *Journal of Catalysis*, vol. 241, no. 2, pp. 389–399, 2006.

[171] D. Bose, S. Sridharan, H. Dhawan, P. Vijay, and M. Gopinath, "Biomass derived activated carbon cathode performance for sustainable power generation from Microbial Fuel Cells," *Fuel*, vol. 236, pp. 325–337, 2019.

[172] R. V. S. P. Sanka *et al.*, "Nitrogen-doped graphene stabilized copper

nanoparticles for Huisgen [3+ 2] cycloaddition 'click' chemistry," *Chemical Communications*, vol. 55, no. 44, pp. 6249–6252, 2019.

[173] R. Fleischman, R. Amiel, J. Czerwinski, A. Mayer, and L. Tartakovsky, "Buses retrofitting with diesel particle filters: Real-world fuel economy and roadworthiness test considerations," *Journal of Environmental Sciences*, vol. 67, pp. 273–286, 2018.

[174] T. R. Dallmann, R. A. Harley, and T. W. Kirchstetter, "Effects of diesel particle filter retrofits and accelerated fleet turnover on drayage truck emissions at the Port of Oakland," *Environmental science & technology*, vol. 45, no. 24, pp. 10773–10779, 2011.

[175] F. Wang, Z. Li, K. Zhang, B. Di, and B. Hu, "An overview of non-road equipment emissions in China," *Atmospheric environment*, vol. 132, pp. 283–289, 2016.

[176] B. Guan, R. Zhan, H. Lin, and Z. Huang, "Review of the state-of-the-art of exhaust particulate filter technology in internal combustion engines," *Journal of Environmental Management*, vol. 154, pp. 225–258, May 2015.

[177] A. Mohammadiha, H. Malakooti, and V. Esfahanian, "Development of reduction scenarios for criteria air pollutants emission in Tehran Traffic Sector, Iran," *Science of The Total Environment*, vol. 622, pp. 17–28, 2018.

[178] A. Mayer, J. Czerwinski, J.-L. Pétermann, M. Wyser, and F. Legerer, "Reliability of DPF-Systems: Experience with 6000 Applications of the Swiss Retrofit Fleet," in *SAE Technical Paper*, 2004.

[179] C. Kurien and A. K. Srivastava, "Review on post-treatment emission control technique by application of diesel oxidation catalysis and diesel

particulate filtration," *Journal of Thermal Engineering*, vol. 5, no. 2, pp. 108–118, 2019.

[180] C. Kurien, A. K. Srivastava, and E. Molere, "Emission control strategies for automotive engines with scope for deployment of solar based e-vehicle charging infrastructure," *Environmental Progress & Sustainable Energy*, vol. Earlycite, 2019.

[181] X. Pu *et al.*, "Diesel particulate filter (DPF) regeneration using non-thermal plasma induced by dielectric barrier discharge," *Journal of the Energy Institute*, vol. 91, no. 5, pp. 655–667, Oct. 2018.

[182] E. Jiaqiang, M. Liu, Y. Deng, H. Zhu, and J. Gong, "Influence analysis of monolith structure on regeneration temperature in the process of microwave regeneration in the diesel particulate filter," *Can. J. Chem. Eng*, vol. 94, pp. 168–174, 2016.

[183] G. Matte-Deschênes, D. Vidal, F. Bertrand, and R. E. Hayes, "Numerical investigation of the impact of thermophoresis on the capture efficiency of diesel particulate filters," *The Canadian Journal of Chemical Engineering*, vol. 94, no. 2, pp. 291–303, 2016.

[184] M. K. Das, P. P. Mukherjee, and K. Muralidhar, "Equations Governing Flow and Transport in Porous Media," in *Modeling Transport Phenomena in Porous Media with Applications*, Springer, 2018, pp. 15–63.

[185] B. R. Strazisar, R. R. Anderson, and C. M. White, "Degradation of monoethanolamine used in carbon dioxide capture from flue gas of a coal-fired electric power generating station," 2001.

[186] IARC, "Known and Probable Human Carcinogens," *American Cancer Society*, 2016. [Online]. Available:

https://www.cancer.org/cancer/cancer-causes/general-info/known-and-probable-human-carcinogens.html.

[187] S. A. Halim and J. Swithenbank, "Simulation study of parameters influencing microwave heating of biomass," *Journal of the Energy Institute*, 2018.

[188] S. L. Birla and K. Pitchai, *18. Simulation of microwave processes*, Second Edi. Elsevier Ltd, 2017.

[189] P. P. Falciglia, P. Roccaro, L. Bonanno, G. De Guidi, F. G. A. Vagliasindi, and S. Romano, "A review on the microwave heating as a sustainable technique for environmental remediation/detoxification applications," *Renewable and Sustainable Energy Reviews*, vol. 95, pp. 147–170, 2018.

[190] L. Punathil and T. Basak, "Microwave Heating of Food Materials: Theoretical Investigations," in *Reference Module in Food Science*, Elsevier, 2017.

[191] M. Regier, "Microwave Heating," in *Reference Module in Food Science*, Elsevier, 2017.

[192] S. Curet, O. Rouaud, and L. Boillereaux, "Heat transfer models for microwave thawing applications," in *Excerpt from the Proceedings of the COMSOL Users Conference, Paris*, 2006.

[193] I. Imenokhoyev, A. Matthes, H. Gutte, and G. Walter, "Numerical 3D-FEM-simulation made by COMSOL Multiphysics of a microwave assisted cleaning system for a diesel sooty particle filter and its experimental validation," in *Proceeding Book, Int. COMSOL Multiphysics Conf., Ludwigsburg*, 2011, vol. 26, no. 28.10.

173

[194] C. Kurien, A. K. Srivastava, K. Anand, and N. Gandigudi, "Modelling of Microwave-Based Regeneration in Composite Regeneration Emission Control System," in *Intelligent Communication, Control and Devices*, Springer, 2020, pp. 313–320.

[195] A. B. Epenetus, C. S. Meera, S. Mohan, and M. K. Gupta, "Development and motion control of spatial serial robotic manipulator under varying disturbances," *World Journal of Engineering*, 2019.

[196] Z. Meng *et al.*, "Particle emission characteristics of DPF regeneration from DPF regeneration bench and diesel engine bench measurements," *Fuel*, vol. 262, p. 116589, Feb. 2020.

[197] J. Rodríguez-Fernández, M. Lapuerta, and J. Sánchez-Valdepeñas, "Regeneration of diesel particulate filters: Effect of renewable fuels," *Renewable Energy*, vol. 104, pp. 30–39, Apr. 2017.

[198] P. Chen and J. Wang, "Air-fraction modeling for simultaneous Diesel engine NOx and PM emissions control during active DPF regenerations," *Applied Energy*, vol. 122, pp. 310–320, Jun. 2014.

[199] P. Chen, U. Ibrahim, and J. Wang, "Experimental investigation of diesel and biodiesel post injections during active diesel particulate filter regenerations," *Fuel*, vol. 130, pp. 286–295, Aug. 2014.

[200] A. Misra, K. Panchabikesan, E. Ayyasamy, and V. Ramalingam, "Sustainability and Environmental Management: Emissions Accounting for Ports," *Strategic Planning for Energy and the Environment*, vol. 37, no. 1, pp. 8–26, 2017.

[201] Z. Gong, J. Wang, K. Zhang, B. Li, and W. Wu, "Complex Rare-earth oxides leached from the rare-earth concentrate to prepare the catalyst for selective catalytic reduction of NO with NH3," *Minerals*

Engineering, vol. 146, p. 106135, Jan. 2020.

[202] Y. You *et al.*, "Low-temperature selective catalytic reduction of N2O by CO over Fe-ZSM-5 catalysts in the presence of O2," *Journal of Hazardous Materials*, vol. 383, p. 121117, Feb. 2020.

[203] C. Niu *et al.*, "The deposition of VWOx on the CuCeOy microflower for the selective catalytic reduction of NOx with NH3 at low temperatures," *Journal of Colloid and Interface Science*, vol. 561, pp. 808–817, Mar. 2020.

[204] J. Baleta, M. Martinjak, M. Vujanović, K. Pachler, J. Wang, and N. Duić, "Numerical analysis of ammonia homogenization for selective catalytic reduction application," *Journal of Environmental Management*, vol. 203, pp. 1047–1061, Dec. 2017.

[205] Z. Zhao *et al.*, "Density functional theory (DFT) studies of vanadium-titanium based selective catalytic reduction (SCR) catalysts," *Journal of Environmental Sciences*, vol. 90, pp. 119–137, Apr. 2020.

[206] D. Zhang *et al.*, "VxMn(4 − x)Mo3Ce3/Ti catalysts for selective catalytic reduction of NO by NH3," *Journal of Environmental Sciences*, vol. 88, pp. 145–154, Feb. 2020.

[207] C. Kurien and A. K. Srivastava, "Active Regeneration of Diesel Particulate Filter Using Microwave Energy for Exhaust Emission Control," *Advances in Intelligent Systems and Computing*, vol. 624, pp. 1233–1241, 2018.

[208] H.-H. Chen, S.-C. Shen, X. Chen, and S. Kawi, "Selective catalytic reduction of NO over Co/beta-zeolite: effects of synthesis condition of beta-zeolites, Co precursor, Co loading method and reductant," *Applied Catalysis B: Environmental*, vol. 50, no. 1, pp. 37–47, Jun. 2004.

[209] S. Zinatloo-Ajabshir, N. Ghasemian, and M. Salavati-Niasari, "Green synthesis of Ln2Zr2O7 (Ln = Nd, Pr) ceramic nanostructures using extract of green tea via a facile route and their efficient application on propane-selective catalytic reduction of NOx process," *Ceramics International*, vol. 46, no. 1, pp. 66–73, Jan. 2020.

[210] M. Hosseinpour, M. Akizuki, A. Yoko, Y. Oshima, and M. Soltani, "Novel synthesis and characterization of Fe-ZSM-5 nanocrystals in hot compressed water for selective catalytic reduction of NO with NH3," *Microporous and Mesoporous Materials*, vol. 292, p. 109708, Jan. 2020.

[211] H. Zhang, J. Wang, and Y. Wang, "Removal of NO x sensor ammonia cross sensitivity from contaminated measurements in Diesel-engine selective catalytic reduction systems," *FUEL*, vol. 150, no. x, pp. 448–456, 2015.

[212] H. Hua *et al.*, "Understanding of the high hydrothermal stability of a catalyst prepared from Mn slag for low-temperature selective catalytic reduction of NO," *Journal of Hazardous Materials*, vol. 381, p. 120935, Jan. 2020.

[213] C. Lee, "Numerical and experimental investigation of evaporation and mixture uniformity of urea–water solution in selective catalytic reduction system," *Transportation Research Part D: Transport and Environment*, vol. 60, pp. 210–224, May 2018.

[214] H. T. Xu, Z. Q. Luo, N. Wang, Z. G. Qu, J. Chen, and L. An, "Experimental study of the selective catalytic reduction after-treatment for the exhaust emission of a diesel engine," *Applied Thermal Engineering*, vol. 147, pp. 198–204, Jan. 2019.

[215] F. Ferella, "A review on management and recycling of spent selective catalytic reduction catalysts," *Journal of Cleaner Production*, vol. 246, p. 118990, Feb. 2020.

[216] R. Rogóż, Ł. J. Kapusta, J. Bachanek, J. Vankan, and A. Teodorczyk, "Improved urea-water solution spray model for simulations of selective catalytic reduction systems," *Renewable and Sustainable Energy Reviews*, p. 109616, Nov. 2019.

[217] M. Casapu, A. Bernhard, D. Peitz, M. Mehring, M. Elsener, and O. Kröcher, "A Niobia-Ceria based multi-purpose catalyst for selective catalytic reduction of NOx, urea hydrolysis and soot oxidation in diesel exhaust," *Applied Catalysis B: Environmental*, vol. 103, no. 1–2, pp. 79–84, Mar. 2011.

[218] G. Tokazhanov, E. Ramazanova, S. Hamid, S. Bae, and W. Lee, "Advances in the catalytic reduction of nitrate by metallic catalysts for high efficiency and N2 selectivity: A review," *Chemical Engineering Journal*, vol. 384, p. 123252, Mar. 2020.

[219] J. Baleta, M. Vujanović, and K. Pachler, "Numerical modeling of urea water based selective catalytic reduction for mitigation of NOx from transport sector," *Journal of Cleaner Production*, vol. 88, pp. 280–288, Feb. 2015.

[220] F. Yan, L. Wei, J. Hu, J. Zeng, S. Zheng, and J. Wang, "Simultaneous optimization of urea dosing and ammonia coverage ratio of selective catalytic reduction system in diesel engine by using physico-chemical model based NSGA-II algorithm," *Applied Thermal Engineering*, vol. 154, pp. 46–62, May 2019.

[221] K. Liu, Q. Yu, B. Wang, J. San, W. Duan, and Q. Qin, "Binary copper-

manganese based catalysts with urea for low-temperature selective catalytic reduction of NO: Performance, characterization and mechanism," *Applied Surface Science*, p. 144755, Nov. 2019.

[222] D. Carder, R. Ryskamp, M. Besch, and A. Thiruvengadam, "Emissions Control Challenges for Compression Ignition Engines," *Procedia IUTAM*, vol. 20, no. X, pp. 103–111, 2017.

[223] E. Cao and K. Jiang, "Neurocomputing Adaptive unscented Kalman filter for input estimations in Diesel-engine selective catalytic reduction systems," *Neurocomputing*, pp. 1–7, 2016.

[224] Y. Chen, W. Peng, S. Wang, F. Zhang, G. Zhang, and X. Fan, "Supported nano-sized gold catalysts for selective reduction of 4,4′-dinitrostilbene-2,2′-disulfonic acid using different reductants," *Dyes and Pigments*, vol. 95, no. 2, pp. 215–220, 2012.

[225] P. Polverino, F. D'Aniello, I. Arsie, and C. Pianese, "Investigation of the energy requirements for the on-board generation of oxy-hydrogen on vehicles," *Energy Procedia*, vol. 148, pp. 962–969, 2018.

[226] A. Rimkus, J. Matijošius, M. Bogdevičius, Á. Bereczky, and Á. Török, "An investigation of the efficiency of using O2 and H2 (hydrooxile gas -HHO) gas additives in a ci engine operating on diesel fuel and biodiesel," *Energy*, vol. 152, pp. 640–651, 2018.

[227] Ç. Conker, "A novel fuzzy logic based safe operation oriented control technique for driving HHO dry cell systems based on PWM duty cycle," *International Journal of Hydrogen Energy*, 2018.

[228] B. Subramanian and S. Ismail, "Production and use of HHO gas in IC engines," *International Journal of Hydrogen Energy*, vol. 43, no. 14, pp. 7140–7154, 2018.

[229] S. Thangaraj and N. Govindan, "Evaluating combustion, performance and emission characteristics of diesel engine using karanja oil methyl ester biodiesel blends enriched with HHO gas," *International Journal of Hydrogen Energy*, vol. 43, no. 12, pp. 6443–6455, 2018.

[230] E. Uludamar, "Effect of hydroxy and hydrogen gas addition on diesel engine fuelled with microalgae biodiesel," *International Journal of Hydrogen Energy*, vol. 43, no. 38, pp. 18028–18036, 2018.

[231] M. K. Baltacıoğlu, "A novel application of pulse width modulation technique on hydroxy gas production," *International Journal of Hydrogen Energy*, 2018.

[232] H. T. Arat, "Simulation of diesel hybrid electric vehicle containing hydrogen enriched CI engine," *International Journal of Hydrogen Energy*, 2018.

[233] A. A. Al-Rousan and S. A. Musmar, "Effect of anodes-cathodes inter-distances of HHO fuel cell on gasoline engine performance operating by a blend of HHO," *International Journal of Hydrogen Energy*, vol. 43, no. 41, pp. 19213–19221, 2018.

[234] J. M. R. Matienzo, "Influence of addition of hydrogen produced on board in the performance of a stationary diesel engine," *International Journal of Hydrogen Energy*, vol. 43, no. 37, pp. 17889–17897, 2018.

[235] P. Chelladorai, E. G. Varuvel, L. J. Martin, and N. Bedhannan, "Synergistic effect of hydrogen induction with biofuel obtained from winery waste (grapeseed oil) for CI engine application," *International Journal of Hydrogen Energy*, vol. 43, no. 27, pp. 12473–12490, 2018.

APPENDIX I

S1.1 C PROGRAM FOR INTERFACING PN SENSOR AND DIFFERENTIAL PRESSURE SENSOR WITH ARDUINO UNO INTERFACE

Sl.no	Sensor and Programming Language
1.	Differential Pressure Sensor

```
 /* PIN1 = GND
 *  PIN2 = A0
 *  PIN3= 5V
 *  PIN4 = Al
 */
const float SensorOffset = 102.0;
// the setup routine runs once when you press reset:
void setup() {
  // initialize serial communication at 9600 bits per seco
  Serial.begin(9600);
}

// the loop routine runs over and over again forever:
void loop() {
  // read the input on analog pin 0:
  float sensorValue = (analogRead(A0)-SensorOffset)/100.0;
  // print out the value you read:
  float sensorValuel = (analogRead(Al)-SensorOffset)/100.0
   float sensorValue2=(sensorValue-sensorValuel);

  Serial.print("Air Pressure Difference: ");
  Serial.print(sensorValue2,2);
  Serial.println(" kPa");

  delay(1000);          // delay in between reads for stabil
}
```

2	Particle Number Sensor
| | ```
    /* PIN 3=VCC
 *   PIN5 =GND
 *   PIN2= 8
 */
#include<string.h>
#include<stdio.h>
byte buff[2];
int pin = 8;//DSM501A input D8

long duration;
long starttime;
long endtime;
long sampletime_ms = 3000;
long lowpulseoccupancy = 0;
float ratio = 0;
float concentration = 0;

int i=0;
void setup()
{
  Serial.begin(9600);
  pinMode(8,INPUT);
  starttime = millis();
}
void loop()
{

  duration = pulseIn(pin, LOW);
  lowpulseoccupancy += duration;
  lowpulseoccupancy=(lowpulseoccupancy);
  endtime = millis();
  if ((endtime-starttime) > sampletime_ms)
   {
``` |

```
{
    ratio = (lowpulseoccupancy-endtime+starttime
    + sampletime_ms)/(sampletime_ms*10.0);
    concentration = 1.1*pow(ratio,3)-3.8*
    pow(ratio,2)+520*ratio+0.62;
    concentration=(concentration/1000);
    Serial.print("lowpulseoccupancy:");



    Serial.print(lowpulseoccupancy);
    Serial.print("\n");
    Serial.print("ratio:");
    Serial.print("\n");
    Serial.println(ratio);
    Serial.print("DSM501A:");
    Serial.println(concentration);
    Serial.print(";\n\n");
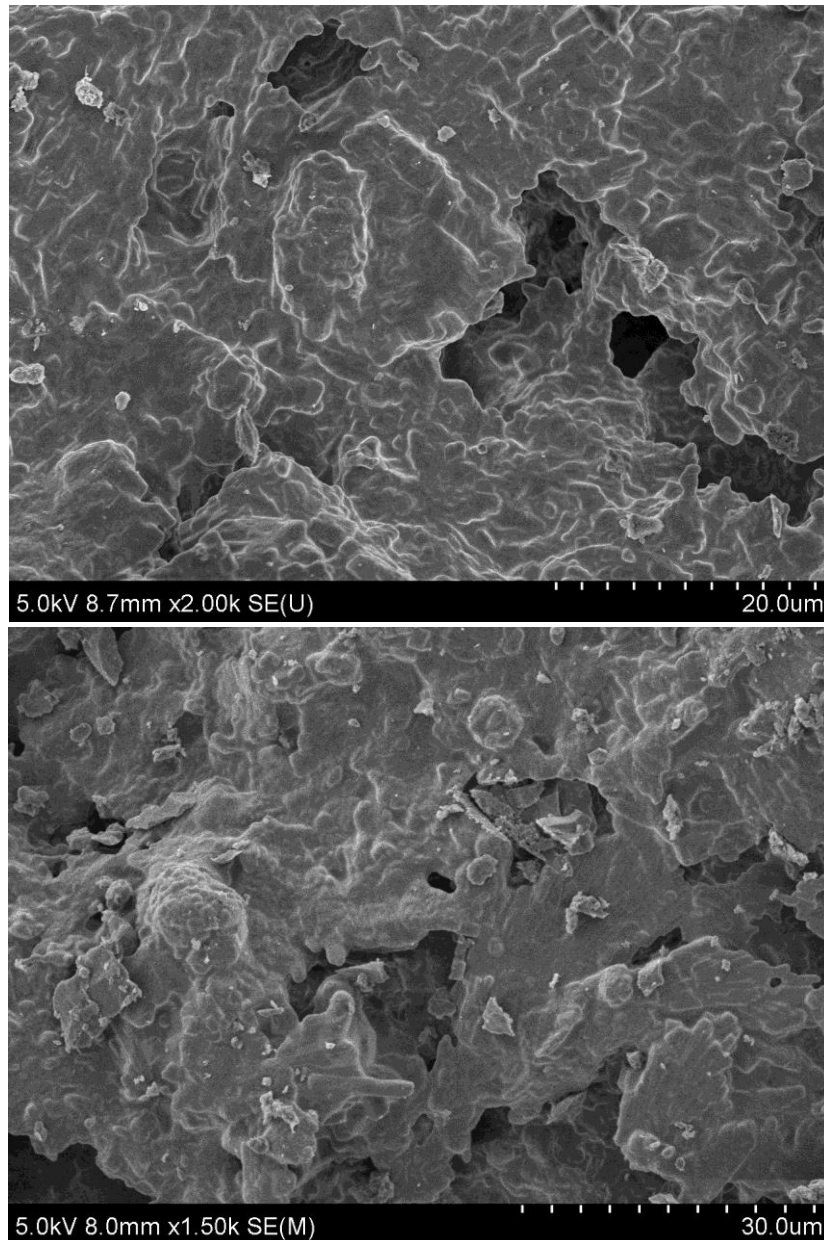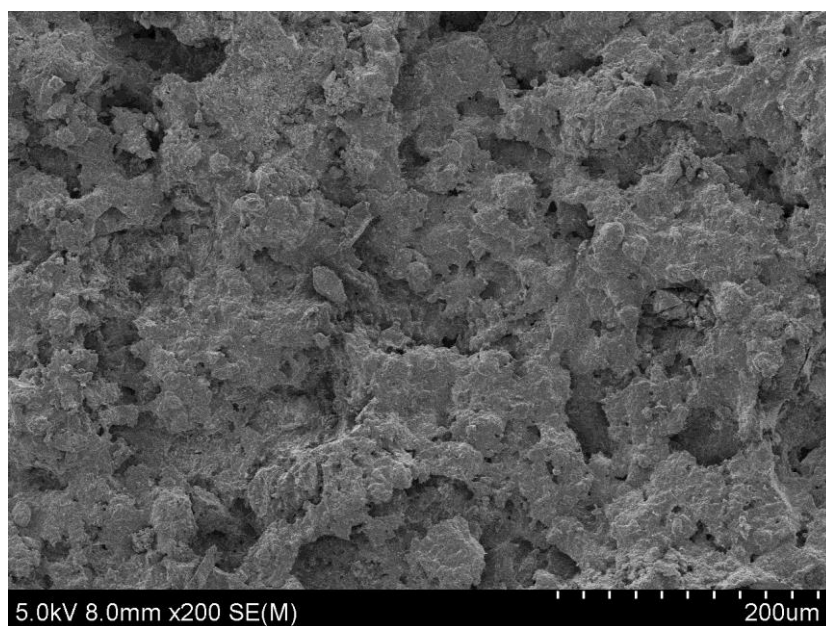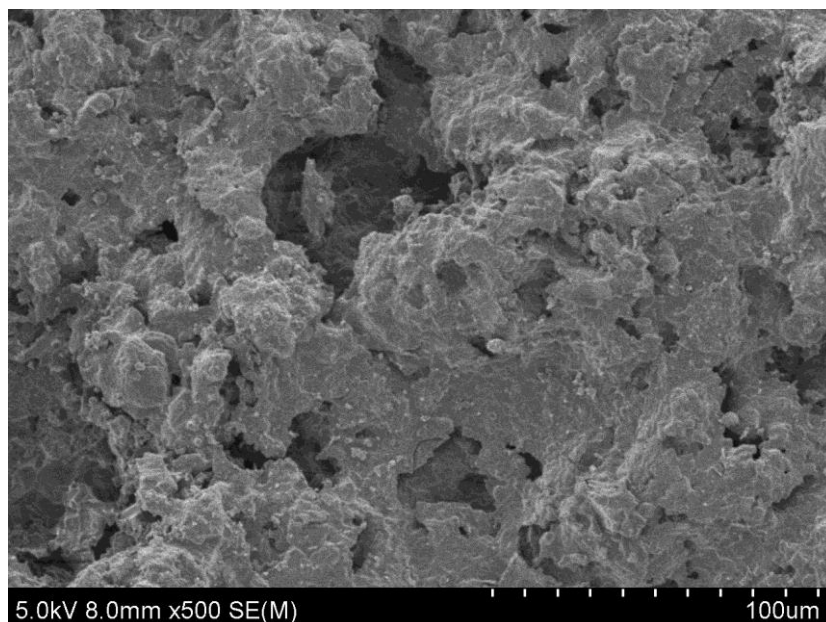
    lowpulseoccupancy = 0;
    starttime = millis();
  }
}
```

APPENDIX II

S2.1 EQUATIONS USED FOR CALCULATING PERFORMANCE PARAMETERS OF ENGINE

Sl. No	Parameter	Formula	
1	Mass of fuel consumed, m_f (kg/hr)	$m_f = \dfrac{fuel\_consumed\_cc \times 10^{-6} \times \rho_{diesel}}{t}$	
2	Density of air, ρ_{air} (kg/m^3)	$\rho_{air} = \dfrac{1.01325 \times 10^5}{287 \times (273 + T_4)}$	
3	Head of air, h_a (m)	$h_a = \dfrac{h_{manometer} \times \rho_{water}}{\rho_{air}}$	
4	Actual mass of air consumed, m_{act} (kg/hr)	$m_{act} = C_d \times \dfrac{\pi}{4} \times d^2 \times \sqrt{2gh_a} \times \rho_{air} \times 3600$	
5	Theoretical mass of air, m_{th} (kg/hr)	$m_{th} = \dfrac{\pi}{4} \times d_{bore}^{\ 2} \times L \times \dfrac{N}{2} \times 4 \times \rho_{air} \times 60$	
6	Volumetric efficiency, η_{vol} (%)	$\eta_{vol} = \dfrac{m_{act}}{m_{th}} \times 100$	
7	Air fuel ratio, A/F_ratio	$A/F\_ratio = \dfrac{m_{act}}{m_f}$	
8	Brake power, BP (kW)	$BP = \dfrac{V \times I}{1000 \times \eta_g}$	
9	Heat Input, Q (kJ)	$Q = \dfrac{m_f \times CV}{3600}$	
10	Specific Fuel Consumption, SFC (Kg/kWh)	$SFC = \dfrac{m_f}{BP}$	
11	Brake Thermal Efficiency, η_{bth} (%)	$\eta_{bth} = \dfrac{BP}{Q} \times 100$	
12	Torque, T (N-m)	$T = \dfrac{BP \times 60 \times 1000}{2\pi N}$	
13	Constants: $\rho_{diesel} = 832$ kg/m^3 $\rho_{water} = 1000$ kg/m^3	$C_d = 0.62$ $d_{orifice} = 0.020$ m $d_{bore} = 0.069$m	$L = 0.082$m $\eta_g = 0.70$

S2.2 ACCURACY OF MEASUREMENTS/UNCERTAINTIES

Sl. No	Parameter	Measuring range	Accuracy	Uncertainty (%)
1	CO	0 to 9.999%	0.001%	3.8
2	HC	0 to 15000ppm	1ppm	3.09
3	CO_2	0 to 20%	0.01%	1.5
4	Temperature	0 to 1000 deg. C	1 deg. C	0.12
5	Brake Power	-	-	3
6	Volume flow rate of air	-	-	0.52
7	Fuel consumption	-	-	1.69
8	Volumetric efficiency	-	-	1.47

APPENDIX III

S3.1 SEM IMAGES OF DPF SUBSTRATE

Figure S 3.1 SEM images of the DPF cordierite substrate before soot loading at magnification of (a) 20 micron and (b) 30 micron

Figure S 3.2 SEM images of the DPF cordierite substrate before soot loading at magnification of (a) 100 micron and (b) 200 micron

Figure S 3.3 SEM images of the DPF cordierite substrate after soot loading at magnification of (a) 20 micron and (b) 30 micron

Figure S 3.4 SEM images of the DPF cordierite substrate after soot loading at magnification of (a) 100 micron and (b) 200 micron

APPENDIX IV

S4.1 ISOSURFACE TEMPERATURE CONTOURS FOR MICROWAVE REGENERATION

Figure S.4.1 . Contours of Iso-surface temperature distribution in Microwave Regeneration System after 150 Seconds of Regeneration at Power Rating of (a) 100 W (b) 200 W (c) 300 W and (d) 400 W

Figure S.4.2 . Contours of Iso-surface temperature distribution in Microwave Regeneration System after 150 Seconds of Regeneration at Power Rating of (a) 500 W (b) 600 W and (c) 700 W

CANEON KURIEN

EDUCATION

2014-2016   M.Tech in Pipeline engineering, University of Petroleum & Energy Studies (UPES), Dehradun, India.

2010-2014   B.Tech in Mechanical Engineering, Calicut University, Kerala, India.

PUBLICATIONS

PATENTS

1. "*Microwave-Assisted Composite Regeneration System for Diesel Particulate Filter*". Ajay Kumar, Caneon Kurien and Deepak Kumar, Patent Application No. 201911035506, REQUEST FOR EXAMINATION DATE 04/09/2019; PUBLICATION DATE (U/S 11A) :20/09/2019.

ARTICLES

1. Kurien, Caneon, Ajay Kumar Srivastava, Niranjan Gandigudi, and Karan Anand. "*Soot deposition effects and microwave regeneration modelling of diesel particulate filtration system.*", Journal of the Energy Institute, Elsevier (2020) https://doi.org/10.1016/j.joei.2019.07.005, Volume 93, Issue 2, Pages 463 – 473. **[SCI]**

2. Kurien, Caneon, Ajay Kumar Srivastava, and Salome Lesbats, "*Experimental and Computational Study on the Microwave Energy Based Regeneration and Filtration in Diesel Particulate Filter*", Journal of the Energy Institute, Elsevier, Article in Press (Available online), (2020) https://doi.org/10.1016/j.joei.2020.05.008 **[SCI]**

3. Kurien, Caneon, and Ajay Kumar Srivastava. "*Impact of Electric Vehicles on Indirect Carbon Emissions and Role of Engine Post-Treatment Emission Control Strategies.*" Volume 16, Issue 2, Integrated

environmental assessment and management, Wiley, Page no. 234 – 244. https://doi.org/10.1002/ieam.4206 (2020) **[SCI]**

4. Kurien, Caneon Ajay Kumar Srivastava and Joris Emeric Molere, "*Emission Control Strategies for Automotive Engines with Scope for Deployment of Solar Based E-Vehicle Charging Infrastructure*", Environmental Progress and Sustainable Energy, Wiley, https://doi.org/10.1002/ep.13267 , Volume 39, Issue 1, May 2019. **[SCI]**

5. Kurien, Caneon, Ajay Kumar Srivastava, and Joris Naudin. "*Modelling of regeneration and filtration mechanism in diesel particulate filter for development of composite regeneration emission control system.*" Archive of Mechanical Engineering, Volume no. 65, issue no. 2 (2018). https://doi.org/10.24425/123025**[ESCI]**

6. Kurien, Caneon and Ajay Kumar Srivastava. "*Review on Post-Treatment Emission Control Technique by Application of Diesel Oxidation Catalysis and Diesel Particulate Filtration.*" Journal of Thermal Engineering Vol 5, No. 2 (2019): 108-118. https://doi.org/10.18186/thermal.532252 **[ESCI]**

7. Kurien, Caneon, and Ajay Kumar Srivastava. "*Investigation on gas conversion efficiency and filtration behavior of Diesel Oxidation Catalysis System* ", Australian Journal of Mechanical Engineering, Taylor and Francis, Article in press. http://doi.org/10.1080/14484846.2019.1704491 **[ESCI]**

8. Kurien, Caneon, and Ajay Kumar Srivastava. "*Advancement in the Design of Automotive Catalytic Filter for Meeting Environmental Emission Norms.*" Nature Environment and Pollution Technology 17.2 (2018): 433-438.**[SCOPUS]**

9. Kurien, Caneon, and Ajay Kumar Srivastava. "*Geometrical Modelling and Analysis of Automotive Oxidation Catalysis System for Compliance with Environmental Emission Norms.*" Nature Environment & Pollution Technology 17.4 (2018).**[SCOPUS]**

10. Kurien, Caneon, and Ajay Kumar Srivastava. "*Active Regeneration of Diesel Particulate Filter Using Microwave Energy for Exhaust Emission Control.*" Intelligent Communication, Control and Devices. Springer,

Singapore, 2018. 1233-1241 (2018) https://doi.org/10.1007/978-981-10-5903-2_129 .**[SCOPUS]**

11. Kurien, Caneon, Ajay Kumar Srivastava, and Deepak Kumar. "*Geometric Design Validation of Oxidation Catalysis System in Composite Regeneration Emission Control System.*" International Journal of Vehicle Structure and Systems, Vol 11, Issue 1 (2019) http://dx.doi.org/10.4273/ijvss.11.1.16 **[SCOPUS]**

12. Kurien, Caneon, Srivastava A.K., Anand K., Gandigudi N. (2020) *Modelling of Microwave-Based Regeneration in Composite Regeneration Emission Control System*. In: Choudhury S., Mishra R., Mishra R., Kumar A. (eds) Intelligent Communication, Control and Devices. Advances in Intelligent Systems and Computing, vol 989. Springer, Singapore. https://doi.org/10.1007/978-981-13-8618-3_33 **[SCOPUS]**

13. Kurien, Caneon, and Ajay Kumar Srivastava. "*Solid Reductant Based Selective Catalytic Reduction System for Exhaust Emission Control of Compression Ignition Engines*", Nature Environment and Pollution Technology, Vol 18, no. 3 (2019): 1207-1212. **[SCOPUS]**

CONFERENCE PRESENTATIONS

1. Presented a technical paper on, "*Components of design and flow analysis of Diesel Oxidation Catalyst (DOC) filter for exhaust emission control*" at International Conference on 21st Century Energy Needs - Materials, Systems and Applications (ICTFCEN 2016), held at Indian Institute of Technology (IIT) Kharagpur.

2. Presented a technical paper on, "*Active Regeneration of Diesel Particulate Filter Using Microwave Energy for Exhaust Emission Control*", at International Conference on Intelligent Communication, Control and Devices (ICICCD 2017), held at University of Petroleum and Energy Studies (UPES), Dehradun.

3. Presented a technical paper on, "*Scope of Artificial Intelligence Techniques for Exhaust Emission Prediction of CI Engines and Renewable Energy Applications*" at International Conference on Advances in

Computing Applications (ICACA 2018), held at National Institute of Technology (NIT) Uttarakhand.

4. Presented a technical paper on, "*Modelling of Microwave Based Regeneration in Composite Regeneration Emission Control System*", at International Conference on Intelligent Communication, Control and Devices (ICICCD 2018), held at University of Petroleum and Energy Studies (UPES), Dehradun.

PLAGIARISM CERTIFICATE

1. We Dr. AJAY KUMAR SRIVASTAVA (Internal Guide), _____(Co Guide/ External Guide) certify that the Thesis titled

    COMPOSITE REGENERATION AND PARTICULATE FILTRATION BY APPLICATION OF MICROWAVE ENERGY FOR EXHAUST EMISSION CONTROL OF CI ENGINES

    submitted by Scholar Mr__CANEON KURIEN____having SAP ID 500056861____has been run through a Plagiarism Check Software and the Plagiarism Percentage is reported to be __12__%.

2. Plagiarism Report generated by the Plagiarism Software is attached.

_____28.08.2020_

Signature of the Internal Guide   **Signature of External Guide/ Co Guide**

Signature of the Scholar

COMPOSITE REGENERATION AND PARTICULATE FILTRATION BY APPLICATION OF MICROWAVE ENERGY FOR EXHAUST EMISSION CONTROL OF CI ENGINES